SYNTHESIS, CHARACTERIZATION AND CATALYTIC PROPERTIES OF METAL PHTHALOCYANINES ENCAPSULATED IN LARGE PORE ZEOLITES

A thesis

submitted to the

UNIVERSITY OF PUNE

for the degree of

DOCTOR OF PHILOSOPHY

in Chemistry

by

SINDHU SEELAN

M.Phil

CATALYSIS DIVISION

NATIONAL CHEMICAL LABORATORY

PUNE 411008, INDIA

SEPTEMBER, 2000

DEDICATED TO MY BELOVED PARENTS AND REVERED GUIDE

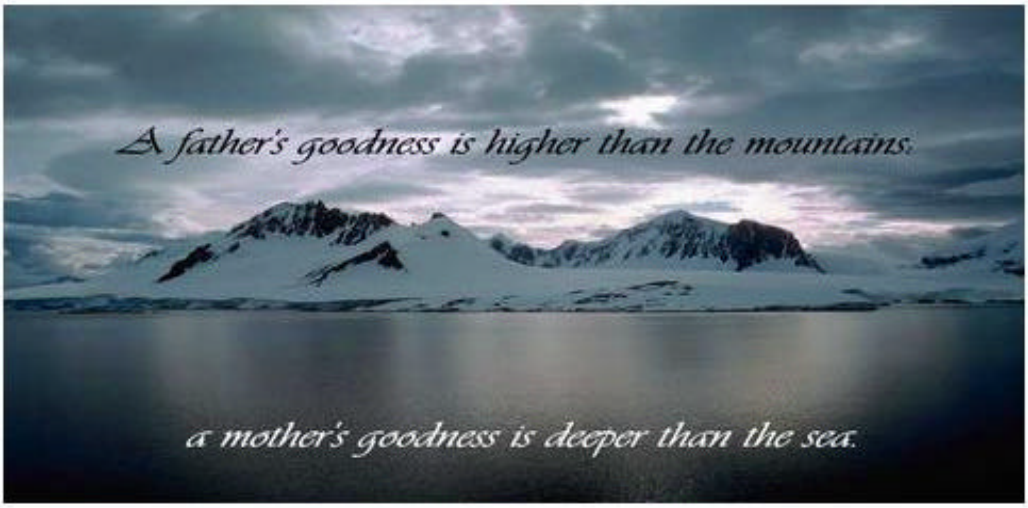

For their love and concern, for sowing in me,
the value of education and knowledge,
for their unlimited, unhesitant moral support,
for which I am forever grateful and highly
indebted to them.

CERTIFICATE

Certified that the work incorporated in the thesis **Synthesis, Characterization and Catalytic Properties of Metal Phthalocyanines Encapsulated in Large Pore Zeolites** submitted by **Miss Sindhu Seelan**, for the degree of Doctor of Philosophy in Chemistry, was carried out by the candidate under our supervision in the Catalysis Division, National Chemical Laboratory, Pune, India. Materials obtained from other sources have been duly acknowledged in the thesis.

Dr. S. Sivasanker — **Research Guide**

Dr. D. Srinivas — **Reseach Co-Guide**

ACKNOWLEDGMENTS

I acknowledge with respect the valuable guidance and support given by Dr. S. Sivasanker, Deputy Director, National Chemical Laboratory, Pune during the course of this work. His constant encouragement, insight and close attention to details have ensured the successful completion of this work.

I wish to express my sincere gratitude and indebtness to Dr. D. Srinivas, National Chemical Laboratory for his expert co-guidance, thought provoking discussions and the help rendered throughout the course of this investigation without which I would not have completed this work successfully.

I wish to offer my sincere thanks to Dr. A.V. Ramaswamy, Head, Catalysis Division for providing me all the facilities to carry out the research work.

I am grateful to Dr. B.S. Rao, Dr. H.S. Soni, Dr. S.G. Hegde, Dr. Mr.& Mrs. Gopinathan, Dr. R. Vetrivel, Mrs. N. Jacob, Dr. S. Awate, Dr.A.A.Belhekar, Dr. S.P.Mirajkar, Dr. C.V.V. Satyanarayana, Dr. V.Ramaswamy, Dr. A.J. Chandwadkar. Dr. K.R. Kamble, Dr. S. Deshpande, Miss. Violet, Dr. S.A.Pardhy, Mr. K.Ramakrishnan, Katti, Madhu and all other scientific and non-scientific staff of Catalysis and Inorganic Division for their help and cooperation given to me in completing my research work successfully.

I specially thank Mr. & Mrs. Viswambharan for their cooperation and timely help during my research.

I record my appreciation and heart-felt thanks to beloved Anil for helping and encouraging me in all possible manners throughout this work.

I thank my friends, Karuna, Sharvari, Raja, Bennur, Abhimanyu, Sabde, Sridevi, Jai, Siddesh, Suhas.K, Suhas.C, Sivaramakrishna, Anand, Tapan, Tapas, Venkatathri, Raghavan, Gnaneswar and many others from whom I have received valuable help, encouragement and friendly working environment.

I thank Mr.Suresh Waghmode for the help in molecular modelling work.

My special thanks to my friend Tahseen and my brother Abbas for their love and support.

My heart felt thanks to Mrs. Jaya Sivasanker for her invaluable encouragement and moral support, without which this thesis would not have taken its present shape.

I am extremely grateful to my father, mother and grandmother for their love, total support and valuable blessings.

My sincere thanks are due to Dr. P. Ratnasamy, Director, NCL, for allowing me to carry out the research at NCL and to submit the work in the form of a thesis for the award of the Ph.D degree. Finally I thank the Council of Scientific and Industrial Research, New Delhi for providing me a senior research fellowship.

Sindhu Seelan

CONTENTS

1. INTRODUCTION

1.1 Generalities 1

1.2 Zeolites and Molecular Sieves 2

1.3 Heterogenization of Homogeneous Catalysts 6

1.4 Transition Metal Complexes Encapsulated in Zeolites 8

1.5 Methods of Metal Complex Encapsulation in Zeolites 9

1.5.1 *In situ* preparation of metal complexes 10

1.5.2 Flexible ligand synthesis method 10

1.5.3 Template synthesis method 11

1.5.4 Zeolite synthesis method 13

1.6 Cationic Exchange in Zeolites 15

1.7 Phthalocyanine Complexes – A Brief Review 17

1.8 Characterization of Encapsulated Transition Metal Complexes 18

1.8.1 Chemical analysis 18

1.8.2 X-ray diffraction studies 19

1.8.3 Sorption techniques 19

1.8.4 Thermal analysis 19

1.8.5 Infrared spectroscopy 20

1.8.6 UV-Visible spectroscopy 20

1.8.7 Electron Paramagnetic Resonance (EPR) spectroscopy 21

1.9 Objective of the Thesis 21

1.10 Plan of the Thesis 22

1.11 References 25

2. EXPERIMENTAL

2.1 Preparation of Cu(II) Exchanged NaY Samples 31

2.2	Synthesis of Zeolite-Y Encapsulated Copper Phthalocyanine Complex	31
2.3	Purification of Encapsulated Complexes	33
2.4	Preparation of Back-Exchanged Encapsulated Phthalocyanine Complexes	34
2.5	Preparation of Physical Mixture	35
2.6	Preparation of Encapsulated Copper Phthalocyanine by "Zeolite Synthesis Method"	35
2.7	Preparation of Co(II) Exchanged NaY Samples	36
2.8	Synthesis of Zeolite Y Encapsulated Cobalt Phthalocyanine	37
2.9	Preparation of V Exchanged NaY Samples	37
2.10	Synthesis of Encapsulated Vanadium Phthalocyanine in Zeolite Y	38
2.11	Synthesis of ETS-10 Encapsulated Iron Phthalocyanine	38
	2.11.1 Synthesis of ETS-10	38
	2.11.2 Synthesis of iron phthalocyanine inside the cages of ETS-10	39
2.12	"Neat" Metal Complexes	39
2.13	Physicochemical Characterization	40
	2.13.1 X-ray diffraction	40
	2.13.2 Sorption studies	40
	2.13.3 Chemical and thermal ananlyses	41
	2.13.4 Infrared spectroscopy	42
	2.13.5 Diffuse reflectance UV-Visible spectroscopy (DRUV-Vis)	42
	2.13.6 EPR spectra	43

2.14 Catalytic Activity Studies 43

2.14.1 Styrene epoxidation 43

2.14.2 Phenol hydroxylation 44

2.15 References 45

3. PHYSICOCHEMICAL CHARACTERIZATION

3.1 *Characterization and Effect of Peripheral Substitution on the Spectral and Structural Properties of "Neat" CuPc Complexes* 48

3.1.1 FT-IR spectra of substituted CuPc complexes 50

3.1.2 UV-Vis spectra of substituted CuPc complexes 53

3.1.3 EPR spectra of solid CuPc complexes 57

3.1.4 EPR spectra of substituted CuPc complexes in conc. H_2SO_4 60

3.1.5 Ground state wave function and chemical bonding 65

3.2 Characterization of Copper Phthalocyanine Complexes Encapsulated in Zeolite Y: CuPcY 69

3.2.1 X-ray diffraction 70

3.2.2 Chemical and thermal analyses of zeolite-encapsulated CuPc complexes 71

3.2.3 N_2 adsorption studies on zeolite-encapsulated CuPc complexes 73

3.2.4 FT-IR spectra of zeolite Y encapsulated CuPc 74

3.2.5 UV-Vis spectra of zeolite Y encapsulated CuPc complexes 76

3.2.6 EPR spectra of Cu exchanged NaY: CuY 78

3.2.7 EPR spectra of "neat" and encapsulated CuPc complexes 79

3.3 Characterization of Cobalt Phthalocyanine Encapsulated in Zeolite Y: CoPcY 85

3.3.1 X-ray diffraction 85

3.3.2 Chemical and thermal analyses of CoPcY 85

3.3.3 N_2 adsorption studies 87

3.3.4 *FT-IR spectra of "neat" and encapsulated CoPc complexes* 88

3.3.5 UV-Vis spectra of "neat" CoPc and CoPcY samples 90

3.3.6 EPR spectra of "neat" and encapsulated CoPc complexes 91

3.4 Characterization of Vanadium Phthalocyanine Encapsulated in Zeolite Y: VPcY 96

3.4.1 X-ray diffraction 96

3.4.2 Chemical and thermal analyses of VPcY samples 96

3.4.3 N_2 adsorption studies 98

3.4.4 *FT-IR spectra of VPcY samples* 99

3.4.5 DRUV-Vis spectra of VPcY samples 99

3.4.6 EPR studies on VPcY samples 100

3.5 Characterization of Iron Phthalocyanine Encapsulated in ETS-10: FePc-ETS-10 103

3.5.1 X-ray diffraction of FePc-ETS-10 103

3.5.2 *Thermal analysis of FePc-ETS-10 samples* 104

3.5.3 FT-IR spectra of FePc-ETS-10 samples 106
3.5.4 MAS-NMR studies of FePc-ETS-10 samples 107
3.5.5 SEM of FePc-ETS-10 108
3.5.6 Sorption studies of FePc-ETS-10 samples 109
3.5.7 EPR of FePc-ETS-10 samples 110
3.6 Characterization of Copper(II)hexadecachlorophthalocyanine ($CuCl_{16}Pc$) Encapsulated in Zeolite X 111
3.6.1 X-ray diffraction of $CuCl_{16}PcX$ 112
3.6.2 N_2 and n-hexane adsorption studies of $CuCl_{16}PcX$ 113
3.6.3 FT-IR spectra of $CuCl_{16}PcX$ 113
3.6.4 DRUV-Vis spectra of $CuCl_{16}PcX$ 113
3.6.5 EPR spectra of $CuCl_{16}PcX$ 114
3.7 Molecular Modeling Studies 115
3.8 Conclusion 118
3.9 References 119
4. CATALYTIC PROPERTIES
4.1 Oxidation of Styrene over CuPc and CuPcY Catalysts 121
4.1.1 Epoxidation using "neat" CuPc complexes 123
4.1.2 Epoxidation using encapsulated CuPc complex 124
4.1.2.1 Comparison of catalysts 124
4.1.2.2 Influence of reaction time on styrene epoxidation 126
4.1.2.3 Influence of temperature on styrene epoxidation over encapsulated CuPc 128
4.1.2.4 Influence of solvent on styrene epoxidation 129

4.1.2.5 Influence of styrene : TBHP mole ratio 130

4.2 Hydroxylation of Phenol over MPcY Catalysts (M = Cu, Co, V) 132

4.2.1 Hydroxylation of phenol over CuPcY catalysts 133

4.2.2 Hydroxylation of phenol over CoPcY catalysts 139

4.2.3 Hydroxylation of phenol over VPcY catalysts 145

4.2.4 Comaparitive study of CuPcY, CoPcY and VPcY catalysts in phenol hydroxylation 150

4.3 Conclusions 152

4.4 References 153

5. SUMMARY AND CONCLUSIONS 157

5.1 References 159

CHAPTER 1
INTRODUCTION

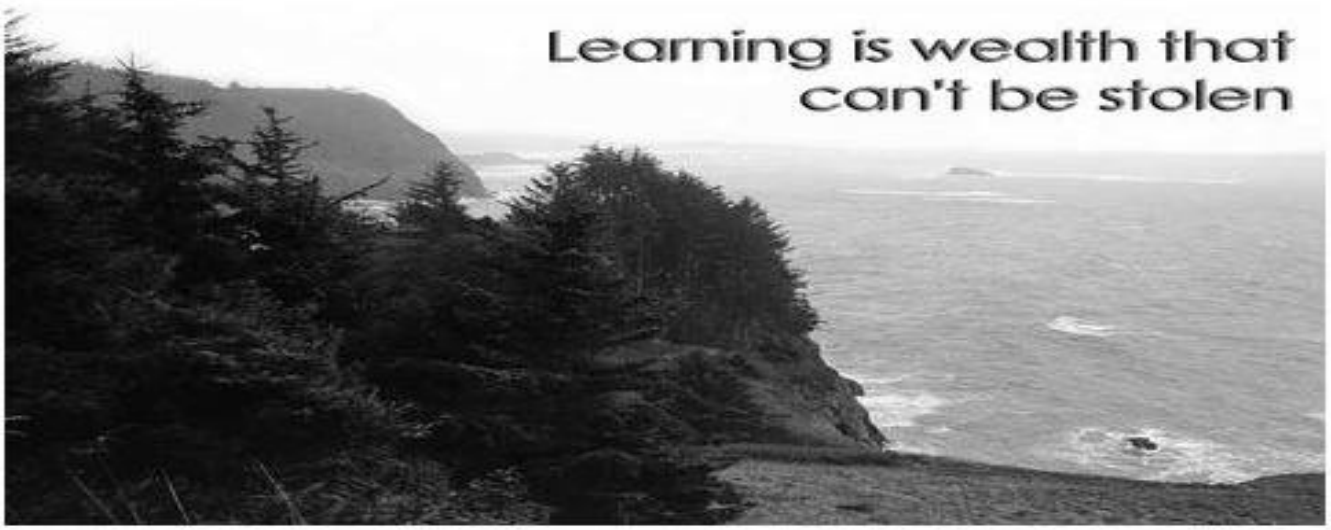

1.1 Generalities

Enzymes are proteins with complex three-dimensional folded structures and are often associated with co-enzymes or other prosthetic groups which may contain metal ions as active sites for biochemical reactions. The difficult chemical transformations, essential to life processes, performed by nature, have long been admired by synthetic chemists. After millions of years of biological evolution enzymes have grown into almost perfect catalysts which are able to catalyze a wide variety of reactions with very high selectivity, under mild conditions. By a judicious choice of enzymes nature performs complex tasks such as reversible oxygen binding (by haemoglobin, myoglobin, tyrosinase) [1,2], selective partial oxidation of unactivated hydrocarbons (Cytochrome P-450, ω-hydroxylase) [3,4], and electron transport (by ferridoxins) [5]. The rate of enzyme catalyzed reactions is often 10^9-10^{12} times higher than the non-enzymatic processes. However, the disadvantages of enzyme catalysts in practical use are their high cost, poor applicability to substrates not occuring in nature, difficulty in manipulation and restricted working conditions which are necessarry for an optimal performance. Their activity is strongly influenced by parameters such as pH, temperature, ionic strength of the reaction medium, pressure, various types of inhibitors, solvent properties etc. Small changes in these parameters change significantly their catalytic activity [6].

Industry widely makes use of heterogeneous inorganic catalysts. Unfortunately, compared to the enzymatic catalysts, heterogeneous inorganic catalysts generally have lower selectivities. As growing environmental concern forces chemists to prepare cleaner and more selective catalysts, semi-organic or completely inorganic mimics of enzymes

should be appropriate as these hybrid – catalysts should in principle possess the high stability of heterogeneous catalysts and the excellent selectivity of enzymes.

Oxidation reactions of organic substrates generally occur with rather low selectivities. The O_2 molecule has a strong double bond and has a triplet ground state, whereas the organic substrates are in a singlet state [7]. The differences in the electronic states can be overcome by using transition metals as catalysts. Even then it is difficult to avoid the formation of free organic radicals which causes an appreciable loss in selectivity. Fortunately, nature has developed enzymatic catalysts which are capable of overcoming these difficulties. An important oxygenase enzyme is Cytochrome P-450 [8] which catalyzes a large number of oxidations.

1.2 Zeolites and Molecular Sieves

Zeolites belong to a family of microporous metal oxides commonly referred to as molecular sieves [9]. These crystalline materials are characterized by well defined pore systems that are composed of channels or cage-like structures. Zeolites are attractive materials as catalyst supports because of their high surface area and stability as well as the shape selectivity that arises from their uniform pore dimensions. Their microporosity also provides the means for physically trapping of guest molecules as opposed to external surface attachment.

The most popular zeolite phase employed in host/guest studies is the synthetic Faujasite (FAU), more commonly known as X and Y type zeolites. The FAU topology involves a three dimensional channel system that opens up to larger cages. Fig. 1.1 illustrates this large cavity or supercage (~ 12 Å in diameter) as well as the restricted

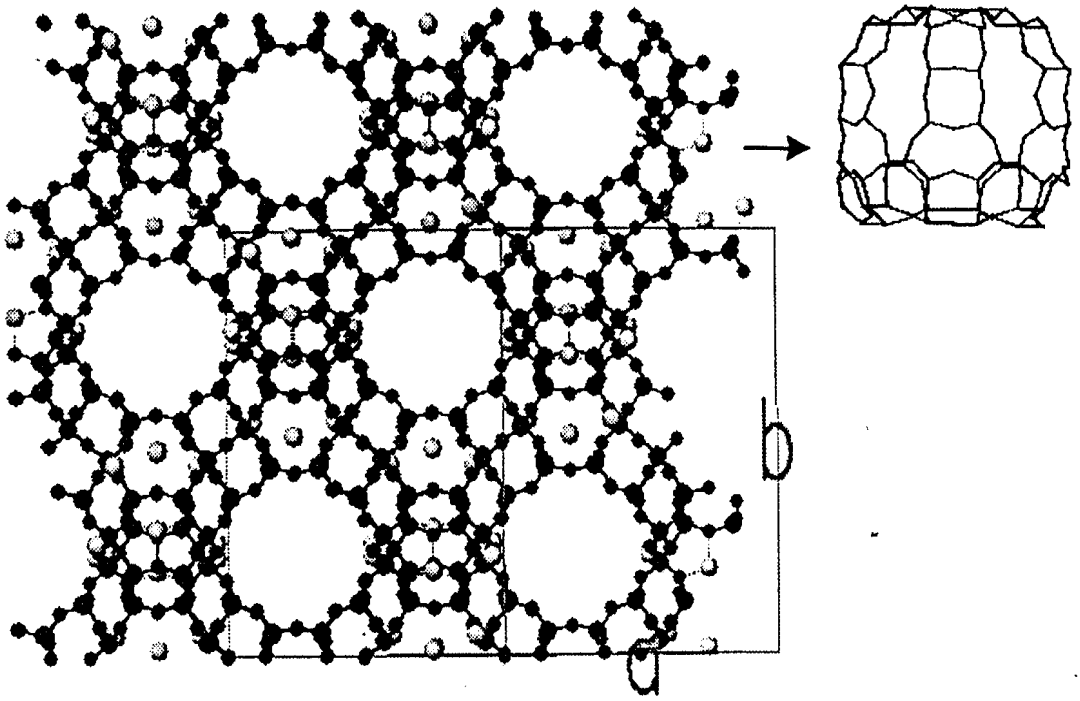

Fig. 1.1 View of NaY along 110 direction illustrating the 7.4 Å channels. A separate view of the supercage can be obtained by 45º rotation [10].

aperatures defined by the 12 membered rings (~ 7.4 Å). One could envision how a guest molecule effectively larger than the supercage windows but small enough to fit inside could be physically trapped but free to move within the confines of the cavity.

Zeolites have crystalline open frame work structures constructed of SiO_4 and AlO_4 tetrahedra linked through oxygen bridges [11,12]. The open framework has pores and cavities of molecular dimensions (3-13 Å) that selects only those molecules with proper size and shape to pass through, hence their common name molecular sieves. They also orient those molecules (based on their physical dimensions) as they gain access to the internal voids of the crystallite.

Zeolites are natural or synthetic crystalline aluminosilicates with a 3-dimensional microporous framework made up of corner sharing of SiO_4 and AlO_4 tetrahedra [11]. The formal isomorphous substitution of Si^{4+} by Al^{3+} in the silicate lattice creates an excess negative charge which is compensated by exchangeable cations. Therefore, zeolites are marked for their ion exchange properties [12]. A general formula for aluminosilicates can be written as:

$$M_{x/n}{}^{n+}[(AlO_2^-)_x(SiO_2)_y].\,zH_2O,$$

where 'n' is the valency of the charge compensating cation M; x assumes values between 0 and 0.5. According to the Lowenstein rule, the ratio x/y is smaller than or equal to 1 [11]. The individual silicon and aluminium tetrahedra (TO_4) are always close to regular, but the shared oxygen linkage can accommodate T-O-T angles from 130-180°. The tetrahedra can be combined to form a variety of frame work structures. Zeolites with different frame work topology have pores which vary in size, shape and dimensionality. The aperature of the pores range from 0.4 to 8 nm, depending on the number of tetrahedra constituting these rings. The pore geometry of the zeolites forms the basis of their molecular sieving properties. Molecules with dimensions exceeding those of zeolite aperatures are excluded from the void volume.

Now-a-days the traditional aluminosilicate zeolites are widely used as heterogeneous catalysts in petroleum and petrochemical industries as well as in environmental pollution control [13]. Their applications are based on the Brönsted acidity of the zeolites and involve hydrocarbons as feed molecules. Brönsted acidity is provided by protons acting as charge compensating cations. By far the most important

use of zeolite catalysts is the application of Ultra Stable Y zeolites in catalytic cracking (more than 300,000 ton of USY-zeolite were used in 1987).

ETS-10 is a novel large-pore titanosilicate with a framework consisting of "TiO_2" rods which run in two orthogonal directions, surrounded by tetrahedral silicate units [14]. The pore structure consists of 12-rings, 7-rings, 5-rings and 3-rings and has a

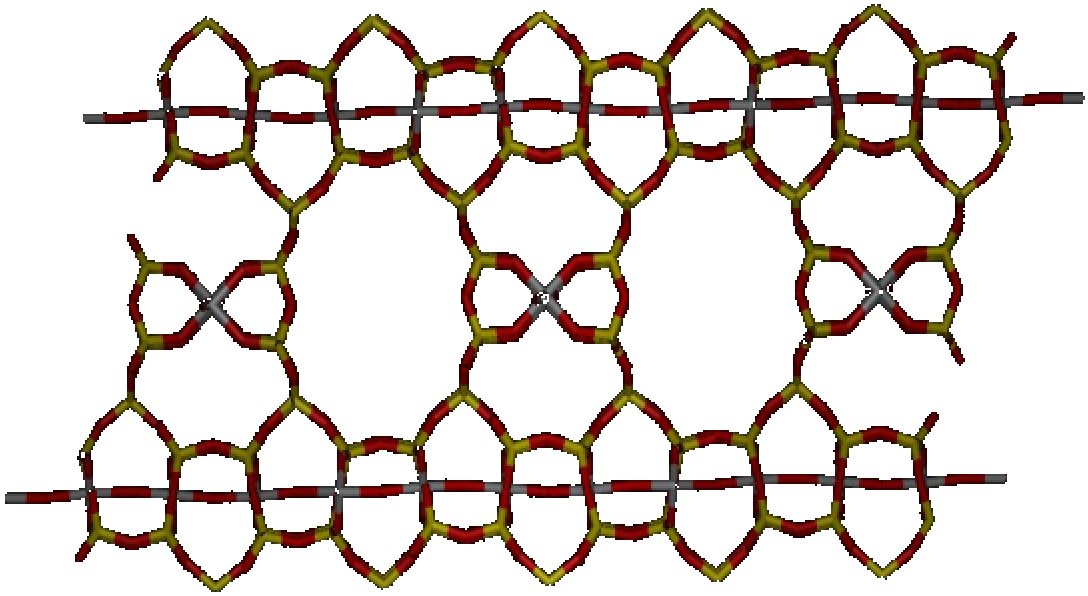

Fig. 1.2 Framework structure of ETS-10 molecular sieve viewed from the 110 plane direction

three-dimensional large-pore channel system whose minimum diameter is defined by 12-ring apertures. The structure contains often some disorders arising from structural faulting along planes parallel to the 12-ring channel directions, and it is possible to describe the structure in terms of an intergrowth of two ordered polymorphs with tetragonal and monoclinic symmetry, respectively (Fig. 1.2). Since ETS-10 contains corner-sharing SiO_4 tetrahedra, for every framework titanium there is an associated

charge of –2. This charge is compensated by extra-framework cations, usually Na^+ and K^+.

Molecular sieves, can act also as hosts for organometallic compounds. In these systems, the complexes will be the active sites and the molecular sieves may be responsible for shape and size selective properties. These supramolecular catalysts resemble enzymes, which consist of a protein mantle and a prosthetic group as the active site [15].

1.3 Heterogenization of Homogeneous Catalysts

Even though the oxidation and hydroxylation of organic compounds using molecular dioxygen is of wide spread occurrence in nature, such processes are not in common practice either in the laboratory or in the industry. Some of the extensively studied systems for the oxidation and hydroxylation of aromatic compounds are the Fenton's reagent (Fe^{2+}- H_2O_2) [16], peracids (R-COOOH $\prod$ RCO_2^- + OH^+), trifluoroacetic acid [17], the Hamilton–Friedman reagent (Fe^{3+}-H_2O_2- Catechol) [18], the Udenfriend reagent (Fe^{2+}-EDTA-ascorbic acid-O_2) [19] and the Cu^{2+}-O_2-morpholine system. All these systems are homogeneous in nature.

The heterogenising of homogeneous catalysts is an active area of research [17-19]. The term heterogenerising refers to a process whereby a homogeneous transition metal complex is immobilized, anchored, incorporated or encapsulated in an inert polymer or inorganic support. These heterogeneous catalysts have several advantages over their homogeneous analogues in (i) fixed-bed and continuous flow through operations, (ii) complete separation of the reaction mixture (products and reactants) from the catalyst, (iii) commercial utility on a large scale owing to the economic debits of

batch type operation and expense of catalyst recovery and recycle, (iv) in maintaining high selectivities of their homogeneous counterparts for many reactions, and (v) preventing dimerization and aggregate formation of the catalyst complex which normally occurs in solution.

Workers from Du-pont were among the early pioneers to exploit the chemistry of natural enzymes [20]. They adopted the strategies of natural enzymes and applied them to the rational design of zeolite based catalysts as both mimics of natural enzymes and for processes of industrial interest [21]. In an attempt to prepare analogs of haemoglobin and myoglobin [22,23] which reversibly bind O_2, cobalt salen complexes were encapsulated in the supercages of zeolite Y [24]. Such encapsulated complexes formed adducts with dioxygen which were more stable than those formed by the same complexes in free solution [17]. In a similar attempt to prepare analogs of Cytochrome P-450, the iron phthalocyanine encapsulated in zeolite Y exhibited remarkable substrate and regioselectivity in the oxidation of unactivated alkanes with molecular oxygen [21-25]. Recently Jacobs et al. [26] have reported a composite catalytic system that achieves realistic mimicry of Cytochrome P-450 by incorporating FePc complex in crystals of zeolite Y, which are in turn embedded in a polydimethylsiloxane membrane. This system oxidizes cyclohexane at room temperature at rates comparable to those of the enzymes.

Selective oxidation of aromatic substrates using solid catalysts, preferably at near ambient conditions and using clean oxidants like O_2 or H_2O_2, is a research area of growing importance in recent years. However, extensive studies have been reported on selective oxidation of organic compounds using singlet oxygen sources such as H_2O_2 and *tert*-butyl hydroperoxide (TBHP) as the oxidants [26, 27]. Since the early work, only a

few studies have been reported on the activation of molecular oxygen by metal complexes (mostly of Fe with ligands such as porphyrins, phthalocyanines and salens) encapsulated in molecular sieves [28-32].

The environment around the metal centre and the conformational flexibility of the protein mantle are the key factors for a metalloprotein to carry out a specific physiological function, for example, dioxygen binding by haemoglobin and myoglobin and oxygen utilization by Cytochrome P-450. Fine tuning of electronic structure by electron withdrawing or donating substituents [33-35] enhances the stability of ligand towards oxidation and improves the catalytic activiy of the complexes.

1.4 Transition Metal Complexes Encapsulated in Zeolites

The potential for coupling the shape selectivity associated with the well-defined channels and cages of zeolites with the reactivity of metal complexes makes these molecular sieves particularly attractive as solid supports. Zeolites have a distinct advantage over conventional support materials in that a metal complex can be physically trapped in the pores and not necessarily bound to the oxide surface. A metal complex of appropriate dimensions might be encapsulatd in a zeolite and yet be free to move within the confines of a cage or channel. This could be viewed as a bridge between a homogeneous and heterogenous system. Herron et al. [24] have referred to such zeolite guest molecules as *ship-in-a-bottle* complexes.

One of the goals of catalysis researchers in recent times has been the synthesis of inorganic mimics of enzymes such as cytochrome P-450. Romanovsky et al. [36-37] were the first to report the synthesis of a metal phthalocyanine inside zeolite NaY in 1977. In the past two decades, the zeolite encapsulated metal complexes have captured the

attention of several groups around the world. The primary interest has been in the development of shape selective catalysts, especially for oxidations. Metal complexes containing salen, porphyrin and phthalocyanine ligands have been the typical active centers used in many studies on the subject [38-42]. Though many porous materials have been used, the most popular ones have been zeolites X and Y possessing large α-cages (~ 12 Å diameter.).

Owing to their large size, (10-14 Å), metal-Schiff-base, porphyrin and phthalocyanine complexes cannot be encapsulated by direct exchange processes in conventional zeolites with channel dimensions between 4–8 Å. Over the years, many methods have been developed for the encapsulation of metal complexes inside zeolite cages. In the following section, the synthetic strategies of metal complex encapsulation are reviewed briefly.

1.5 Methods of Metal Complex Encapsulation in Zeolites

There are four general strategies for the encapsulation of metal complexes in molecular sieves [43]:

(i) the *in situ* preparation method,

(ii) the flexible ligand method,

(iii) the template synthesis method, and

(iv) the zeolite synthesis method.

The encapsulation methods that involve preparing a complex inside a zeolite are limited by the ability of the reagents to diffuse into the crystalline molecular sieve. Zeolites such as Na-A, which have a large cavity (11.9 Å in diameter) but openings that are only 4.1 Å, can not be modified with most ligands or ligand precursors because of the

size restrictions of the cage windows. However, the zeolite can be synthesized around the metal complex, in these cases. For successful encapsulation, the metal complex must meet the requirement of stability under the conditions of crystallization. But this is often not a major restriction since zeolites/molecular sieves can be synthesized under many conditions that include low pH fluoride synthesis, high pH hydroxide mediated synthesis, and crystallization from non-aqueous solvents. The zeolite synthesis approach has been employed to encapsulate metal complexes in a variety of molecular sieves ranging from the small pore clathrasils to the large pore FAU-type zeolites.

1.5.1 *In situ* preparation of metal complexes

This method is employed in the encapsulation of complexes like metal carbonyl clusters [44] of nuclearity greater than three in FAU type zeolites. In this method, the metal ion exchanged Y type zeolite is interacted with CO/H_2 or CO/H_2O to form the encapsulated metal carbonyl cluster. The presence of H_2 or H_2O is necessary for the formation of clusters by the reductive carboxylation of intrazeolite metal ions. Cationic complexes could be easily encapsulated within the supercages of FAU type zeolites.

1.5.2 Flexible ligand synthesis method

The flexible ligand method involves the diffusion of the ligands into the zeolite pores, where, upon complexation with the metal ion, a metal complex is formed. The dimensions of the metal complex are larger than the dimension of the aperture and hence it can not exit. This approach is well suited for the encapsulation of metal-Schiff-base complexes (e.g. Salen complexes) since this ligand offers the desired flexibility. The ligand should have a sufficiently low melting or sublimation point and should be small enough to enter the zeolite cavities. The void volume in the zeolite is filled

homogeneously with the ligand molecule and these form a complex with the cation on heating. The complexes are sterically constrained in the supercages. The flexible ligand method requires ligands of such dimensions that intrazeolite complexation precludes diffusion back out of the zeolite. This imposes severe limitations on the number and type of ligands that might be employed. Additionally, the intrazeolite complexation may occur from the outer parts of the crystal to the inner parts. One would anticipate a heterogeneous distribution of complexes as a consequence of pore blockage. Nevertheless, this approach is probably the easiest in practice. The disadvantage of this method is that it is difficult to control metal speciation; the zeolite often remains in the primary coordination sphere of the transition metal ion. A wide variety of cobalt [23, 45], iron [46], rhodium [47], ruthenium [48], manganese [49] and palladium [50] Schiff base complexes have been encapsulated according to this method within the supercages of faujasites.

1.5.3 Template synthesis method

Metallophthalocyanines and related complexes can be prepared from a variety of reagents but a common mechanism appears to involve the metal ion acting as a template around which the Pc ligand precursors condense [51]. It was first proposed by Romanovsky et al. that this template synthesis could be performed within the confines of a zeolite cavity [36,37]. The template synthesis method involves the diffusion of multidentate ligand into the zeolite pores where, upon complexation with a metal ion, it becomes too large to exit. This method has been successful only for phthalocyanines. The Pc ligand precursors must be able to freely enter the zeolite such that the diffusion of reagents much wider than a benzene ring (6 Å) might be hindered by the 7.4 Å openings.

Therefore, dicyanobenzene (DCB) has been the reagent of choice for the preparation of intrazeolite metal phthalocyanine (MPc) complexes. However, it is possible that other, yet to be studied, Pc ligand precursors will also work. A typical template synthesis involves the reaction of a metal ion exchanged NaX or Y zeolite with an excess of DCB at elevated temperatures (323-573 K), where the DCB is dissolved in a high boiling solvent or melted. Alternatively, the DCB can be sublimed over the metal containing zeolite at high temperature and reduced pressure. Fig. 1.3 shows a representation of 4 DCB molecules positioned near the openings to a FAU supercage with a metal ion near the center of the cavity. Although, this is an acceptable intrazeolite cation position, the ions are mobile and there are more stable locations that include smaller cages which are inaccessible to DCB. Ligation of the metal ion can force the complex to sit in the supercage because of size constraints rendering the metal more accessible to DCB. Once DCB molecules begin to condense around the intrazeolite metal ion (Fig. 1.3), two reducing equivalents are required to form the Pc ligand. This approach which has been sucessful only for phthalocyanines is also called as *in situ* ligand synthesis method by some workers [12].

The synthesis of zeolite encapsulated phthalocyanine complexes of Cu [52], Co [36,37,52], Fe [32,53], Ni [36,54], Ru [53,55], Rh [55], Os [53,56], perhalogenated-phthalocyanines [57,58], t-butyl-phthalocyanines [59], cobalt porphyrin [60], Mn [61], Ti [61] and H_2Pc [61], nitrophthalocyanines [61], Fe and Mn tetramethylporphyrins [27,62] as well as tetraphenyl porphyrin complexes [63] by the above method has been reported. Even though there are reports on the encapsulation of Fe and Mn tetramethyl and

tetraphenyl porphyrins in zeolite Y by the above method, no convincing data on intrazeolite formation of these complexes are available.

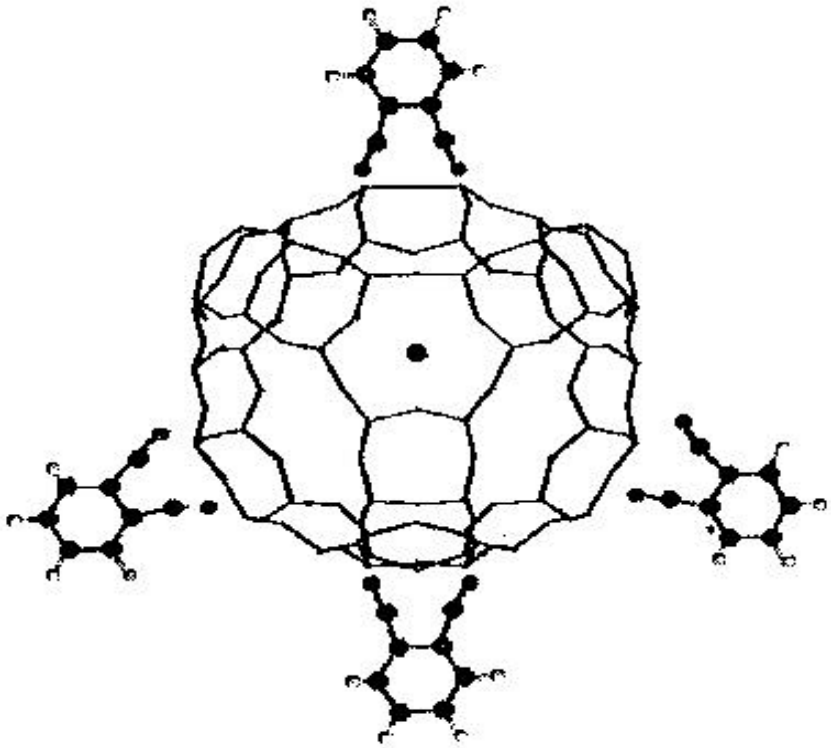

Fig. 1.3 The "template synthesis" of MPc inside the supercage of X or Y type zeolite involves the reaction of four DCB molecules with an intrazeolite metal ion or complex [10].

1.5.4 Zeolite synthesis method

The limitations and disadvantages associated with the flexible ligand and template synthesis methods for encapsulating metal complexes in zeolites have led to this method in which a zeolite is crystallized around a metal complex, i.e., building the bottle around the ship. This has the advantges of encapsulating a well defined intrazeolite complex

without contamination from free ligand as well as uncomplexed and partially complexed metal ions. This method is not applicable to those complexes that are not stable during zeolite synthesis. Besides, large ligands such as phthalocyanines (13 Å diameter) may be far larger than the intra crystalline voids of many zeolites..

Fig. 1.4 shows a representation of the encapsulation process during synthesis, where the MPc complex is mixed with silica, alumina, NaOH and water to form a gel which is then heated to ~373 K to crystallise the zeolite. The gel is composed of silicate and aluminate species that interact with the MPc complexes in such a manner that a portion of the complexes becomes incorporated into the NaX crystals. However, if the metal complex is added to the aluminate solution or aluminophosphate gel, a heterogeneous mixture results and there is virtually no encapsulation in the zeolites. In a similar way metal complexes were also incorporated in ZSM-5 and mordenite [64,65]. The metal complex possibly plays the role of a template in directing the synthesis. The aggregation of the metal complexes in the aqueous synthesis medium can be overcome by careful design of the zeolite synthesis procedure. More recently, crown ethers have been employed as templates for zeolites. Although, metal complexes of the crown ethers are introduced in to the gel, it is clear that under synthesis conditions a sodium complex is formed which acts as the template.

Metal phthalocyanine [66-67] and perflurophthalocyanine [68] complexes were encapsulated in NaX during zeolite crystallization. A close examination of the gel chemistry reveals a dependence on the order of mixing, aging and crystallization time as well as the amount and type of metal phthalocyanine complex. A normal NaX synthesis requires little or no aging, whereas the metal phthalocyanines modified gels may require

aging overnight to produce highly crystalline zeolites. If the metal complexes were cationic, one might expect the encapsulation to be even more favourable. The disadvantage involved in this method is that the complex should be stable during all

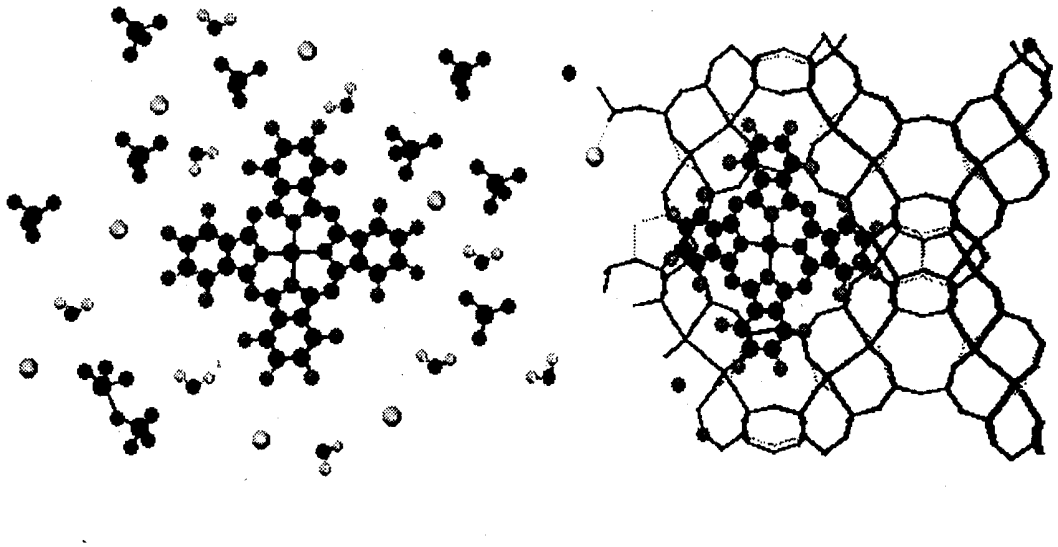

Fig. 1.4 A representation of MPc encapsulation during zeolite NaX synthesis [10].

stages of the zeolite synthesis and crystallization. Further in the case of zeolites requiring a supplementary template molecule, removal of this template may necessitate calcination which may also damage the complex during the process.

1.6 Cationic Exchange in Zeolites

The importance of molecular sieves has grown during the past 3-4 decades. Molecular sieves have become of great importance, especially in the petroleum industry as selective absorbents and catalysts [69,70]. In both these applications the properties of the molecular sieves depend on the cations present and on their distribution. Zeolite Y has a lower Al : Si ratio than X and therefore requires fewer cations to compensate for the Al atoms. The factors influencing the cation distribution are as follows: **(i)** The alumino-

silicate framework has a strongly electronegative character. **(ii)** The negative charge on the framework is lower in Y than in X; approximately 56 univalent ions per unit cell are

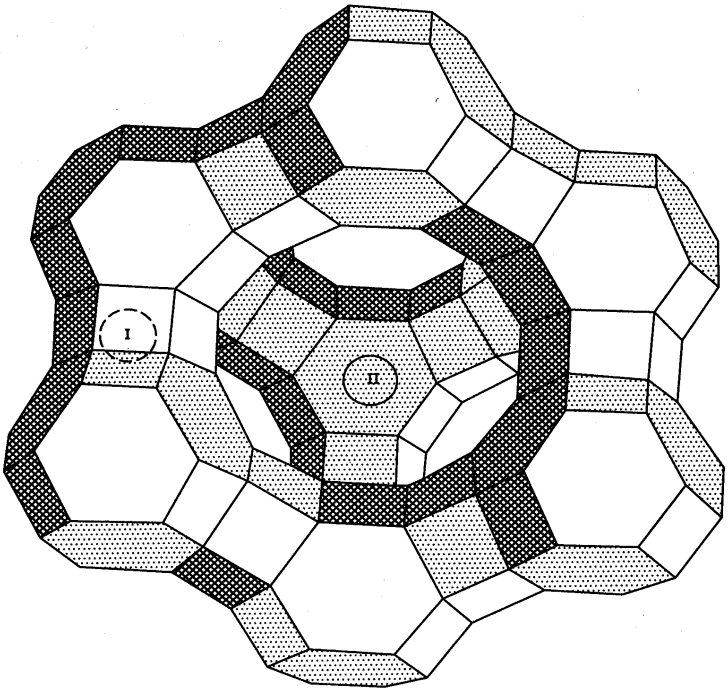

Fig. 1.5 A perspective view of a part of the faujasite structure. Aluminium atoms lie on the corners, oxygen atoms near the edges. Type I and II sites are indicated.

required for compensation in Y and 86 in X. **(iii)** The aluminium distribution is necessarily non-uniform and this must cause local variations in charge density. **(iv)** Cation sites exist at points where the framework oxygen atoms provide the highest coordination. Cations may also occupy the hydrated region in the large cages. **(v)** A lower number of cations is required when the cation charge is greater than one. Moreover, local charge compensation is difficult for these ions if the negative charge density on the

framework is low. **(vi)** Cations of high field strength are more stable in polarizable sites relative to other sites.

Cationic transition metal complexes can be encapsulated by direct ion exchange with the counter ions balancing the negative charge of AlO_4 tetrahedra of the zeolite framework. It is an essential condition that the complex is stable and sufficiently small to pass through the pore zeolite openings of the zeolite [71].

1.7 Phthalocyanine Complexes – A Brief Review

The analogy to porphyrins makes the understanding of the chemical and physical behaviour of phthalocyanines (Pc) especially important in the long-term investigation of natural life processes. The molecular structure of phthalocyanine ligand is shown in Fig. 1.6. The two central hydrogen atoms in the structure are replaceable by a wide range of metals and metalloids.

The compounds so obtained are usually insoluble in common solvents, but have some slight solubility in higher boiling aromatic solvents such as quinoline, chlorobenzene, pyridine and chloronaphthalene. Many of them sublime at high temperatures and may often be purified by sublimation. However, not all phthalocyanines sublime; recrystallization from chlorobenzene, quinoline, or chloronaphthalene may then be employed. Certain more slouble phthalocyanines may be Soxhlet-extracted with lower boiling solvents such as acetone or alcohol. The complexes are all intensely coloured – purple, blue or green compounds with a beautiful red reflex. Most of them are thermally very stable and many will sublime unchanged at 673 $K/10^{-6}$ mm. Copper phthalocyanine has been shown [72] to be stable even at 1173 K in *vacuo*. The phthalocyanines often exist in two or more polymorphic modifications, which may be

distinguished by IR and X-ray diffraction techniques. Although phthalocyanines in which the central metal ion has an oxidation state of +2 are the most common, complexes are known in all oxidation states from 0 to +6 [73].

1.8 Characterization of Encapsulated Transition Metal Complexes

One of the major objectives of the study on the characterization of intrazeolite transition metal complexes is to confirm that the complex is located inside the cavities of the zeolite and not on its external surface. Eventhough the external surface area of zeolites may be several orders of magnitude lower than its internal surface area, the small amount of transition metal complexes adsorbed on the external surface, may give a disproportionately higher contribution to the catalytic activity of the material. Hence, it is essential to ensure that the complex located on the external surface is completely removed. This is especially important in the case of zeolites containing very low loadings of metal complexes. A variety of techniques have been used to characterize intrazeolite complexes [24]. The complexes were characterized by elemental (C / N) analysis, X-ray diffraction studies, thermal and gravimetric analysis, N_2 adsorption studies, FT-IR, diffuse reflectance UV-Visible and EPR spectroscopic techniques.

1.8.1 Chemical analysis

Chemical analysis includes elemental analysis of carbon, nitrogen and hydrogen as well as that of the transition elements. In addition to techniques like X-ray fluorescence and EDAX it is also preferable to carry out the chemical analysis after digestion of the zeolite. It is important to note that in the case of those methods (other than "zeolite synthesis" method) wherein the complexation may not be quantitative,

elemental analysis does not necessarily reflect the amount of the transition metal in the complex formed. Part of the ligands or metal may remain in the uncomplexed state.

1.8.2 X-ray diffraction studies

X-ray powder diffraction is an indispensable technique for phase identification and purity. XRD also provides valuable information on crystallinity as well as any change in unit cell parameters that might arise from intrazeolite *ship-in-a-bottle* complexes.

The encapsulated metal phthalocyanine complexes, have never shown an expansion of X or Y zeolite unit cell in spite of the fact that the complex has a tight fit inside the supercages [55,57,58,73,74].

1.8.3 Sorption techniques

Sorption experimets can provide direct evidence for the presence of the complex inside the zeolite cavities and not merely on the external surface of the crystals. The extent of pore blocking can be ascertained from the decrease in the pore volume on encapsulation of the metal complex. Sorption data can also indicate the volume of the space available for substrate molecules. The BET surface area of zeolites X and Y is drastically reduced when phthalocyanine and porphyrin complexes [32] are incorporated.

1.8.4 Thermal analysis

Differential thermal analysis (DTA) and thermogravimetric analysis (TGA) [75] have been used to characterize intrazeolite metal phthalocyanine complexes prepared by the “template method”. The amount of encapsulated metal phthalocyanine complexes can be estimated from the weight loss and is generally more accurate than the spectrometric method of analysis. The encapsulated complexes generally decompose at a

higher temperature than the free complexes. Hence this technique can also be used to estimate the amount of complexed metal in the final catalyst.

1.8.5 Infrared spectroscopy

Infrared spectroscopy is probably the most widely applied analytical tool for the characterization of zeolite *ship-in-a-bottle* complexes. Either diffuse reflectance or transmission IR spectra can provide information on the zeolite lattice as well as the nature of guest molecules. IR spectra also provide the information on the nature of vibrations in the complex molecule. Due to the high sensitivity of the CO ligand to its environment, for example the spectra of metal carbonyl clusters have been used to confirm their intrazeolite location. Similarly, bands associated with C=N and C-O stretching modes of phthalocyanine molecules may be shifted when inside the zeolite cages due to ligand distortion or formation of hydrogen bonds with the zeolite supercages. Such shifts have been noted for several encapsulated metal carbonyl clusters [76-78]. Mid-IR spectroscopic results for intrazeolite and metal phthalocyanine, metal salen complexes have been reported [21,24,73].

1.8.6 UV-Visible spectroscopy

The diffuse relfelctance UV-Vis spectra can be useful in evaluating intrazeolite complexation as well as any structural perturbation. UV-Vis spectroscopy, usually in the diffuse reflectance mode, gives information on the electronic state of the central metal atom as well as ligand geometry in intrazeolite complexes.

Mayer et al. and Zakharov and Romanovsky [79,80] had observed that the most intense band for metal phthalocyanine complexes in zeolite occurs at 600-900 nm arising from a phthalocyanine based π-π^* transition known as Q bands. On encapsulation, the Q

bands were red shifted to higher wavelength. This shift was attributed to distortion of the planar phthalocyanine complex as a result of steric interactions within the supercages since the phthalocyanine ligand is slightly larger than the 12 Å diameter of the supercage.

1.8.7 Electron Paramagnetic Resonance (EPR) spectroscopy

EPR studies can give information on the nuclearity (monomeric or dimeric structure) of encapsulated complexes in addition to the oxidation state of the metal ion in the zeolite *ship-in-a-bottle* complexes. The structural integrity of the complexes on encapsulation can also be ascertained.

1.9 Objective of the Thesis

The present work is to study of the synthesis of metal phthalocyanine complexes encapsulated inside the α-cages of zeolites NaY by "template synthesis" method. TGA, sorption measurements and spectroscopic techniques including FT-IR, diffuse reflectance UV-Vis and EPR are to be employed to prove the encapsulation of metal complexes inside the pores of zeolites. These well characterized materials are to be studied for catalytic activity in the oxidation of styrene and hydroxylation of phenol. The catalytic activities of the encapsulated complexes and those of "neat" metal phthalocyanine complexes are to be compared. The effect of molecular confinement on the structure and activity of metal phthalocyanine complexes is to investigated. The objectives of the thesis in the present investigation are as follows:

1. To encapsuate metal phthalocyanine (MPc) complexes, (M = Cu, Co and V) inside the pores and channels of NaY and FePc inside the pores of ETS-10 molecular sieve.
2. To establish techniques to characterize the encapsulated MPc complexes and to differentiate them from adsorbed complexes.

3. To evaluate the catalytic activity of "neat" and zeolite encapsulated MPc complexes and to understand the role of molecular confinement on structure-activity relations.
4. Finally, to evaluate how closely the zeolite encapsulated metal complexes mimic the metalloenzymes and proteins.

1.10 Plan of the Thesis

The thesis is divided into five chapters including this introductory Chapter 1.

Chapter 2 describes the synthetic methodologies employed in the present work to encapsulate the metal complexes inside the pores of zeolites NaY and ETS-10 and the purification techniques adopted. The encapsulated complexes reported in this section are: copper phthalocyanine, cobalt phthalocyanine, vanadium phthalocyanine and iron phthalocyanine.

Chapter 3 deals with the physico-chemical characterization of the "neat", adsorbed and encapsulated MPc complexes. In the case of "neat" complexes , spectroscopic studies were performed both on solid samples and in conc. H_2SO_4 solutions. The complexes were characterized by elemental (C/N) analysis, atomic absorption spectroscopy (for metal ion estimation), thermogavimetric and differential thermal analysis (TGA/DTA), N_2 adsorption studies (for the determination of pore volume and surface area), FT-IR, diffuse reflectance UV-Vis and EPR spectroscopic techniques.

The metal complexes investigated are as follows:

"Neat" complexes

Copper phthalocyanine (β-form), CuPc;

Copper 4,4',4",4"'-tetraazaphthalocyanine, CutetraazaPc;

Copper phthalocyaninetetrasulfonicacid tetrasodium salt, $Cu(SO_3Na)_4Pc$;

Copper tetranitrophthalocyanine, $Cu(NO_2)_4Pc$;

Copper octachlorophthalocyanine, $CuCl_8Pc$,;

Copper hexadecachlorophthalocyanine, $CuCl_{16}Pc$;

Cobalt phthalocyanine, CoPc; and

Iron phthalocyanine, FePc.

Complexes adsorbed on zeolites

Copper phthalocyanine on Y, CuPcY(m); and

Cobalt phthalocyanine on Y, CoPcY(m).

Complexes encapsulated in zeolites

Copper phthalocyanine in Y, CuPcY;

Cobalt phthalocyanine in Y, CoPcY;

Vanadium phthalocyanine in Y, VPcY; and

Iron phthalocyanine in ETS-10, FePc-ETS-10.

Chapter 4 deals with the catalytic properties of "neat" and encapsulated complexes. The complexes were evaluated for styrene epoxidation and hydroxylation of phenol. Hydrogen peroxide and *tert*-butulhydroperoxide (TBHP) were used as oxidants. The effects of various factors like solvent, temperature, reactant to oxidant mole ratio, catalyst concentration etc. on the catalytic activity were investigated.

Chapter 5 describes the summary and conclusions. The present work demonstrates that metal phthalocyanine complexes can be encapsulated in the supercages of zeolite-Y. Spectroscopic (FT-IR, diffuse reflectance UV-Vis and EPR) studies have revealed distortion from the square planar geometry (D_{4h}) of MPc complexes to a

puckered conformation (C_{2v}). This change in molecular structure modulates the redox properties of the central metal ion and facilitates the coordination of the substrate or oxidant molecules in the axial position. Such molecular forces have also been noted at the site of the active site in metalloproteins by the surrounding protein manifold. The unusual molecular and electronic structures of the active sites in metalloproteins and zeolites are the driving forces for the enhanced selective catalytic activities. By and large, the present work demonstrates that the zeolite encapsulated complexes indeed mimic the metalloenzymes and proteins.

1.11 References

1. D. A. Robb, in R. Lontie (Ed); "*Copper Proteins and Copper Enzymes*" CRC press, Boca Raton, Florida, (1984) 207.
2. E. T. Adman, C. B. Anfinsen, J. T. Edsall, F. M. Richards and D. S. Eisenberg (Eds); " *Advances in Protein Chemistry*", Vol. 42, Academic press, New York, (1991) 45.
3. R. E. White and M. J. Coon., *Ann. Rev. Biochem*., 49 (1980) 315.
4. M. Hamburg, B. Samuelsson, I. Bjorkhem, H. Danielsson, and O. Hayaishi (Ed); " *Molecular Mechanisms of Oxygen Activation*" Academic Press, New York, (1974) 29.
5. J. C. M. Tsibris and R. D. Woody., *Coord. Chem. Rev*., 5 (1970) 417.
6. S. L. Neidleman, *Aspects of Enzyme Catalysis, Chem. Industr.*, 18 (1984) 3.
7. B. Meunier., *Bull. Chem. Soc. Fr*., (1986) 578.
8. R. W. Estabrook., *Biochem. Soc. Trans*., 18 (1990) 34.
9. R. Szostak., "*Molecular Sieves: Principles of Synthesis and Identification*", Van

Nostrand Reinfold, New York, (1989).

10. K. J. Balkus, Jr., in *"Phthalocyanines- Properties and Applications"*., Vol. 4 (1996) 85.
11. D. W. Breck, " *Zeolite Molecular Sieves*", Wiley, New York, (1974).
12. D. E. De Vos, F. Thibault-Starzyk, P. P. Knops-Gerrits, R. F. Parton and P. A. Jacobs., *Macromol. Symp*., 80 (1994) 157.
13. J. W. Ward., *Molecular Sieve Catalysts, Appl. Ind. Catal*., 3 (1984) 271.
14. M.W. Anderson, O. Terasaki, T. Ohsuna, A. Phillippou, S.P. Mackay, A. Ferreira, J. Rocha, S. Lidin, *Nature.*, 367 (1994) 347.
15. J. M. Thomas., *Advanced Catalysts*: *Interfaces in the Physical and Biological Sciences, Angew, Chem. Adv. Mater*., 101(1989) 1105.
16. F. Haber and J. Weiss., *Proc. Roy. Soc. (London) A* 147 (1934) 332.
17. J. Manassen, F. Basolo and R. E. Burwell Jr. (Eds); "*Catalysis, Progress in Research"* Plenum, New York (1973)177.
18. J. C. Bailar Jr., *Catal. Rev. Sci. Eng*., 10 (1974) 17.
19. J. P. Candlin and H. Thomas, *"Homogeneous Catalysis – II*, D. Forster and J. F. Roth (Eds) ; American Chemical Society, Washington, D. C., (1974) 212.
20. N. Herron and C. A. Tolman., *J. Am. Chem. Soc*., 109 (1987) 2837.
21. N. Herron., CHEMTECH, (1989) 542.
22. J. P. Collman, R. R. Gagne, T. R. Hallbert, J. C. Marchon and C. A. Reed., *J. Am. Chem. Soc*., 95 (1973) 7868.
23. R. D. Jones, D. A. Summerville and F. Basolo., *Chem. Rev*., 79 (1979) 139.
24. N. Herron., *Inorg. Chem*., 25 (1986) 4717.

25. D. R. Corbin and N. Herron., *J. Mol. Catal*., 86 (1994) 343.

26. R. F. Parton, I. F. J. Vankelecom, M. J. A. Casselman, C. P. Benzoukhanova, J. B. Uytterhoeven and P. A. Jacobs, *Nature*, 370 (1994) 541.

27. R. Parton, D. De Vos and P. A. Jacobs, " *Zeolite Microporous Solids : Synthesis, Structure and Reactivity*," E. G. Derouane, F. Lemos, C. Naccache and R. F. Ribeiro (Eds), Khumer Academic Publishers, London (1991) 555.

28. J. E. Lyons, P. E. Ellis, Jr. and H. K. Myers, Jr., *J. Catal*., 155 (1995) 59.

29. P. E. Ellis, Jr. and J. E. Lyons., *Coord. Chem. Rev*., 105 (1990) 181.

30. A. Zsigmond, F. Notheisz, M. Bartok and J. E. Backval., *Stud. Surf. Sci. Catal*., 78 (1993) 417.

31. E. R. Birnbaum, M. W. Grinstaff, J. A. Labinger, J. E. Bercaw and H. B. Gray., *J. Mol. Catal*., 104 (1995) L 119.

32. H. Diegruber, P. J. Plath, E. G. Schulz-Elkoff and M. Mohl., *J. Mol. Catal*., 24 (1984) 115.

33. P. P. K. Gerrits, D. De Vos and P. A. Jacobs., *Nature*, 369 (1994) 543.

34. J. E. Lyons and P. E. Ellis, Jr., *Appl. Catal*. A., 84 (1992) L 1.

35. B. B. Corden, R. S. Drago and R. P. Perito., *J. Am. Chem. Soc*., 107 (1985) 2903.

36. V. Y. Zakharov, and B. V. Romanovsky., *Sov. Mosc. Univ. Bull*., 32 (1977) 16.

37. V. Yu. Zakharov, O. M. Zakharova, B. V. Romanovsky and R. E. Mardalishvili, *React. Kinet*. *Catal. Lett*., 6 (1977) 133.

38. C. R. Jacobs, S. P. Varkey and P. Ratnasamy, *Appl. Catal. A*: General 168 (1998) 353.

39. R. Raja and P. Ratnasamy., *Stud. Surf. Sci. Catal*., 101 (1996) 181.

40. E. Armengol, A. Corma, V. Fornes, H. Garcia and J. Primo., *Appl. Catal*., 181 (1999)305.

41. K. J. Balkus, Jr., *J. Electroanal. Chem*., 345 (1993) 157.

42. Bi – Zeng Zhan and Xiao – Yuan Li., *Chem. Commun*., (1998) 349.

43. K. J. Balkus, Jr. and A. G. Gabrielov., *Journal of Inclusion Phenomena and Molecular Recognition in Chemistry*., 21 (1995) 159.

44. M. Lehikawa, *Adv. Catal*., 38 (1992) 283.

45. F. Bedioui, E. DeBoysson, J. Devynck and K. J. Balkus, Jr., *J. Chem. Soc*., *Faraday. Trans*., 87 (1991) 3831.

46. L. Gaillon, N. Sajot, F. Bedioui, J, Devynck and K. J. Balkus, Jr., *J. Electroanal. Chem. Interface. Electochem*., 345 (1993) 157.

47. K. J. Balkus, Jr., A. A. Welch and B. E. Gnade, *Zeolites*., 10 (1990) 722.

48. F. Bedioui, L. Roue, L. Gaillon, J. Devynck, S. L. Bell and K. J. Balkus., Jr., *Petrol. Preprints.*, 38 (1993) 529.

49. C. Bowers and P. K. Dutta., *J. Catal*., 122 (1990) 271.

50. S. Kowalak, R. C. Weiss and K. J. Balkus, Jr., *J. Chem. Soc., Chem. Commun*., (1991)57.

51. B. D. Berezin., *Coordination Compounds of Porphyrins and Phthalocyanines*., J. Wiley., New York (1981)

52. J. P. Ferraris, K. J. Balkus, Jr., and A. Schade., *J. Inclus. Phenom. Mole. Recog. Chem.*,14 (1992) 163.

53. B. V. Romanovsky and A. G. Gabrielov., *J. Mol. Catal*., 74 (1992) 293.

54. A. G. Gabrielov, A. N. Zakharov and B. V. Romanovsky., *Coord. Chem*., 14 (1988)

214.

55. K. J. Balkus, Jr., A. A. Welch and B. E. Gnade., *J. Inclu. Phenom. Mol. Recog. Chem*., 10 (1991)141.

56. B. V. Romanovsky and A. G. Gabrielov., *Stud. Surf. Sci. Catal*., 72 (19920 443.

57. A. G. Gabrielov, K. J. Balkus, Jr., F. Bedioui and J. Devynck., *Micropor. Mater*., 2 (1994) 119.

58. K. J. Balkus, Jr., A. G. Gabrielov, F. Bedioui and J. Devynck., *Inorg. Chem*., 33 (1994) 67.

59. M. Ichikawa, T. Kimura and A. Fukuoka., *Stud. Surf. Sci. Catal*., 60 (1991) 335.

60. X. Wang, Y. Liang, Y. Lui, L. Yu. Y. Li, F. Li and X. Cao, *Gaodeng Xuexiao*, 14 (1993) 14.

61. R. Parton, *Dissertation*, Katholick University Leuven, (1993).

62. Y. W. Chan and R. B. Wilson., *Preprint Papers-ACS, Div, Fuel. Chem*., 33 (1988) 453.

63. T. Kimura, A. Fukuoka and M. Ichikawa, *64th CATSJ Meeting* Abstr. No. 1A09. 31 (1989) 357.

64. L. A. Rankel and E. W. Valyocsik, U. S. Patent 4,500,503 (1985).

65. L. A. Rankel and E. W. Valyocsik., U. S. Patent 4,388,285 (1983).

66. K. J. Balkus, Jr., and S. Kowalak, U. S. Patent 5,167,942 (1992).

67. K. J. Balkus, Jr., S. Kowalak, K. T. Ly and C. D. Hargis., *Stud. Surf. Sci. Catal*., 69 (1991) 93.

68. A. G. Gabrielov, K. J. Balkus, Jr., F. Bedioui, and J. Devynck., *Microporous Materials*., 2 (1994) 119.

69. T. I. Bary and L. A. Lay., *J. Phys. Chem. Solids*., 29 (1968) 1395.

70. T.I. Bary and L. A. lay., *J. Phys. Chem. Solids*., 27 (1966) 1821.

71. P. Peigneur, J. H. lunsford, W. De Wilde and R. A. Schoonheydt., *J. Phys. Chem.*, 81 (1977) 1179.

72. E. A. Lawton., *J. Phys.Chem*., 62 (1958) 384.

73. N. Herron., *J. Coord. Chem*., 19 (1988) 25.

74. R. F. Parton, L. Utytterhoeven, and P. A. Jacobs., *Stud. Surf. Sci. Catal*., 59 (1991) 395.

75. Z. Jiang and Z. X. Fenzi Cuihua, 6 91992) 467., [CA 118 : 212554 (1992)]

76. L. L. Sheu, H. Knozinger, and W. M. H. Sachtler., *Catal. Lett*., 2 (1989) 129.

77. S. Kawi and B. C. Gates., *J. Chem. Soc., Chem. Commun*., 702 (1992).

78. A. De Mallmann and D. Barthomeuf., *Catal. Lett*., 5 (1990) 293.

79. G. Meyer, D. Wohrle., D. Mohl and G. Schultz- Ekloff., *Zeolites*., 4 (1984) 30.

80. A. N. Zakharov and B. V. Romanovsky., *J. Inclu. Phenom*., 3 (1985) 389.

CHAPTER 2
EXPERIMENTAL

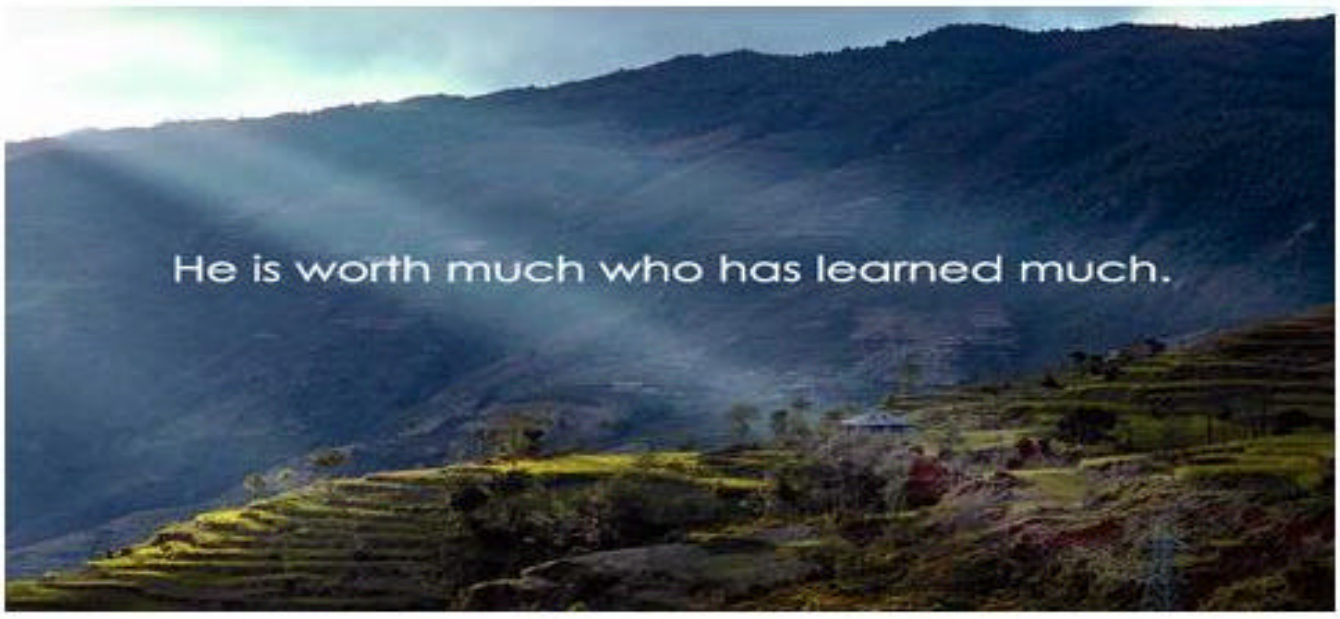

During the past 15 years much attention has been paid to the synthesis of zeolite included metal phthalocyanine complexes (MPc) and the catalytic behaviour of these systems [1-4]. Metallo-phthalocyanines in zeolites were first synthesized in 1977 by Zakharov and Romanovskii [5]. The synthesis is restricted by the rigid geometry of the intracrystalline void space of the zeolite, more specifically the dimensions of the channels and cavities and their respective pore mouths. The largest diameter of MPc complexes is ~ 1.5 nm which is very close to the supercage diameter of zeolite Y, but the apertures of 12-membered ring zeolites are only 0.7 to 0.8 nm. It is therefore not possible to synthesize MPc in zeolites by adsorption of phthalocyanine molecules. However, metal phthalocyanine complexes can be encapsulated in molecular sieves by *in situ* synthesis methods. The first *in situ* synthesis of metal phthalocyanine inside the large cages of zeolite Y was reported by Pinnavaia *et al*. [1]. After encapsulation, it is impossible to remove MPc complexes by methods other than zeolite dissolution or complete calcination. The zeolite-encapsulated metal phthalocyanine complexes are thus the true examples of "ship-in-a-bottle" systems.

This chapter describes the synthetic methodologies employed in the present work to encapsulate the MPc complexes inside the pores of zeolites NaY and ETS-10. It also describes in brief the sample purification and characterization techniques. The encapsulated complexes reported in this section are: copper phthalocyanine (CuPc), cobalt phthalocyanine (CoPc), vanadium phthalocyanine (VPc) and iron phthalocyanine (FePc).

2.1 Preparation of Cu(II) Exchanged NaY Samples

Copper exchanged NaY [CuY(0.25)] was prepared by ion exchange of zeolite NaY with Cu(II) ions. To 5 g of NaY taken in a round bottom flask was added 0.0475 g of $Cu(NO_3)_2.3H_2O$ (0.25 wt. %) dissolved in 100 ml of distilled water. The pH of the suspension was adjusted to 4.0. The reaction mixture was heated on a hot water bath for 6-8 h. Then, the solid was separated by filteration. CuY(0.25), thus prepared, was washed several times with distilled water till the washings did not contain any dissloved Cu(II) ions.

Samples of CuY(0.6) and CuY(1.2) were prepared in a similar manner except that 0.114 and 0.228 g, respectively, of $Cu(NO_3)_2.3H_2O$ dissolved in 100 ml of distilled water were used, in the preparation of samples. The colour of the Cu-exchanged zeolite was pale blue.

2.2. Synthesis of Zeolite-Y Encapsulated Copper Phthalocyanine Complex

Copper phthalocyanine (CuPc) encapsulated in zeolite Y (CuPcY) samples were prepared by the "template synthesis" method using 1,2 dicyanobenzene (DCB) [6-16]. The generalized procedure is schematically shown below.

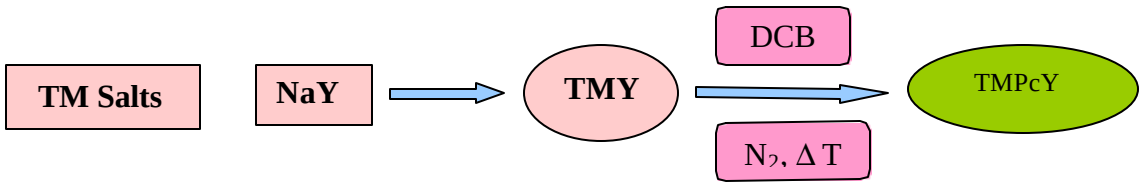

TM= transition metal; DCB = dicyanobenzene

In a typical synthesis, CuY (0.6), prepared as described above, was initially degassed for 8 h at 373 K and then exposed to DCB (2.23 g) vapours at 473 K for 24 h

under N_2 atmosphere. The synthesis was carried out in a specially made glass reactor (Fig. 2.1). The unreacted DCB, phthalocyanine and other organic matter sticking to the surface of the zeolite were removed by Soxhlet extraction (described below in detail) with different solvents till all the organic material adhering to the outer surface of the zeolite crystallites was removed. The sample thus prepared was labeled as CuPcY(0.6).

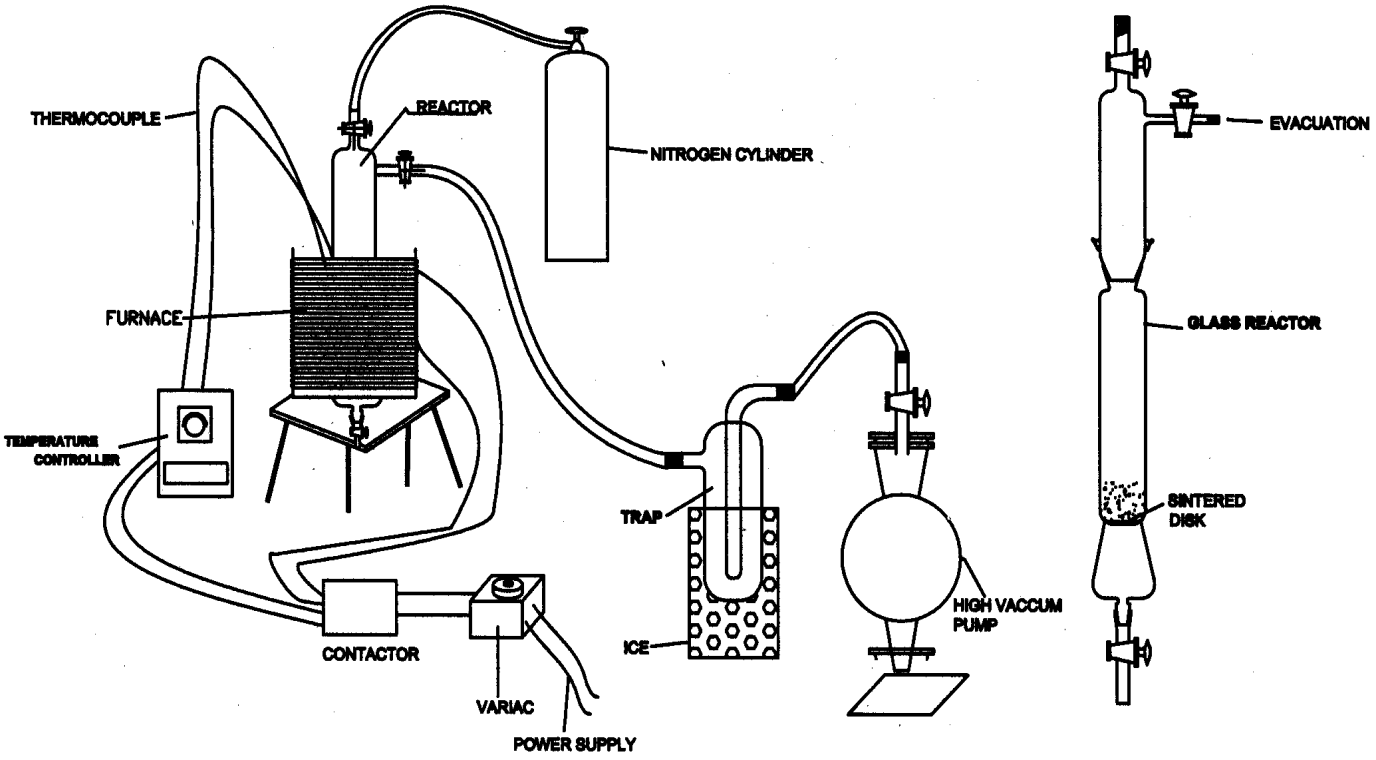

Fig. 2.1 Apparatus used in the synthesis of MPcY samples

CuPcY(1.2) was prepared in a similar manner except that CuY(1.2) was used in place of CuY(0.6). The samples were dried at 393 K in an oven for 24 h before use. The encapsulated complexes were greenish blue in colour.

2.3 Purification of Encapsulated Complexes

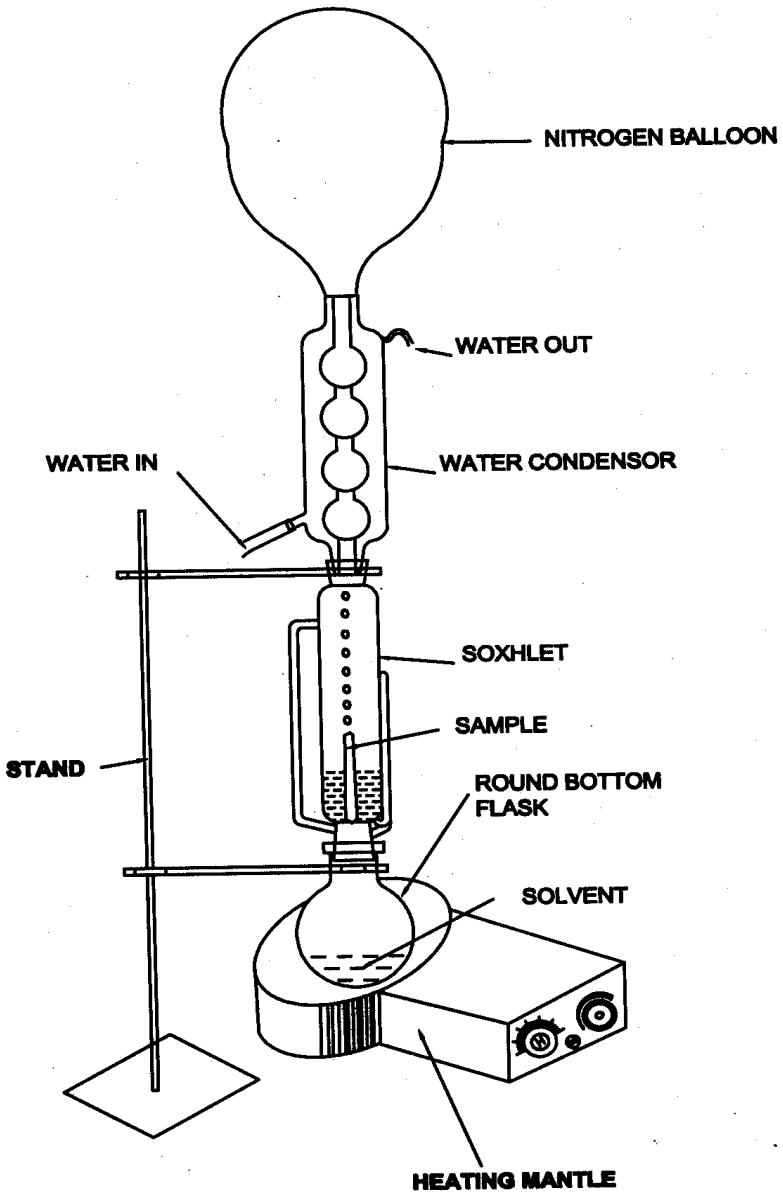

Fig. 2.2 Soxhlet apparatus used for the purification of MPcY samples

In the "template synthesis" method, in addition to the metal complex inside the pore of the zeolite, the unreacted DCB, the uncomplexed phthalocyanine and other organic matter are usually formed at the outer surface of the zeolite crystallites. These organics were removed by Soxhlet extraction with different solvents. (Fig. 2.2 shows the apparatus used for Soxhlet extraction). In this method, the sample is taken in a thimble made of Whatmann filter paper (No. 1) and was placed inside the Soxhlet apparatus. The Soxhlet apparatus was fitted with a water condenser at the top. It was attached to a round bottom flask (250 ml) containing a suitable solvent upto $3/4^{th}$ of its capacity.

The samples were initially extracted with acetone (s.d.fine chem. Ltd., India, 99.5%) for 48 h followed by pyridine (s.d.fine chem. Ltd., India, 99.0%) for 120 h; Pyridine was found to be effective in removing the surface-bound phthalocyanines. The extraction was continued till the extract became colourless. Then, the material was extracted with acetonitrile (s.d fine chem. Ltd., India, 99.0%) for 48 h to remove the residual pyridine and organics from the sample. A final extraction was done with acetone for 24 h. Then the sample was taken out from thimble and dried at 372 K for 8-10 h. The encapsulated CuPc complexes, thus purified were designated as CuPcY(n), where n refers to the metal weight percent.

2.4 Preparation of Back-Exchanged Encapsulated Phthalocyanine Complexes

Due to restrictions of void space, only the ions present in the supercages form MPc complexes while those in the sodalite cages remain uncomplexed. The uncomplexed Cu ions were removed by back exchanging of CuPcY(1.2) with $CaCl_2$.

This experiment was carried out by taking a weighed amount of the catalyst (0.5 g) and 10 ml of 1 M $CaCl_2$ solution.

0.5 g of CuPcY was taken in a round bottom flask and to that 10 ml of 1 M $CaCl_2$ solution was added. The mixture was heated to 333 K while stirring continuously for 5-6 h. After that the supernant liquid was decaned and the solid catalyst was washed thrice with deionized water. The whole procedure was repeated three times and finally the back exchanged CuPcY was dried in an air oven at 373 K for 6-8 h. The back exchanged encapsulated CuPc complex was designated as CuPcY(1.2)-Ca.

2.5 Preparation of Physical Mixture

A physical mixture of "neat" CuPc (Aldrich, USA) and zeolite Y was prepared to compare physico-chemical characteristics of the encapsulated phthalocyanine complexes with surface-adsorbed complexes. The physical mixture was prepared by thoroughly mixing 0.005 g of CuPc with 5 g zeolite NaY using a pestle and mortar. Necessary care was taken to avoid any damage to the zeolite structure while mixing. This sample was designed as CuPcY(m).

2.6 Preparation of Encapsulted Copper Phthalocyanine by "Zeolite Synthesis"

Method

As efforts to prepare perchloro CuPc using tetrachloro-1,2-dicyanobenzene by the template method were not successful, the "zeolite synthesis" method adopted by Balkus *et al*. [6] was used. A commercial sample containing sixteen peripheral Cl atoms (BASF; Heliogen green) was used. In this method, the complex was encapsulated during synthesis of zeolite X as follows:

2.4 g of NaOH (s.d.fine chem. Ltd., India; 97.0%), 3g of fumed silica (Aldrich, USA, 99.5%) and 6.0 ml of deionized water were taken in a polypropylene bottle and stirred to form a slurry. To this was added 0.225 g of $CuCl_{16}Pc$ and then the mixture was stirred till a uniform slurry was formed. A slurry containing 6.75 g aluminium isopropoxide (Aldrich USA, 98.0%), 2.4 g NaOH and 9.0 ml of distilled water was prepared seperately in another polypropylene beaker and then transferred to the slurry containing fumed silica. Then 24 ml of distilled water was added to the mixture and stirred for 24 h. The gel was then hydrothermally treated for 17 h at 373 K. The solid crystalline product was cooled, filtered and finally washed with water. Organic matter on the outer surface was removed by Soxhlet extraction using different solvents as described in the previous section. The complex was denoted as $CuCl_{16}Pc$ (ZS).

2.7 Preparation of Co(II) Exchanged NaY Samples

To 10 g of NaY taken in a round bottom flask was added 0.245 g of cobaltous acetate (s.d.fine.chem.Ltd.,India ; 99.5%) dissolved in 100 ml of distilled water. The pH of the suspension was adjusted to 4.0. The reaction mixture was heated on a hot water bath (at 373 K) for 6 h. Then, the solid was separated by filtration and washed several times with distilled water till the washings did not contain any Co(II) ions. The sample was designated as CoY(0.6).

A similar procedure described above was adopted for the preparation of CoY(1.0) and CoY(1.2) taking 0.4227 g and 0.507 g, respectively, of $(CH_3.COO)_2Co.4H_2O$ dissolved in 100 ml of distilled water.

2.8 Synthesis of Zeolite-Y Encapsulated Cobalt Phthalocyanine

Cobalt phthalocyanine (CoPc) encapsulated in zeolite Y [CoPcY(0.6)] was synthesized by ion-exchange of Co(II) ions in NaY followed by template synthesis using 1,2 dicyanobenzene (DCB) [9-16].

CoY(0.6), prepared as above, was degassed for 8 h at 373 K in vacuum and finally exposed to DCB (5.0 g) vapours at 543 K for 24 h under N_2 atmosphere inside a specially made glass reactor (Fig. 2.1). Unreacted DCB, uncomplexed phthalocyanine and other organic matters on the surface of the zeolite were removed by Soxhlet extraction with different solvents viz., acetone (48 h), pyridine (120 h), acetonitrile (48 h) and again acetone (24 h) to remove the residual pyridine. After the extraction, the sample was dried at 373 K. This sample was designated as CoPcY(0.6).

The other encapsulated CoPc samples, CoPcY(1.0) and CoPcY(1.2), were also prepared in a similar manner except that CoY(1.0) and CoY(1.2), respectively, were used in place of CoY(0.6). The final product greenish blue in colour was dried at 393 K in an oven for 24 h.

2.9 Preparation of V Exchanged NaY Samples

To 10 g of NaY taken in a round bottom flask was added 0.426 g of vanadyl sulfate trihydrate ($VOSO_4.3H_2O$; Aldrich USA) dissolved in 100 ml of distilled water. The pH of the suspension was adjusted to 4.0. The reaction mixture was heated on a hot water bath (373 K) for 6 h. Then, the solid was separated by filtration and washed several times with distilled water till the washings did not contain any V(IV) ions. The sample was designated as VY(1.0).

A similar procedure as above was adopted for the preparation of VY(1.2) and VY(1.6) except that 0.511 and 0.681 g of $VOSO_4.3H_2O$ dissolved in 100 ml of distilled water were used.

2.10 Synthesis of Encapsulated Vanadium Phthalocyanine in Zeolite Y

Vanadium phthalocyanine (VPc) encapsulated in zeolite Y [VPcY(1.0)] was synthesized by ion-exchange of V(IV) ions in NaY followed by template synthesis using 1,2 dicyanobenzene (DCB) [9-16]. VY(1.0%), prepared as above, was degassed for 8 hrs at 373 K in vacuum and finally exposed to DCB (5.0 g) vapors at 523 K for 24 h under N_2 atmosphere inside a specially designed glass reactor (Fig. 2.1). Unreacted DCB, uncomplexed phthalocyanine and other organic matters on the surface of the zeolite were removed by Soxhlet extraction with different solvents viz., acetone (48 h), pyridine (120 h), acetonitrile (48 h) and again acetone (24 h) to remove the residual pyridine. After the extraction the sample was removed and dried at 373 K. This sample is designated as VPcY(1.0).

The other encapsulated samples VPcY(1.2) and VPcY(1.6) were also prepared in a similar method except that VY(1.2) and VY(1.6) were used in place of VY(1.0). The final greenish blue products were dried at 393 K in an oven for 24 h and were designated as VPcY(1.2) and VPcY(1.6), respectively.

2.11 Synthesis of ETS-10 Encapulated Iron Phthalocyanine

2.11.1 Synthesis of ETS-10

The hydrothermal synthesis of ETS-10, using $TiCl_4$, was carried out with a gel of the following molar composition following the published procedure [17]:

$$3.70\ Na_2O : 0.95\ K_2O : TiO_2 : 5.71\ SiO_2 : 171\ H_2O$$

In a typical synthesis, a solution of 9.3 g of NaOH in 40 g of distilled water was added to a vigorously stirred solution of 52.5 g of sodium silicate (UCIL,India; 98.0%; 28.6% SiO_2, 8.82% Na_2O, 62.58% H_2O) and 40 g of distilled water. This was followed dropwise addition of 32.75 g of titanium tetrachloride ($TiCl_4$) solution (25.42 wt% $TiCl_4$, 25.92 wt% HCl, 48.6 wt% H_2O) to the colourless gel with rapid stirring. 7.8 g of potassium fluoride ($KF.2H_2O$; Loba Chemie, India 96.0%) was then added to the above gel (pH = 11.2 ± 0.1) and the mixture was stirred well. The mixture was then transferred to a stirred stainless steel autoclave (Parr Instruments, USA) and crystallization was carried out at 473 K with a stirring speed of 300 r.p.m for 14-16 h. After crystallization the products were filtered and washed with deionized water till the pH of the filtrate was about 10.7. It was dried at 373 K for 8-10 h. The product was identified as ETS-10. The yield of the sample was 85 to 90%.

2.11.2 Synthesis of iron phthalocyanine inside the cages of ETS-10

Iron phthalocyanine was encapsulated inside the pores of ETS-10 by taking 5 g of ETS-10 and 50 ml solution of 84 mg of ferrocene ($C_{10}H_{10}Fe$; >98.0%) in acetone. The solution was dried in air at 343 K and the dried products were mixed with 5 g DCB. This mixture was heated in an inert atmosphere at 453 K for 4 h. The product was then Soxhlet extracted with acetone (48 h), followed by acetonitrile (120 hrs) and again finally with acetone (24 h) to remove the unreacted DCB, Pc and other organic matter present at the external surface of ETS-10. The final product was then dried at 353 K. The sample was designed as FePc-ETS-10.

2.12 "Neat" Metal Phthalocyanine Complexes

"Neat" complexes of CuPc, $CuCl_8Pc$, $CuCl_{16}Pc$, $Cu(SO_3Na)_4Pc$, Cu tetraazaPc and $Cu(NO_3)_4Pc$ were obtained from commercial sources (Lona Industries, India and Aldrich Chemical Co., USA). The complexes were purified by sublimation or recrystallization from dichloronaphthalene.

2.13 Physicochemical Characterization

The characterization of zeolite encapsulated metal complexes generally requires a battery of techniques as detailed below to convincingly prove the intrazeolite location of metal complexes. It is necessary to remove surface species by Soxhlet extraction with a series of solvents before the following characterization techniques are used.

2.13.1 X-ray diffraction

XRD provides valuable information on crystallinity as well as changes in unit cell parameters that might arise from the *in situ* generation of intrazeolite complexes. The effect of encapsulation on the zeolite frame work was identified from X-ray powder diffraction studies (Rigaku, Model D/MAX III VC, Japan ; Ni filtered Cu-Kα radiation, λ = 1.5404 Å; graphite crystal monochromator, computer assisted automated diffractometer).

2.13.2 Sorption studies

Inclusion of MPc molecules inside the voids of molecular sieves can dramatically reduce the adsorption capacity of modified zeolites. This can be investigated by nitrogen adsorption studies. A commercial adsorption unit (Omnisorb 100CX; Coulter Corporation, USA) was used for measurements of nitrogen adsorption to determine the surface areas. The samples (approx. 300 - 400 mg) were activated at 473 K for 16 h in

high vaccum (~10^{-5}mm). After the treatment, the anhydrous weights of the samples were recorded. The samples were then cooled to 77 K using liquid nitrogen and allowed to adsorb nitrogen gas. Finally knowing the amount of N_2 adsorbed at different equilibrium pressures, the BET surface area was calculated. The anhydrous weight of the sample was used in the surface area calculation. To obtain the surface area, the results were fitted into the equation, Surface area = V_m x N x A_m, where, V_m is the monolayer volume, N is the Avagadro's number and A_m is the cross sectional area of adsorbent.

2.13.3. Chemical and thermal analyses

Chemical analyses of carbon and nitrogen were done using a Carbo Erba Elemental Analyser (EA 1108). The total Pc content was estimated from the carbon content of the samples. The amount of CuPc in CuPcY samples was estimated as follows. The sample (0.1 g) (after extraction of occulded organic material) was treated with warm conc. H_2SO_4 (2 ml) and stirred well to break down the zeolite and also dissolve the CuPc complex. The mixture was next diluted with 10 ml of ice cold water. The dissolved CuPc precipitated while the uncomplexed Cu ions went into solution. The mixture was filtered and the filtrate analysed for uncomplexed Cu. The amount of CuPc was estimated from the total Cu content and the uncomplexed Cu estimated as above. This procedure could be adopted in the case of CuPcY samples as CuPc is known to be stable in conc. H_2SO_4. This method of analysis could not be carried out in the case of CoPcY, VPcY and FePc-ETS-10 due to fear of demetallation of these complexes in conc. H_2SO_4.

Thermogravimetric and differential thermal analyses (TG/DTA) of the crystalline phase (to determine the amount of intrazeolite MPc) were performed simultaneously on

an automatic derivatograph Setaram TG-DTA 92. The thermograms of the samples were recorded under the following conditions.

Weight of the sample ~ 30 mg

Heating rate = 10 K min^{-1}

Atmosphere = flowing air

Preheated and finely powdered α-alumina was used as the reference material. Experiments were performed in the temperature range 273–1273 K. The weight loss enabled the determination of organic content as well as the thermal stability of the encapsulated complexes.

2.13.4 Infrared spectroscopy

Mid-IR spectroscopy was used to study the bands associated with the characteristic vibration modes of the Pc ligand viz., C=N and C=C stretching modes. The infrared spectra of the samples were recorded on a Nicolet 60 SXB FT-IR spectrophotometer in the wavenumber range 400-1300 cm^{-1}. The spectra were recorded for nujol mulls.

2.13.5 Diffuse reflectance UV-Vis spectroscopy (DRUV-Vis)

UV-Vis spectra of MPc modified zeolites were used to evaluate the intrazeolite complexation as well as any structural perturbations that might arise as a consequence of encapsulation. The diffuse reflectance UV-Visible spectra (DRUV-Vis) of the samples were obtained in the wavelength range 200-900 nm using a Shimadzu (Model UV-2101 PC) spectrometer. The spectra were recorded in solid state and in H_2SO_4 medium.

2.13.6 EPR spectra

EPR spectroscopy was used to investigate the state of the metal (M) in MPc encapsulated inside the zeolite. The EPR spectra of samples were recorded on a Bruker EMX spectrometer operating at X-band frequency and 100 kHz field modulation. The samples were taken in Suprasil quartz tubes of 4.5 mm o.d. The measurements at 77 K were carried out using a quartz insert dewar. Spectral manipulations and simulations were done using Bruker WINEPR and Simfonia software packages. Microwave frequency was calibrated using a frequency counter fitted in the microwave bridge (Bruker ER 041XG-D) and the magnetic field was calibrated by a ER 035M NMR gaussmeter.

2.14 Catalytic Activity Studies

The samples were tested for their catalytic activity in styrene epoxidation using TBHP as oxidant and phenol hydroxylation using H_2O_2 as oxidant. The influence of encapsulation on the activity and product selectivity in these reactions was investigated.

2.14.1 Styrene epoxidation

Styrene epoxidation was carried out in a 50 ml double necked round bottom flask fitted with a water condenser and kept in an oil bath (Fig. 2.3). Styrene (s.d. fine chem. Ltd, India, 99.0%; 4.8 mmol), acetonitrile (5 g) and tertiary-butylhydroperoxide (TBHP Aldrich, USA; 4.8 mmol) and the catalyst (0.050 g) were taken in the flask and the reaction was performed while stirring the reaction mixture for 48 h. The products were collected at different time intervals and analysed by gas chromatography (HP 5880A ; 50 m x 0.2 mm, HP1 capillary column). The catalytic studies were carried out at different temperatures, styrene to H_2O_2 mole ratios and amounts of catalysts.

2.14.2 Phenol hydroxylation

In a typical oxidation reaction, the catalyst (0.1 g) was added to phenol (C_6H_5OH) (1.0 g) in a suitable solvent, e.g. water (20 ml). Aqueous hydrogen peroxide (Merck, India; 30 wt.%; 0.5 ml) was added after the desired temperature was attained. The catalytic runs were carried out in a double necked flask (100 ml capacity) fitted with a

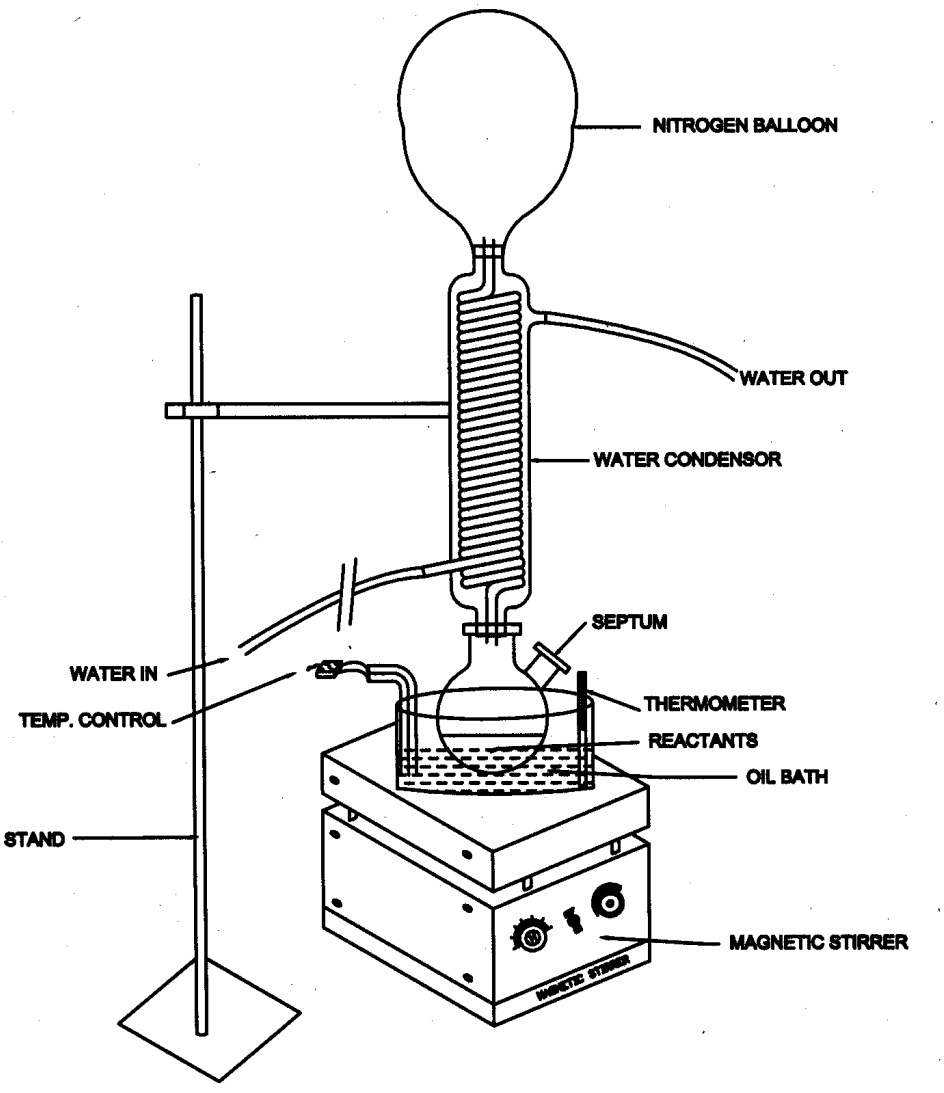

Fig. 2.3 Experimental set up for catalytic reactions

condenser (Fig. 2.3). The reaction mixture was stirred using a magnetic stirrer for 12 h. The temperature of the reaction vessel was maintained using an oil bath. Periodically, the samples were taken out at different time intervals and centrifuged to remove the solid catalyst. The products were analysed by a gas chromatograph (HP 5880 A ; FID; 50 m x 0.2 mm capillary column). Influence of temperature, catalyst concentration and other parameters on the activity and selectivity for the different products were monitored.

2.15 References

1. T. Pinnavaia, M. Tzou, S. Landau and R. Raythatha., *J. Mol. Catal*., 27 (1984) 195.
2. G. Brindley and R. Sempels., *Clay. Miner*., 12 (1977) 229.
3. D. Vaughan., *Catal. Today*., 2 (1988) 187.
4. G. Bartley., *Catal. Today*., 2 (1988) 233.
5. V. Yu. Zakharov, B. V. Romanovsky., *Vestn. Mosk. Univ., Ser. Khim*., 18 (1977) 143.
6. K. J. Balkus, Jr. and A. G. Gabrielov., *J. Incl. Phenom. Mol. Recog. Chem*., 21 (1995) 159.
7. R. Parton, D. De Vos and P. A. Jacobs in *Proceedings of NATO Advanced Study Institute on Zeolite, Microporous Solids* : *Synthesis, Structure and Reactivity*, E. G. Derouane, F. Lemos, C. Naccache, F. R. Riberio (Eds), Kluwer, Do-drecht, 555 (1992) 578.
8. D. E. De Vos, F. Thibault–Starzyk, P. P. Knops-Gerrits, R. F. Parton and P. A. Jacobs., *Macromol. Symp*., 80 (1994) 157.
9. S. Seelan, A. K. Sinha, D. Srinivas and S. Sivasanker., *J. Mol. Catal. A : Chemical* 157 (2000) 163.

10. V. Yu. Zakharov, O. M. Zakharova, B. V. Romanovsky and R. E. Mardelishvili., *React. Kinet. Catal. Lett*., 6 (1977) 133.

11. G. Meyer, D. Wöhrle, M. Mohl, G. Schulz–Eklof, *Zeolites*, 4 (1984) 30.

12. N. Herron, G. D. Stucky and C. B. Tolman, *J. Chem. Soc. Chem. Commun*., (1986) 1521.

13. M. Ichikawa, T. Kimura and A. Fukuoka., *Stud. Surf. Sci. Catal*., 60 (1991) 335.

14. V. Yu. Zakharov and B. V. Romanovsky., *Vestn., Mosk. Univ., Khim*., 18 (1977) 142.

15. B. V. Romanovsky, in Y. Yermakov and V. Likholobov (eds.), *Homogeneous and Heterogeneous Catalysi*s, VNU Science, Utrecht, 1986, p.343.

16. R. Raja and P. Ratnasamy., *J. Catal*., 170 (1997) 244.

17. T.K. Das, A.J. Chandwadkar and S. Sivasanker, *Chem.Commun*., (1996) 1105.

CHAPTER 3
PHYSICOCHEMICAL CHARACTERIZATION

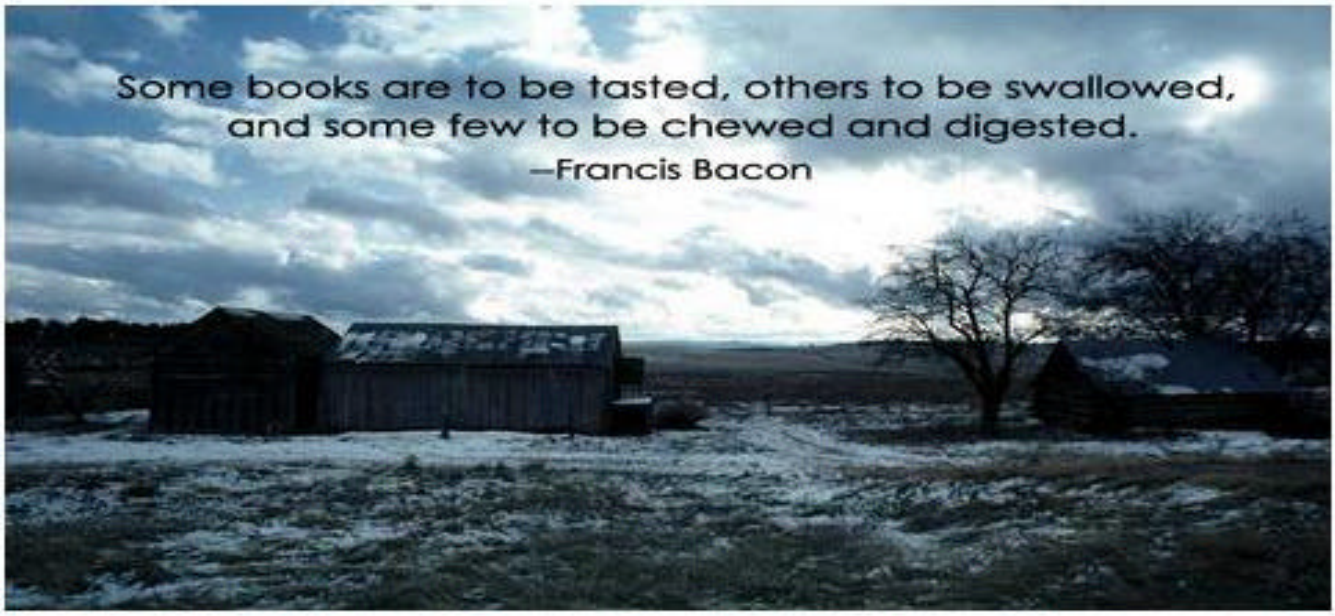

This chapter describes the physicochemical characteristics of "neat" and zeolite-encapsulated Cu, Co, V and Fe phthalocyanine complexes. The complexes were characterized by microanalysis (C, H and N), atomic absorption spectroscopy (AAS), thermal analysis (TGA and DTG), sorption studies and FT-IR, UV-Vis and EPR spectroscopic techniques. *Ab initio* UHFS DV-Xα calculations have revealed that the electronic structure of metal phthalocyanine (MPc) complexes is sensitive to peripheral substituents on the Pc moiety and central metal ion [1]. Hence, by introducing appropriate electron donating and withdrawing substituents in the macrocyclic Pc ring, one could, in principle, fine tune the electronic structure, suitably, to design a desired catalyst. This chapter describes the effects of peripheral substitution on the spectral and the molecular electronic structural properties of CuPc complexes.

In the case of encapsulated CuPc, CoPc, VPc and FePc complexes, the characterization studies presented in this chapter reveal the effect of molecular confinement on the structure of MPc complexes. Generally, the MPc complexes have a tendency to adsorb on the surface of the zeolites in addition to their encapsulation in the supercages. Hence, it is highly desirable to differentiate the zeolite-encapsulated complexes from the surface-adsorbed complexes. A systematic spectral study has been carried out to differentiate the encapsulated from the surface-adsorbed MPc complexes. Also attempts were made to quantitatively estimate the amount of MPc complex encapsulated in zeolites. The results of the characterization studies are presented in the following sections.

3.1 Characterization and Effect of Peripheral Substitution on the Spectral and Structural Properties of "Neat" CuPc Complexes

The complexes, copper phthalocyanine (CuPc), copper 4,4',4'',4'''-tetraazaphthalocyanine (CutetraazaPc), copper phthalocyaninetetrasulfonic acid tetrasodium salt ($Cu(SO_3Na)_4Pc$), copper tetranitrophthalocyanine ($Cu(NO_2)_4Pc$), copper octachlorophthalocyanine ($CuCl_8Pc$), and copper hexadecachlorophthalocyanine ($CuCl_{16}Pc$) have been investigated. Molecular structures of these complexes are shown in Fig. 3.1. Microanalytical data, presented in Table 3.1, confirmed the purity of the complexes.

Table 3.1

Microanalytical data of substituted CuPc complexes

Complex	Elemental Analysis (wt.%)[a]		
	C	H	N
CuPc	66.3 (66.7)	2.7 (2.8)	19.4 (19.4)
$CuCl_{16}Pc$	35.0 (34.0)	0.0 (0.0)	9.9 (9.9)
$CuCl_8Pc$	46.1 (45.1)	1.6 (0.9)	11.6 (13.1)
$Cu(NO_2)_4Pc$	49.7 (49.7)	1.4 (1.6)	21.8 (22.2)

[a] Calculated values are in parentheses.

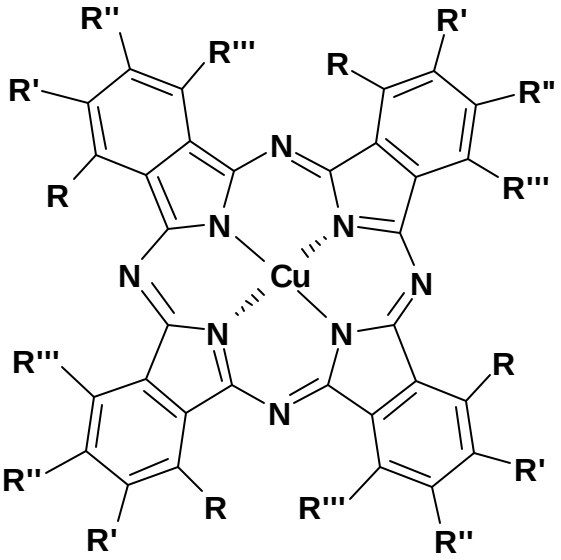

Complex	R	R'	R''	R'''
CuPc	H	H	H	H
$CuCl_8Pc$	Cl	H	Cl	H
$CuCl_{16}Pc$	Cl	Cl	Cl	Cl
$Cu(NO_2)_4Pc$	NO_2	H	H	H
$Cu(SO_3Na)_4Pc$	SO_3Na	H	H	H

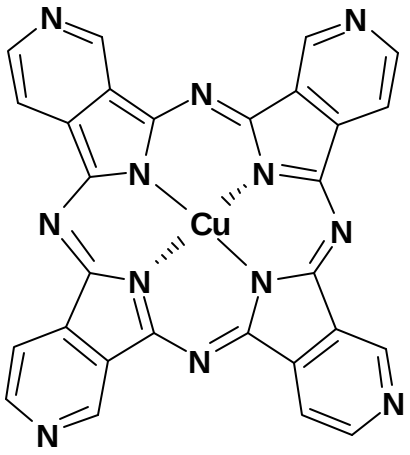

Cut et r aaza Pc

Fig. 3.1 Molecular structure of substituted CuPc complexes

3.1.1 FT-IR spectra of substituted CuPc complexes

Substitution has a significant effect on the FT-IR spectra of CuPc complexes. The spectra of the complexes as nujol mulls are shown in Figs. 3.2 to 3.4. Significant shifts in

Table 3.2

FT-IR data of substituted CuPc complexes

Complex	FT-IR data (cm^{-1})			
	ν(C=N)	ν(C=C)	ν(C-N)	Skeletal
CuPc	1589	1419	1090	1508, 1288
$CuCl_{16}Pc$	1556	1391	1096	1497, 1277
$CuCl_8Pc$	1568	1438	1088	1500, 1300
Cu $(NO_2)_4Pc$	1597		1090	1505, 1254
Cu $(SO_3Na)_4Pc$	1591	1420	1090	1503, 1286

peak positions and changes in peak intensities were observed as a consequence of substitution. The bands were, in general, weaker and broader in substituted complexes than in "neat" CuPc indicating a lower molecular symmetry of the Pc moiety in substituted complexes. The FT-IR spectral data of selected vibrational modes are listed in Table 3.2. The distinct changes in the peak positions of ν(C=N), ν(C=C), ν(C-N) and skeletal vibrational modes reveal conformational changes of Pc moiety as a consequence of peripheral substitution.

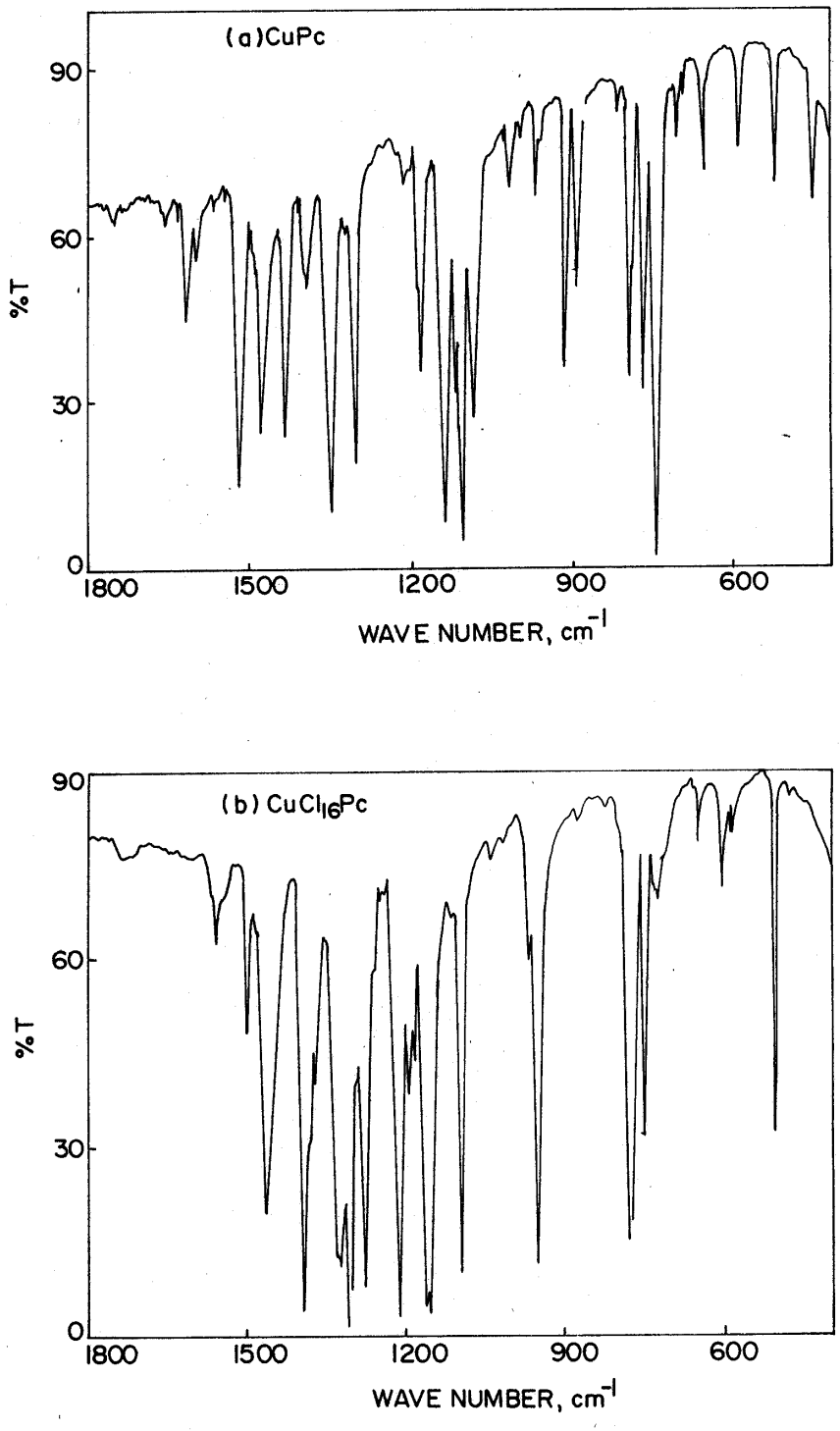

Fig.3.2 FT-IR spectra of (a) CuPc (b) $CuCl_{16}Pc$ as nujol mulls

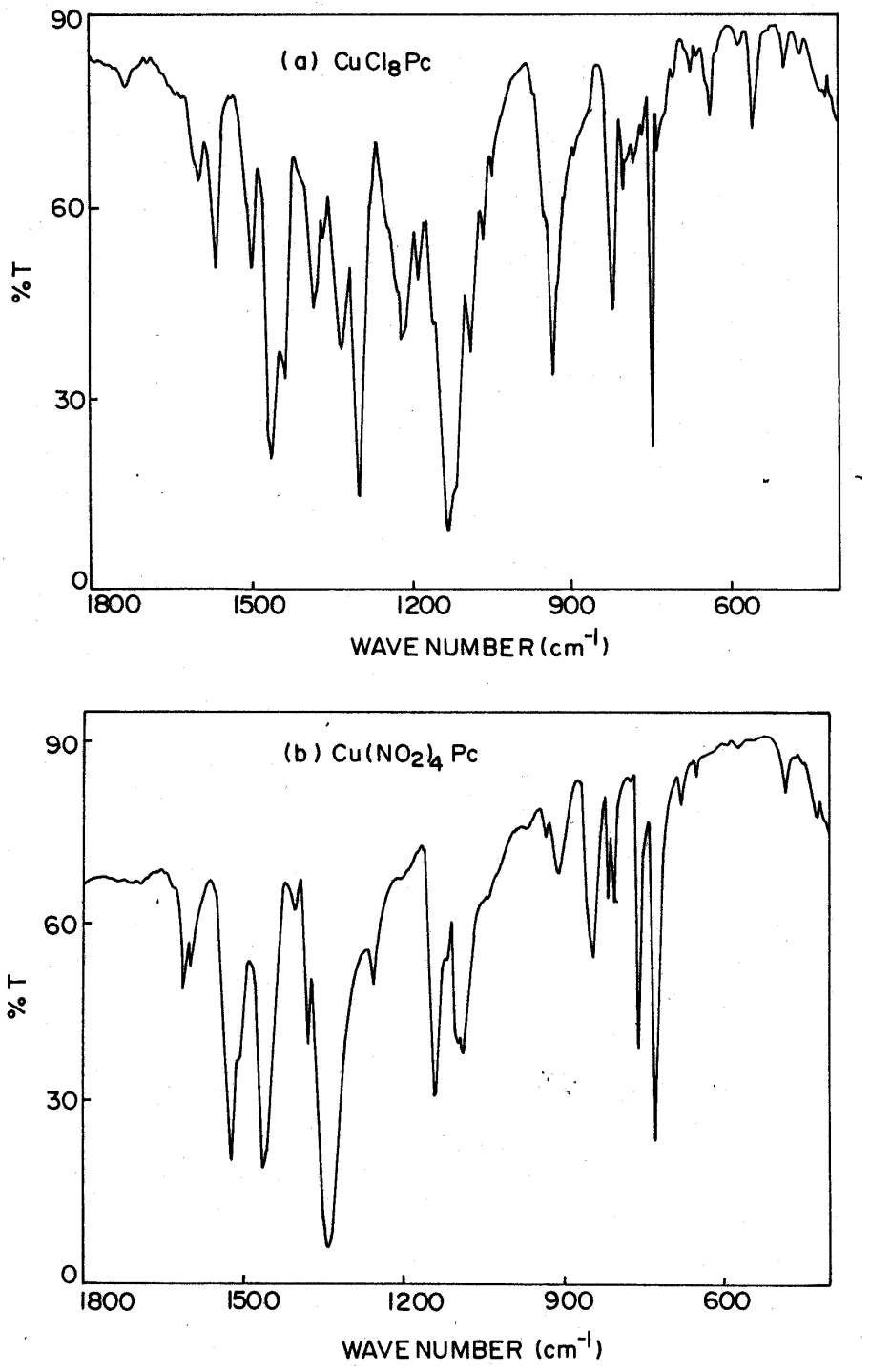

Fig.3.3 FT-IR spectra of (a) $CuCl_8Pc$ (b) $Cu(NO_2)_4Pc$ as nujol mulls

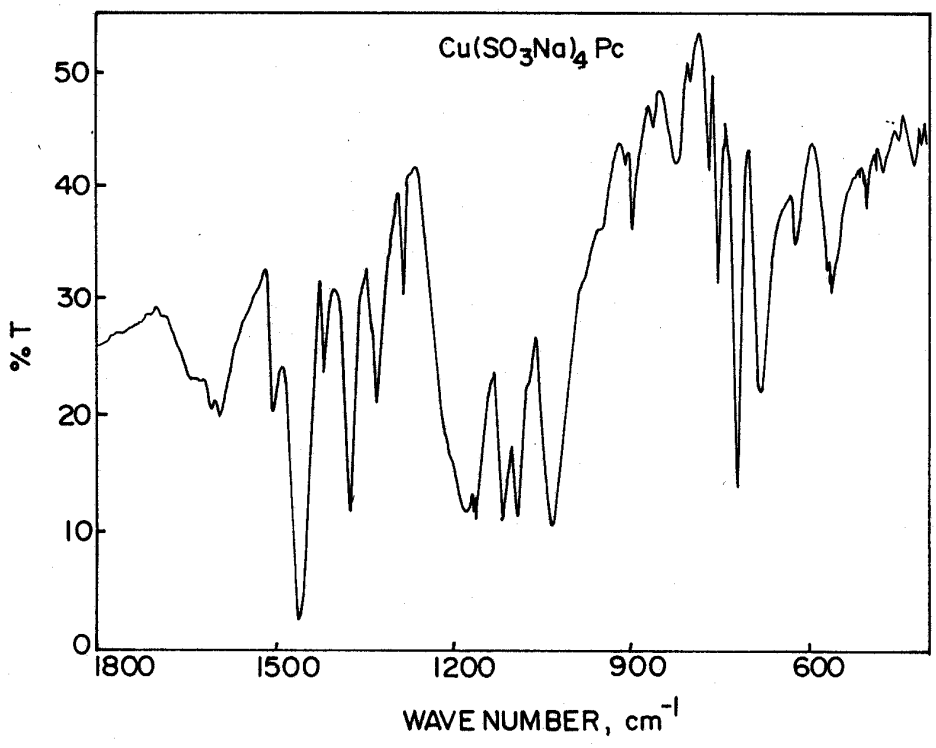

Fig.3.4 FT-IR spectra of $Cu(SO_3Na_4)Pc$ as nujol mulls

3.1.2 UV-Vis spectra of substituted CuPc complexes

Fig. 3.5 presents the effect of peripheral substitution on DRUV-Vis spectra of solid CuPc complexes. The d-d bands were masked by dominant ligand centered π - π^* charge transfer transitions (Q-bands; Q(0,0) and Q(1,0)). For symmetry lower than D_{4h}, these bands show vibrational overtones Q(0,1) and Q(1,1) as shoulders or resolved bands [2]. These bands appeared in the wavelength range 550 - 780 nm. Peripheral substitution considerably affects the band positions and intensities (Fig. 3.5). The Q-bands were diffused in $CuCl_8Pc$, $Cu(NO_2)_4Pc$ and $Cu(SO_3Na)_4Pc$. On the contrary, CuPc and $CuCl_{16}Pc$ showed resolved bands. The spectral variation is probably due to changes in the

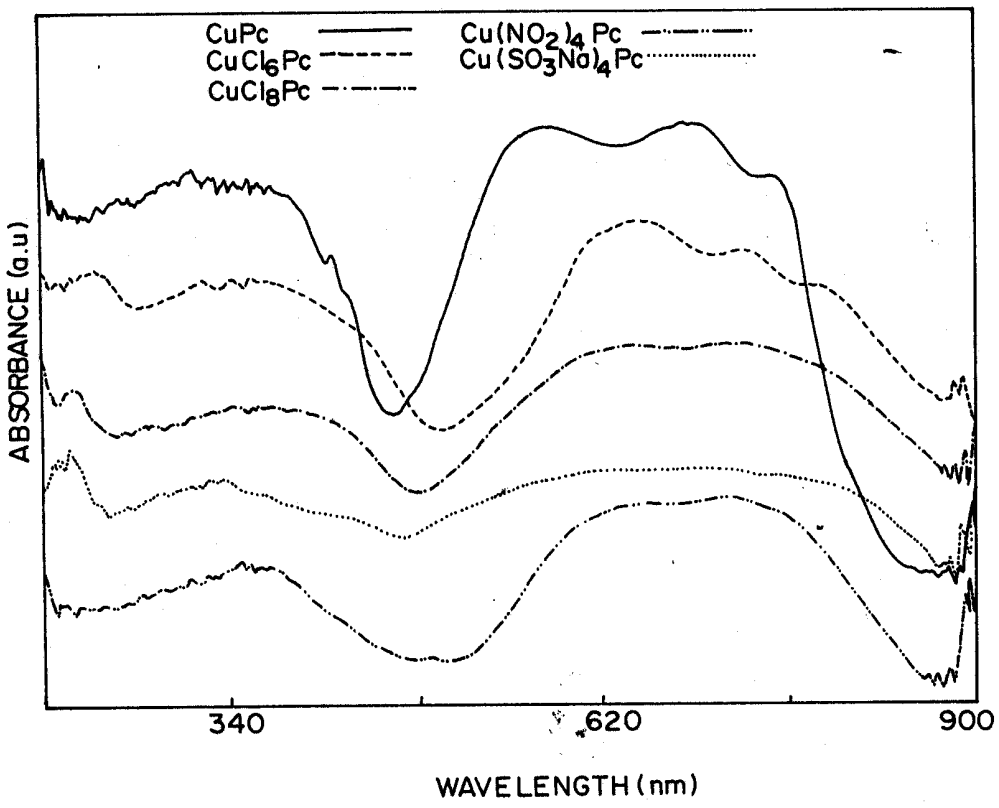

Fig. 3.5 DRUV-Visible spectra for the solid samples of substituted CuPc

molecular conformation. The electronic spectral data of the solid complexes are presented in Table 3.3.

The UV-Vis spectra of the complexes in conc. H_2SO_4 are shown in Fig. 3.6. Unlike the solid complexes, the spectra in conc. H_2SO_4 solutions were sharp and well resolved. The effect of substitution has manifested on spectral features and the positions of the Soret and Q-bands. In addition to these bands of ligand origin, the spectra in solutions also showed two weak d-d transitions in the range 620 - 690 nm. The positions of the

Table 3.3

Electronic spectral data of solid substituted CuPc complexes

Complex	Soret band (nm)	Q-bands (nm)
CuPc	429	545, 588, 686, 755
$CuCl_8Pc$	437	577, 649, 724, 773
$Cu(SO_3Na)_4Pc$	437	584, 623, 685, 782
$CuCl_{16}Pc$	437	590, 655, 726, 780
$Cu(NO_2)_4Pc$	-	604, 652, 717, 674

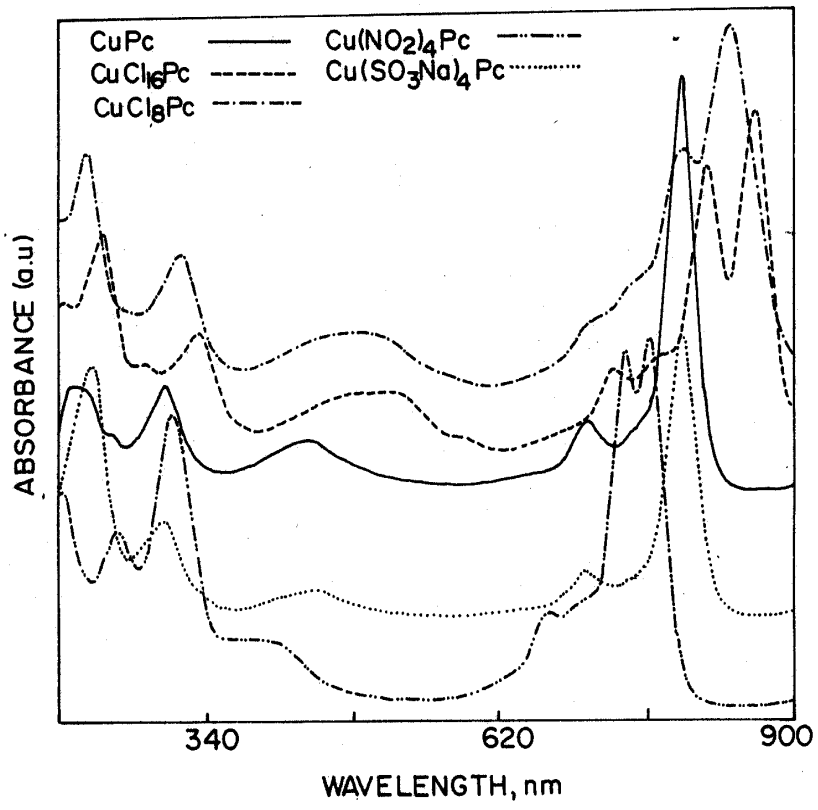

Fig. 3.6 UV-Visible spectra for conc. H_2SO_4 solutions of substituted CuPc

latter bands were sensitive to substituents and vary in the order of increasing energy as follows: $CuCl_{16}Pc$ < $CuCl_8Pc$ < CuPc < $Cu(SO_3Na)_4Pc$ < $Cu(NO_2)_4Pc$. CuPc and $Cu(SO_3Na)_4Pc$ showed only two Q-bands attributable to D_{4h} molecular symmetry in solutions while the rest of substituted complexes showed four Q-bands corresponding to lower molecular symmetry. The Q-band shifted to lower energy in solutions in the order $Cu(NO_2)_4Pc$ < CuPc < $Cu(SO_3Na)_4Pc$ < $CuCl_8Pc$ < $CuCl_{16}Pc$. The macrocyclic Pc moiety adopts a variety of conformations including planar, saddle shaped and puckered [2]. A difference in the conformational geometry introduces changes in the spectral features. The electronic spectral data of the complexes in conc. H_2SO_4 are presented in Table 3.4. It is interesting to note the differences in the UV-Vis spectra in solid and H_2SO_4 solutions.

Table 3.4

UV-Vis data for conc. H_2SO_4 solutions of substituted CuPc complexes

Complex	Electronic spectral data (H_2SO_4 solution) (nm)		
	Soret band	Q-bands	d-d-bands
CuPc	440	702, 792	639, 668
$CuCl_{16}Pc$	465	729,770, 816, 861	584, 656
$CuCl_8Pc$	450	709, 746, 794, 838	569, 661
Cu $(NO_2)_4Pc$	422	668, 705, 740, 764	613
$Cu(SO_3Na)_4Pc$	440	703, 884	630, 668

CuPc and $Cu(SO_3Na)_4Pc$ complexes, which showed only two Q-bands corresponding to D_{4h} molecular symmetry in H_2SO_4, showed four Q-bands in solid state indicating a reduction in the molecular symmetry. This is perhaps due to solid state packing forces and intermolecular interactions. The Q-bands appearing in the wavelength range 545 - 780 nm in solid state have undergone a red shift in H_2SO_4 solutions to the wavelength range 668 - 861 nm. This shift in H_2SO_4 solutions is attributed to protonation of the peripheral nitrogens. The bands were broader in solid state compared to that in solutions. This is due to the fact that intermolecular interactions are less in H_2SO_4 solutions.

3.1.3 EPR spectra of solid CuPc complexes

The solid samples of substituted CuPc, in general, showed broad EPR spectra. The hyperfine features due to copper could not be resolved due to intermolecular dipolar and exchange interactions. However, marked differences were observed in the nature of the EPR spectra (Fig. 3.7) due to peripheral substitution. Except for CutetraazaPc, the spectra for the rest of the complexes were characterized by an axial g tensor, with $g_{||} > g_{\perp}$; CutetraazaPc, on the other hand, showed only an isotropic signal. The spectra were fitted to the following axial spin Hamiltonian. The simulated g parameters are listed in Table 3.5.

$$H = g_{||}\beta H_z S_z + g_{\perp}\beta\ (H_x S_x + H_y S_y) \qquad (1)$$

Here β is Bohr magneton and the rest of the terms carry their usual meaning. The g values for solid samples (Table 3.5) do not represent the molecular values but are averaged due to intermolecular spin-spin interactions. Peripheral substitution has a marked effect on the g values and peak-to-peak linewidth (ΔH) parameters, especially in the parallel region (Table 3.5). The $g_{||}$ value of the complexes decreases in the order $CuCl_{16}Pc$ > CuPc >

$CuCl_8Pc$ > $Cu(SO_3Na)_4Pc$ > $Cu(NO_2)_4Pc$. It is known that phthalocyanine complexes form supramolecular networks in the solid state. The molecules in the unit cell are held together by interacting dipole vectors, H-bonding or π-π stacking interactions [3]. In pure paramagnetic solids the prominent magnetic interactions include exchange, dipole-dipole and psuedo-dipolar interactions [4].

The exchange interaction arises from the combined effect of the electrostatic repulsion of electrons (e^2/r_{12}) and the Pauli exclusion principle. This, for two interacting spins (with $S_1 = S_2 = ½$), is expressed as

$$H_{ex} = - JS_1.S_2 \qquad (2)$$

where J is the exchange coupling constant; its value is negative if the spins are coupled antiferromagnetically and positive if they are coupled ferromagnetically.

The dipolar interaction between the spins is expressed as follows:

$$H_{dip} = (\mu_1.\mu_2)/r_{12}^3 - 3(\mu_1.r_{12})(\mu_2.r_{12})/r_{12}^5 \qquad (3)$$

where μ_1 and μ_2 are the magnetic dipole moments of the two interacting ions 1 and 2 and r_{12} is the distance between them. The combined effect of spin-orbit coupling and isotropic exchange on the ground and excited energy levels of the interacting molecules leads to an additional contribution to the interaction energy known as anisotropic exchange or psuedo-dipolar coupling. The exchange and the dipolar interactions introduce opposite effects; while the former narrows the signal, the latter broadens the resonance signal.

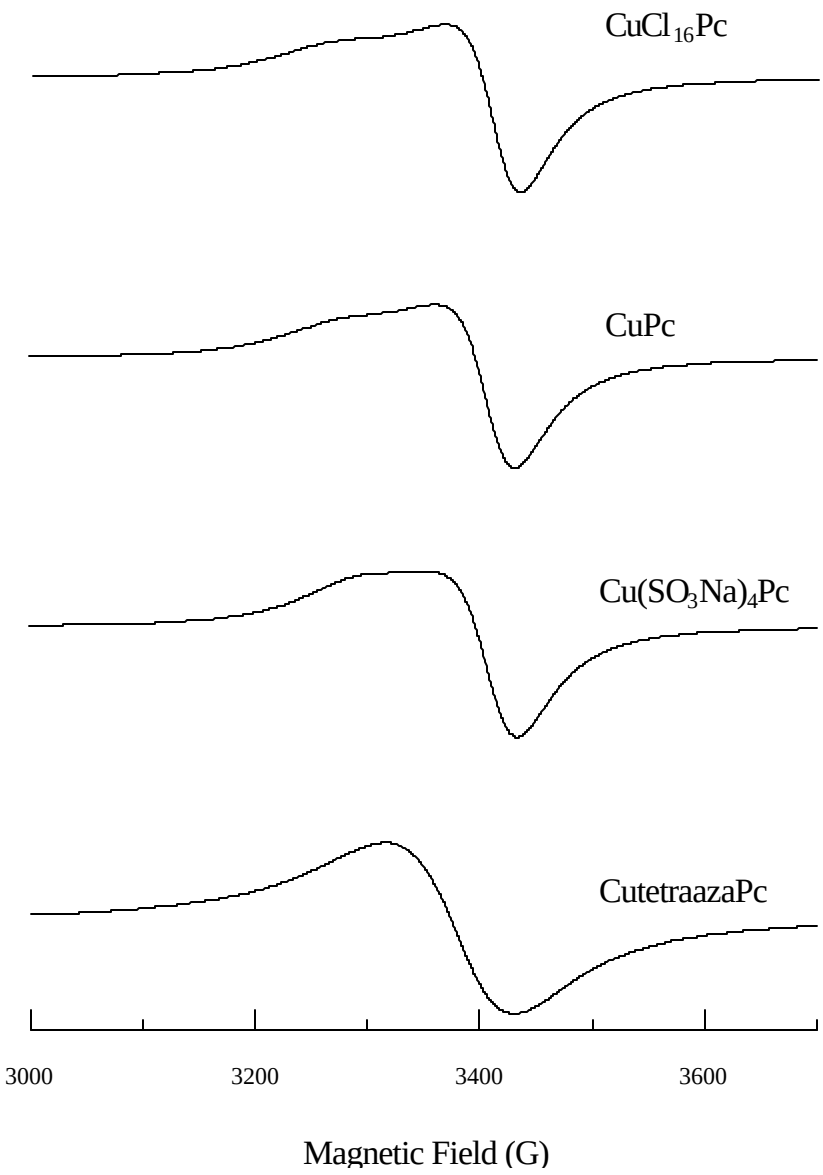

Fig. 3.7 X-band EPR spectra of the powder samples of substituted CuPc complexes at 298 K.

Table 3.5

EPR data for powder samples of substituted CuPc at 298 K

Complex	$g_{\|\|}$	$g_{\perp}$	$\Delta H_{\|\|}$(G)	$\Delta H_{\perp}$(G)
CutetraazaPc[a]	2.069		115	
$Cu(NO_2)_4Pc$	2.123	2.045	65	50
$Cu(SO_3Na)_4Pc$	2.126	2.046	75	55
$CuCl_8Pc$	2.132	2.046	80	55
CuPc	2.133	2.045	85	52
$CuCl_{16}Pc$	2.142	2.045	85	50

[a]Isotropic g value; Estimated error in g values is ±0.002.

The g anisotropy ($\Delta g = g_{\|} - g_{\perp}$) reduces from 0.095 for $CuCl_{16}Pc$ to 0.078 for $Cu(NO_2)_4Pc$ and becomes almost negligible for the CutetraazaPc complex. Similarly, the linewidth, $\Delta H_{\|}$, reduces from 85 G for $CuCl_{16}Pc$ to 65 G for $Cu(NO_2)_4Pc$. From these observations it appears that the exchange interaction is more for the sulfonicacid, nitro and tetraaza-phthalocyanine complexes and varies in the order CutetraazaPc > $Cu(NO_2)_4Pc$ > $Cu(SO_3Na)_4Pc$ > $CuCl_8Pc$ > CuPc > $CuCl_{16}Pc$.

3.1.4 EPR spectra of substituted CuPc complexes in conc. H_2SO_4

Several workers have studied CuPc diluted in metal free phthalocyanine (H_2Pc) and ZnPc to avoid intermolecular interactions [5-10]. While the $g_{\perp}$ values of the pure compounds (Table 3.5) match well, within experimental errors, with the diluted compounds (Table 3.6), the $g_{\|}$ and Δg values are considerably different. For dilute

Table 3.6

EPR data for frozen H_2SO_4 solutions of substituted CuPc at 77K

Complex	species	$g_{\|}$ or g_z	$g_\perp$ or g_x, g_y	$-A_{\|}$ (Cu) ($10^{-4}cm^{-1}$)	$-A_\perp$ (Cu) ($10^{-4}cm^{-1}$)	$A_{\|}$ (^{14}N) ($10^{-4}cm^{-1}$)	$A_\perp$ (^{14}N) ($10^{-4}cm^{-1}$)
CutetraazaPc	I	2.19	2.060	203.5 (201.5)	19.0	13.9	15.2
	II	2.19	2.060	215.0	19.0	13.9	15.2
Cu $(SO_3Na)_4$ Pc		2.19	2.060	204.0	18.0	13.9	15.2
CuPc	I	2.20	2.062	203.5 (200.0)	18.5 (18.5)	13.9	15.2
	II	2.20	2.062	215.5	18.0	13.9	15.2
$CuCl_{16}Pc$		2.20	2.062	204.0	18.0	13.0	15.9
$CuCl_8Pc$		2.20	2.052 2.057	200.0 (196.0)	18.0	13.0	14.3, 14.0

Estimated error in g values is ± 0.002 and in A values is ± 0.5.

samples, the $g_{\|}$ and Δg values are about 2.16 and 0.115, respectively. Complexes, $Cu(SO_3Na)_4Pc$, $Cu(NO_2)_4Pc$ and CutetraazaPc with O and N donor atom substituent groups form relatively close packed structures and hence the dipolar interaction which varies inversely with the distance is expected to be high.

The EPR spectra of frozen CuPc solutions (10^{-3} M) in conc. H_2SO_4 (Fig. 3.8) showed resolved copper hyperfine features in the parallel region. These features,

especially the two at the low field side, were further spit due to superhyperfine interaction due to four equivalent nitrogen nuclei (I = 1). Resolution of superhyperfine features was observed also in the perpendicular region, but, the hyperfine signals due to copper and the superhyperfine features due to nitrogen nuclei overlapped. The hyperfine features due to both the isotopes of copper (^{63}Cu and ^{65}Cu) were also resolved in the low field region. The spectra of the complexes, except the hexadecachloro substituted complex, corresponded to an axial symmetry ($g_x = g_y = g_\perp$ and $A_x = A_y = A_\perp$) while the latter to a rhombic symmetry. The spectra were fitted to the following generalized Hamiltonian.

$$H = \beta_e[g_{||}H_zS_z + g_\perp(H_xS_x + H_yS_y)] + A_{||}^{Cu}S_zI_z + A_\perp^{Cu}(S_xI_x + S_yI_y)$$
$$+ S_x[A_{||}^{N}(I_{1x} + I_{3x}) + A_\perp^{N}(I_{2x} + I_{4x})]$$
$$+ S_y[A_\perp^{N}(I_{1y} + I_{3y}) + A_{||}^{N}(I_{2y} + I_{4y})] + S_z[A_\perp^{N}(I_{1z} + I_{2z} + I_{3z} + I_{4z})] \quad (4)$$

The calculated spin Hamiltonian parameters are listed in Table 3.6. A good agreement between the experimental and simulated EPR spectra of CuPc in conc. H_2SO_4 were observed (Fig. 3.9). The $g_{||}$ and $g_\perp$ values of CuPc, derived from spectral simulations, differ from the reported values [5-10]. Discrepancy was also noticed in the copper and nitrogen hyperfine parameters ($A_\perp^{Cu}$ and A^N values). This is because, the structure of CuPc is sensitive to the concentration of H_2SO_4 and the host lattice (H_2Pc and ZnPc).

The $g_{||}$ values were markedly affected by the substituents. These values (Table 3.6) vary in the order CutetraazaPc < $Cu(SO_3Na)_4$Pc < CuPc < $CuCl_8$Pc < $CuCl_{16}$Pc. Only marginal changes were observed in the A^{Cu} values. The superhyperfine coupling constants due to nitrogen (A^N) are smaller for $CuCl_8$Pc and $CuCl_{16}$Pc than for the rest of the

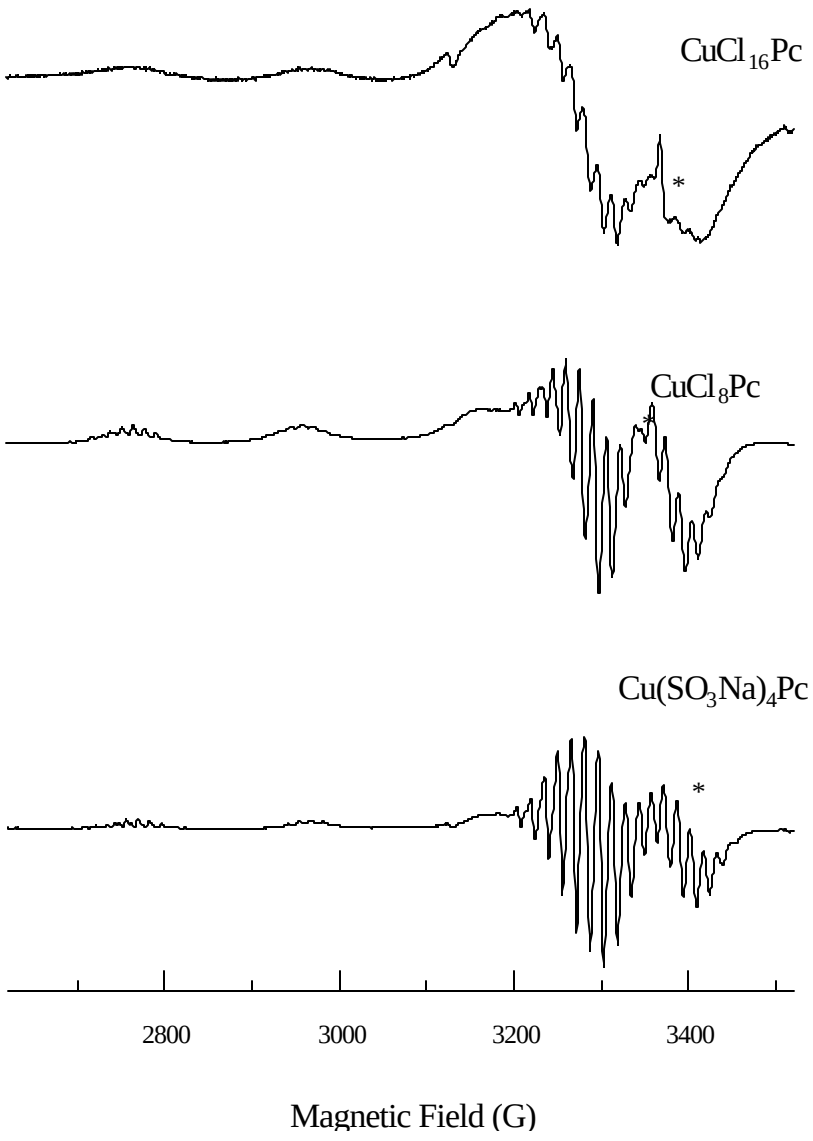

Fig. 3. 8 EPR spectra (77 K) for the frozen H_2SO_4 solutions of substituted CuPc complexes. Asterisk (*) represents a organic free radical impurity.

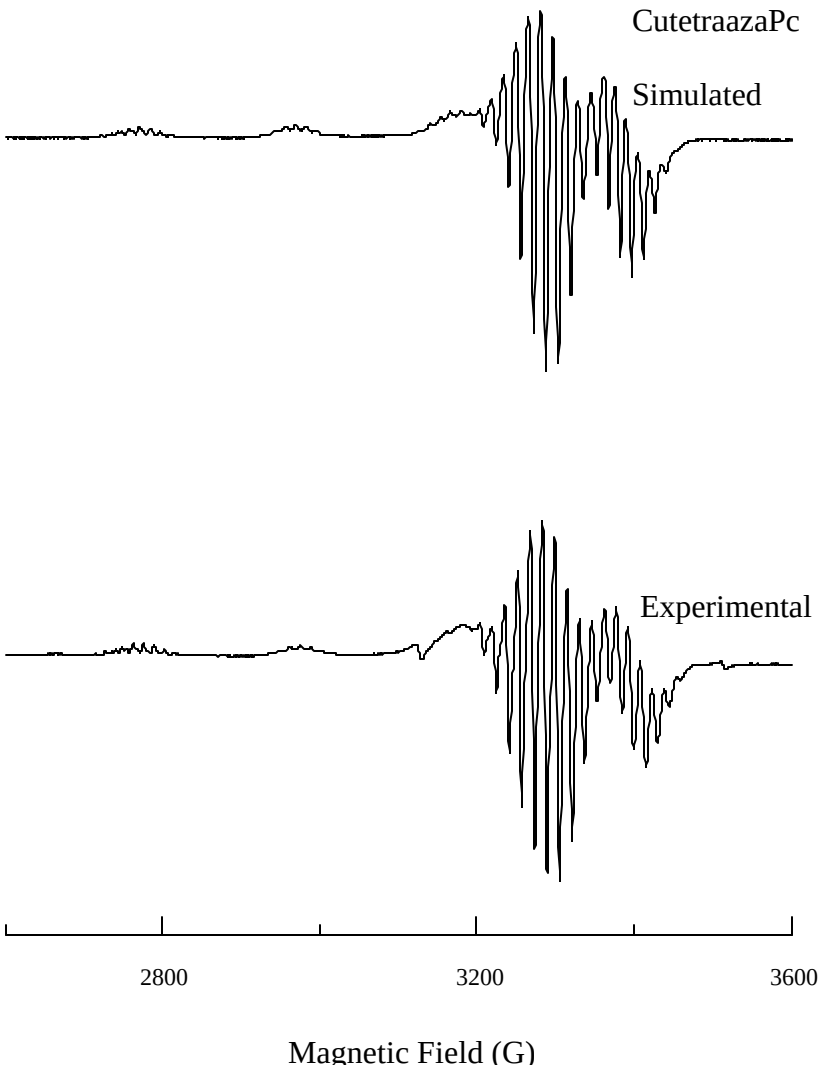

Fig. 3. 9 Experimental and simulated EPR spectra (77 K) of CutetraazaPc in conc. H_2SO_4. Hyperfine features due to ^{63}Cu and ^{65}Cu isotopes are resolved in the parallel region.

complexes and indicate the delocalization of spin density onto the electron withdrawing chlorine atoms. Hence, the peripheral substituents in the phthalocyanine moiety are not passive but contribute to the ground state molecular orbital. The rhombic anisotropy for $CuCl_8Pc$ indicates lower (C_{2v}) symmetry around copper probably due to puckering of the Pc moiety. This observation agrees well with optical spectral results (*vide supra*).

3.1.5 Ground state wave function and chemical bonding

The approach developed by Maki and McGarvey [11] and later by Kivelson and Neiman [12] and Manoharan and Rogers [13] was employed to determine the ground state wave function and the chemical bonding of substituted CuPc complexes. Accordingly, the five anti-bonding orbitals corresponding to the D_{4h} symmetry obtained by a linear combination of the appropriate ligand atomic orbitals and the 3d orbitals of copper can be written as

$$\psi(b_{1g}) = \alpha d_{x^2-y^2} - \alpha'(\sigma_x^1 - \sigma_y^2 + \sigma_x^3 - \sigma_y^4)/2$$

$$\psi(b_{2g}) = \beta d_{xy} - \beta'(p_y^1 - p_x^2 + p_y^3 - p_x^4)/2$$

$$\psi(a_{1g}) = \alpha_1 d_{3z^2-r^2} - \alpha_1'(\sigma_x^1 + \sigma_y^2 + \sigma_x^3 + \sigma_y^4)/2 \qquad (5)$$

$$\psi(e_g) = \begin{matrix} \delta d_{xz} - \delta'(p_z^1 - p_z^3)/\sqrt{2} \\ \delta d_{yz} - \delta'(p_z^2 - p_z^4)/\sqrt{2} \end{matrix}$$

Here, the σ orbitals are obtained by a proper hybridization of 2s and 2p orbitals of the ligand nitrogens, i.e., $\sigma^{(i)} = np^{(i)} -/+ (1-n^2)^{1/2}s^{(i)}$ and $0 \leq n \leq 1$. α and β are the metal d orbital coefficients for the MOs, b_{1g} and b_{2g} representing the in-plane σ and π bonding, respectively, while δ is the coefficient for the MO e_g representing the out-of-plane π

bonding. α' is the coefficient for the ligand orbitals forming b_{1g} molecular orbital and is related by the normalization expression as follows:

$$\alpha^2 + \alpha'^2 - 2\alpha\alpha' S = 1 \qquad (6)$$

Here, S is the overlap integral between the metal $d_{x^2-y^2}$ and ligand σ orbitals. Griffith [14] has reported the energy level ordering of 3d orbitals in copper phthalocyanines and porphyrins as $3d_{xy} < 3d_{xz,yz} < 3\ d_{x^2-y^2}$, with a variable position for $3d_{3z^2-r^2}$. The position of the $3d_{3z^2-r^2}$ orbital, however, depends on the strength and stabilization of the axial distortion. Later, Gouterman and Zerner [15], on the basis of extended Huckel molecular orbital calculation, proposed the 3d orbital ordering with $3d_{xy} < 3d_{xz,yz} < 3d_{3z^2-r^2} < 3d_{x^2-y^2}$. However, in both the cases the ground state wave function is definitely $^2B_{1g}$ with the unpaired electron occupying the non-degenerate b_{1g} molecular orbital. According to Gouterman and Zerner [15], the various states in decreasing energy are listed in eq. 5 and the bonding picture of CuPc is shown in Fig. 3.10.

The expressions for g and hyperfine coupling constants (A^{Cu}) in terms of the MO coefficients can be derived by solving the Hamiltonian in eq. 4 and employing the wave functions given in eq. 5. Accordingly, the expressions for g and A^{Cu} can be written as

$$g_{||} = 2.0023 - (8\lambda\alpha\beta/\Delta E_1)[\alpha\beta - \alpha'\beta S - \alpha'(1-\beta^2)^{1/2}T(n)/2]$$

$$g_{\perp} = 2.0023 - (2\lambda\alpha\delta/\Delta E_2)[\alpha\delta - \alpha'\delta S - \alpha'(1-\delta^2)^{1/2}T(n)/\sqrt{2}$$

$$A_{||} = P\{-\alpha^2(4/7 + k_0) + (g_{||} - 2) + (3/7)(g_{\perp} - 2) - (8\lambda\alpha\beta/\Delta E_1)[\alpha'\beta S + \alpha'(1-\beta^2)^{1/2}T(n)/2] - (6/7)(\lambda\alpha\delta/\Delta E_2)[\alpha'\delta S + \alpha'(1-\delta^2)^{1/2}T(n)/\sqrt{2}]\}$$

$$A_{\perp} = P\{\alpha^2(2/7 - k_0) + (11/14)(g_{\perp} - 2) - (22/14)(\lambda\alpha\delta/\Delta E_2)[\alpha'\delta S + \alpha'(1-\delta^2)^{1/2}T(n)/\sqrt{2}]\} \qquad (7)$$

where $T(n) = n - (1-n^2)^{1/2}R^8(Z_pZ_s)^{5/2}(Z_s-Z_p)/(Z_s+Z_p)^5a_0$ and

$$P = 2\beta\beta_N g_N \langle d_{x^2-y^2} | r^{-3} | d_{x^2-y^2} \rangle.$$

Here, λ is the spin-orbit coupling constant of the free Cu(II) ion, k is the Fermi contact term, $\Delta E_1 = E(B_{1g}) - E(B_{2g})$ and $\Delta E_2 = E(B_{1g}) - E(E_g)$, R is the metal-ligand distance, hydrogen-like radial functions have been used; Z_s an Z_p, represent the effective nuclear

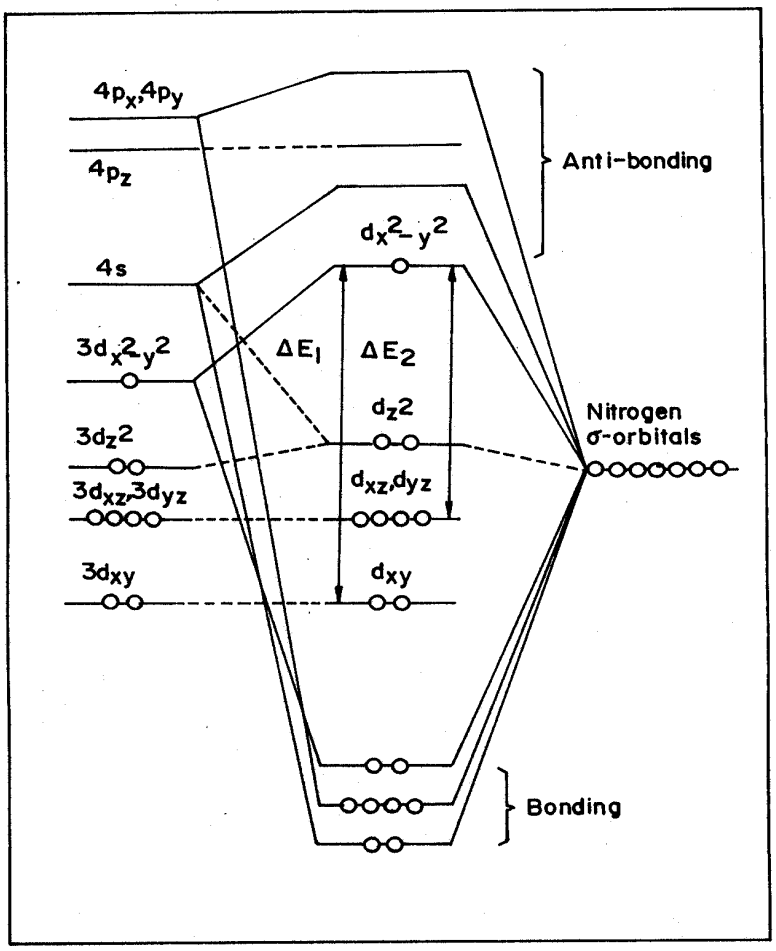

Fig. 3.10 Molecular orbital energy level diagram of CuPc

charges on the s and p orbitals, respectively and a_o is the Bohr radius. Considering the average Cu-N distance of 1.9 Å and the effective charges $Z_{2s} = 4.50$ and $Z_{2p} = 3.54$ for nitrogen and $Z_{3d} = 11.86$ (for Cu) the value of the overlap integral S and the constant T(n) were estimated as 0.093 and 0.333, respectively. The value of λ was chosen to be –828

cm^{-1} while P was 0.036 cm^{-1}; k is about 0.43 with an estimated uncertainty of about 5%. In order to calculate the MO coefficients one should have the knowledge of spin allowed electronic transitions $^2B_{1g} \leftrightarrow {}^2B_{2g}$ (ΔE_1) and $^2B_{1g} \leftrightarrow {}^2E_g$ (ΔE_2). These transitions were in fact resolved in the UV-Vis spectra of H_2SO_4 solutions. The MO coefficients (Table 3.7) were evaluated by substituting the spin Hamiltonian parameters (Table 3.6) in the expressions for g and A^{Cu} values (eq. 7).

The MO coefficients (Table 3.7) are smaller than unity and correspond to covalent nature of bonding between the metal and ligand orbitals. The in-plane σ-bonding parameter (α) is invariant. Peripheral substitution affects the in-plane and out-of-plane π-bonding parameters β^2 and δ^2, respectively. The value of β^2 varies with substituents in the

Table 3.7

MO Coefficients of substituted CuPc complexes

Complex	α^2	α'^2	β^2	δ^2
CuPc	0.83	0.25	0.57	0.71
$CuCl_{16}Pc$	0.83	0.25	0.59	0.77
$CuCl_8Pc$	0.83	0.26	0.60	0.72
$Cu(SO_3Na)_4Pc$	0.83	0.25	0.56	0.70

Estimated error in α^2, α'^2, β^2 and δ^2 is ± 0.005.

order $Cu(SO_3Na)_4Pc$ < CuPc < $CuCl_{16}Pc$ < $CuCl_8Pc$ and δ^2 varies in order $Cu(SO_3Na)_4Pc$ < CuPc < $CuCl_8Pc$ < $CuCl_{16}Pc$ (Table 3.7). From the extended Huckel calculations, Gouterman and Zerner [15], estimated the energy separation between the e_g and b_{2g} orbitals of the order of 1000 cm^{-1} for CuPc. The d-d band positions observed in the present

investigation substantiate the theoretical studies. The spectral studies revealed changes in molecular electronic structure and chemical bonding due to peripheral substitution. The effect of these structural changes on the catalytic activity will be presented in Chapter 4.

By and large, spectroscopic investigations on "neat" substituted CuPc complexes reveal marked effects of peripheral substitution on the molecular and electronic structure. All the substituted complexes studied in this chapter have molecular symmetry lower than D_{4h} in solid state as revealed by UV-Vis spectroscopy. However, the electronic symmetry at the site of central metal ion is D_{4h} except in the chlorosubstituted CuPc complex which has D_{2v} symmetry. The complexes are protonated at the peripheral nitrogens in H_2SO_4 solutions. The effect of intermolecular interactions is clearly manifested in the EPR spectra and g-anisotropy of solid samples. The metal-ligand bonds are covalent as revealed from the MO calculations and bonding parameters. Substituents have also affected the in-plane and out-of-plane π-bonding parameters.

3.2 Characterization of Copper Phthalocyanine Complexes Encapsulated in Zeolite Y: CuPcY

CuPc exists in several crystalline modifications of which the α and β forms have been well characterized. The "neat" CuPc (β form) was deep blue in colour. The encapsulated complexes (CuPcY) were greenish-blue and the physical mixture, CuPcY(m), was light blue in colour. Hence, from the visual examination itself, one could differentiate the physical nature of the complexes. In order to probe further the formation and location of macrocyclic CuPc molecules in zeolite-Y, experiments were performed on the following systems:

(i) Cu(II) exchanged NaY (CuY),

(ii) "neat" CuPc,

(iii) encapsulated CuPc prepared as described in the experimental section using the template synthesis method (CuPcY(1.2) and CuPcY(0.6),

(iv) a physical mixture of "neat" CuPc and NaY (CuPcY(m)), and

(v) H_2SO_4 solutions of CuPc and CuPcY.

3.2.1 X-ray diffraction

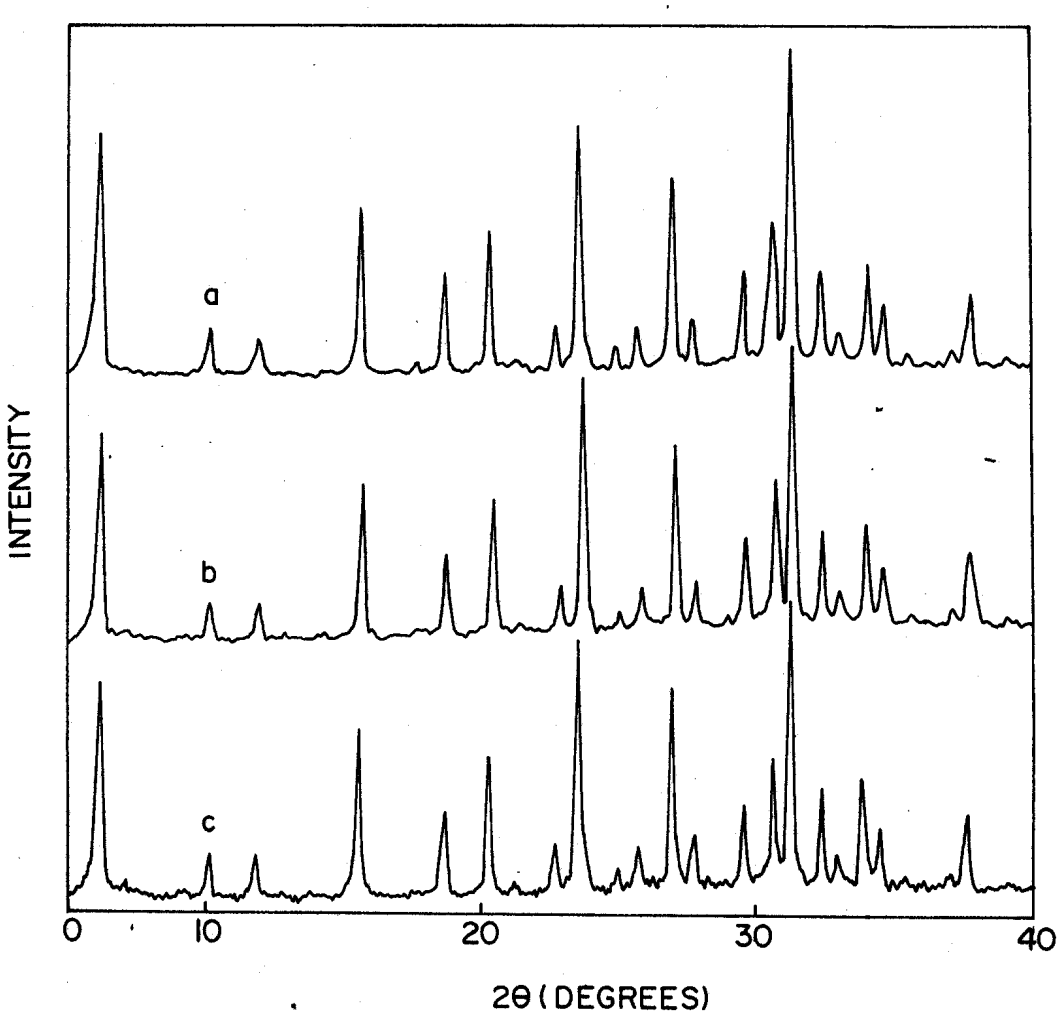

Fig. 3.11 XRD patterns of (a) NaY, (b) CuPcY(1.2) and (c) CuPcY(0.6)

The X-ray diffractograms of NaY, "neat" and enacpsulated CuPc complexes in zeolite Y are shown in Fig.3.11 The XRD patterns of the encapsulated complexes do not reveal any significant differences from those of the pure Y zeolite sample indicating that the molecular sieves had not undergone any structural changes due to the encapsulation of the complexes. Besides, the diffraction lines associated with "neat" CuPc are also not seen in the XRD pattern of CuPcY showing the absence of occluded bulk CuPc in the encapsulated samples.

3.2.2 Chemical and thermal analyses of zeolite-encapsulated CuPc complexes

The chemical analyses of CuPcY samples (Table 3.8) revealed the presence of organic matter with a N/C ratio roughly equal to that of phthalocyanine (36 ± 1 % compared to 29.2 % for Pc). The total organic contents of the samples suggest the presence of 1.6 and 1.3 Pc molecules per unit cell in CuPcY(1.2) and CuPcY(0.6) samples, respectively (Table 3.8).

Table 3.8

Chemical and thermal characterization of CuPcY

Sample	Cu (wt.%)		C/N analysis (wt.%)		molecules/ unit cell	
	Total	As Pc	C	N	Total Pc	CuPc
CuPcY(1.2)	1.2	0.41	5.50	1.91	1.6	0.7
CuPcY(0.6)	0.6	0.46	4.68	1.74	1.3	0.8
CuY(1.2)	1.2	-	-	-	-	-

- degassing of sample done at 423 K and 10^{-5} mm prior to N_2 adsorption.

The thermogravimetric analyses also revealed similar organic contents (weight loss between 473 - 873 K) in the two samples, though accurate quantification was not possible due to the additional water loss from the samples whose magnitude could itself depend on

the organic content (level of encapsulation). The TGA/DTA curves of CuPcY(m) and CuPcY(1.2) are presented in Fig. 3.12. Combustion of Pc occured rapidly in a narrow

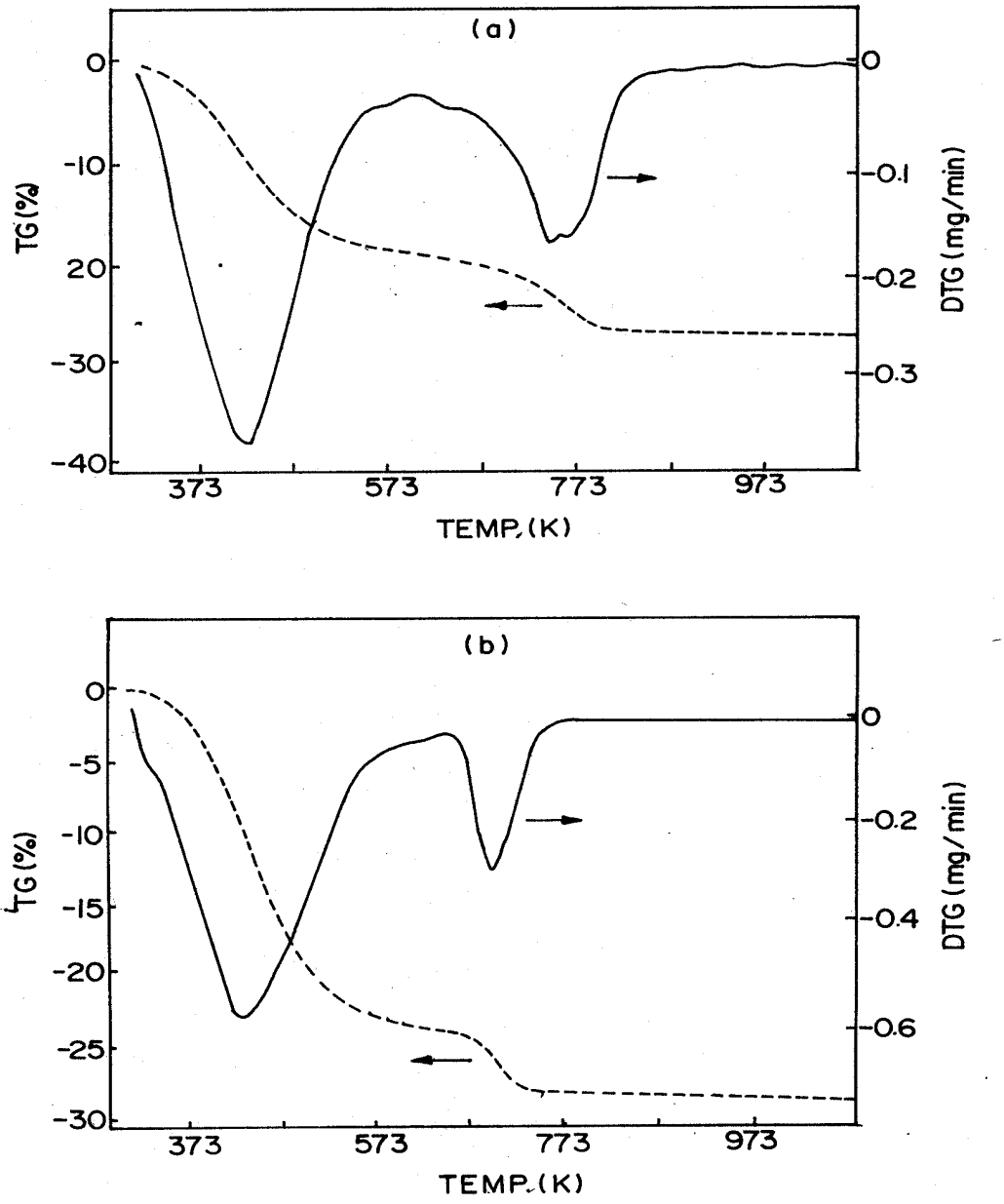

Fig. 3.12 TGA(----) and DTG (—) profiles of (a) CuPcY (1.2) and (b) CuPcY (m)

temperature range with the DTG minimum at about 693 K for the physical mixture (Fig. 3.12(b)), while the combustion occured more slowly, in a much broader temperature range, with the DTG minimum around 750 - 800 K for CuPcY(1.2) (Fig. 3.12(a)). The greater difficulty in combustion of the organics in CuPcY(1.2) reveals that Pc is encapsulated inside the cages and not adsorbed on the external surface.

3.2.3 N_2 adsorption studies on zeolite-encapsulated CuPc complexes

The micropore volume and S_{BET} values of CuPcY(1.2), CuPcY(0.6) and CuY(1.2) are presented in Table 3.9. The surface area was found to decrease on encapsulation. The disproportionately large decrease in the pore volume and surface areas (0.22 to 0.11 ml/g and 573 to 203 m^2 /g, respectively) with a small increase in total Pc content (from 1.3 to 1.6) is probably related to encapsulation occuring mainly in the more accessible cages at the periphery of the crystallites and not uniformly throughout the bulk of the crystallites

Table 3.9

N_2 adsorption data for CuPcY samples

Sample	Cu (wt.%) Total	S_{BET}* (m^2/g)	Pore volume (ml/g)
CuPcY-1(e)	1.2	203	0.11
CuPcY-2(e)	0.6	573	0.22
CuY	1.2	678	0.27

* degassing of sample done at 423 K and 10^{-5} mm prior to N_2 adsorption

As the α-cages of zeolite Y are interlinked, the blockage of one cage at the periphery can reduce the accessibility to many more cages in the interior. A large decrease in pore volume and S_{BET} of zeolite X on encapsulation by CuPc has been reported already by earlier workers [16].

3.2.4 FT-IR spectra of zeolite Y encapsulated CuPc

Representative FT-IR spectra of CuPc, CuPcY(0.6) and CuPcY(m) are shown in Fig. 3.13. The bands at 1462 and 1087 cm^{-1} are attributed to the stretching modes of C=N and C–N, respectively. Those at 1118 and 1065 cm^{-1} correspond to the bending modes of C–H. The spectra gave clear evidence for the formation of macrocyclic copper phthalocyanine molecules inside the supercages of NaY [17 - 20]. While there is no

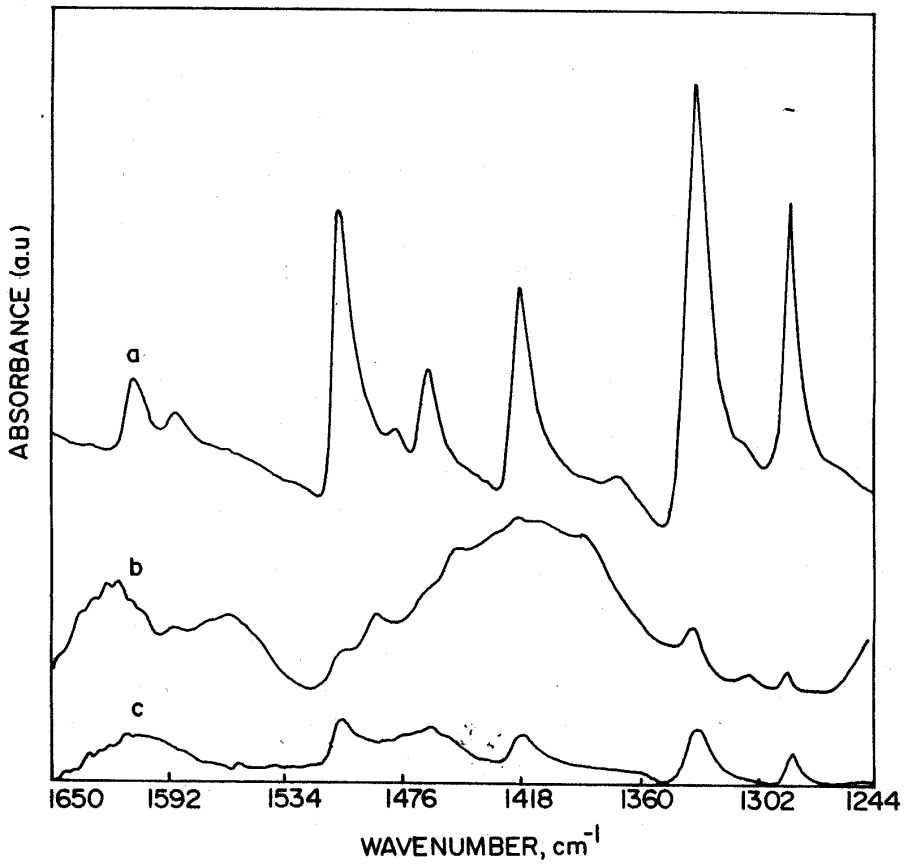

Fig. 3.13 FT-IR spectra of (a) "neat" CuPc as KBr pellet, (b) CuPcY (1.2) and (c) CuPcY (m) as thin films

notable shift in peak positions of the physical mixture CuPcY(m) compared to the "neat" CuPc, the encapsulated materials CuPcY(0.6) exhibited considerable shift in the position

Table 3.10

Assignment of FT-IR bands for CuPc, CuPcY-1(e) and CuPcY(m)

CuPc	CuPcY-1(e)	CuPcY(m)	Assignment
1608	1610	a	
1588	1589	a	
	1576[b]		
1505	1507	1505	
1477	1489[b]	1480	
1462	1463	1462	
			ν(C=N)
1417	1448	1417	and
	1420		ν(C=C)
	1404[b]		
1370	1387[b]	1371	
1332	1333	1332	
1285	1286	1284	
1171	a	a	
1164	a	A	
1118	a	a	δ (C-H)
1099	a	a	
1087	a	a	ν (C-N)
1065	a	a	δ (C-H)

[a] Bands not resolved due to overlap with zeolite bands.
[b] Represents additional bands or band shifted due to encapsulation.

of the peaks at 1477 and 1370 cm^{-1} and also revealed additional peaks at 1404, 1387 and 1306 cm^{-1} (Table 3.10). The band at 1417 cm^{-1} due to ν(C=C) for "neat" CuPc shifts to 1448 cm^{-1} on encapsulation in CuPcY(0.6) samples. This disparity between CuPcY(m) and CuPcY(0.6) could be accounted for by a change in molecular symmetry of CuPc in the encapsulated state. These results are in concurrence with the UV-Vis and EPR spectral data of these materials (*vide infra*).

3.2.5 UV-Vis spectra of zeolite Y encapsulated CuPc complexes

Fig. 3.14 shows DRUV-Vis spectra of CuPc, CuPcY(0.6) and CuPcY(m) in solid state. The spectra of "neat" CuPc and CuPcY(0.6) dissolved in conc. H_2SO_4 are shown in

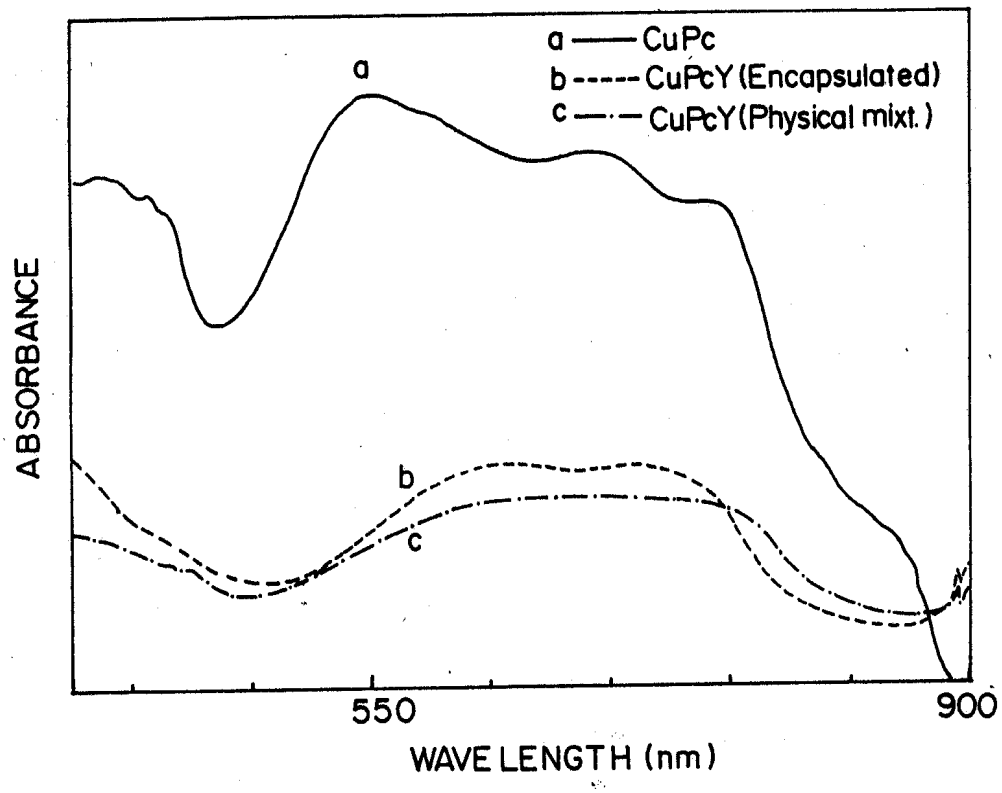

Fig. 3.14 DRUV-Vis spectra of (a) "neat" CuPc, (b) CuPcY(0.6) and CuPcY (m)

Fig. 3.15. The Q-bands of CuPcY(0.6) and CuPcY(m) have red shifted compared to the "neat" complex. The shift was more pronounced in encapsulated complexes CuPcY(0.6). The band at 545 nm for the "neat" CuPc shifted to 581 nm in encapsulated sample and to 574 nm for the physical mixture [21]. The red shift and changes in relative intensities of the Q bands correspond to changes in the molecular structure from planar to puckered geometry and isolation of the molecules. However, the spectra in concentrated sulfuric acid were almost similar for both "neat" CuPc and CuPcY(0.6). In addition to the Q-bands, the Soret band appears around 430 nm. The latter is broad due to overlap of bands attributable to n - π^* transitions [22]. The electronic spectral data are listed in Table 3.11.

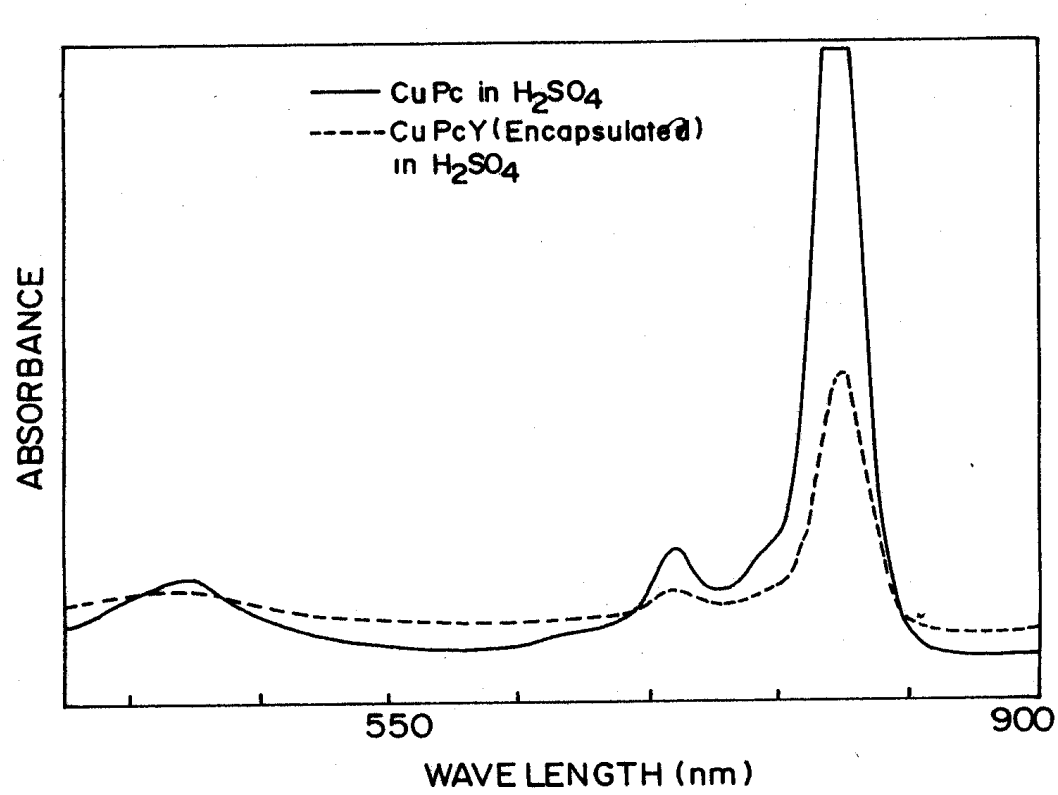

Fig. 3.15 Absorption spectra of (a) "neat" CuPc and (b) CuPcY (0.6) in Conc. H_2SO_4

3.2.6 EPR spectra of Cu exchanged NaY: CuY

EPR spectra for the solid samples of CuY at 298 K (Fig. 3.16(a)) correspond to the presence of two types of Cu(II) species. Species I is characterized by a rhombic g tensor with g_x = 2.083, g_y = 2.095 and g_z = 2.376. Hyperfine features due to copper were resolved only in the g_z region. The values in g_x and g_y regions were obtained by spectral simulations

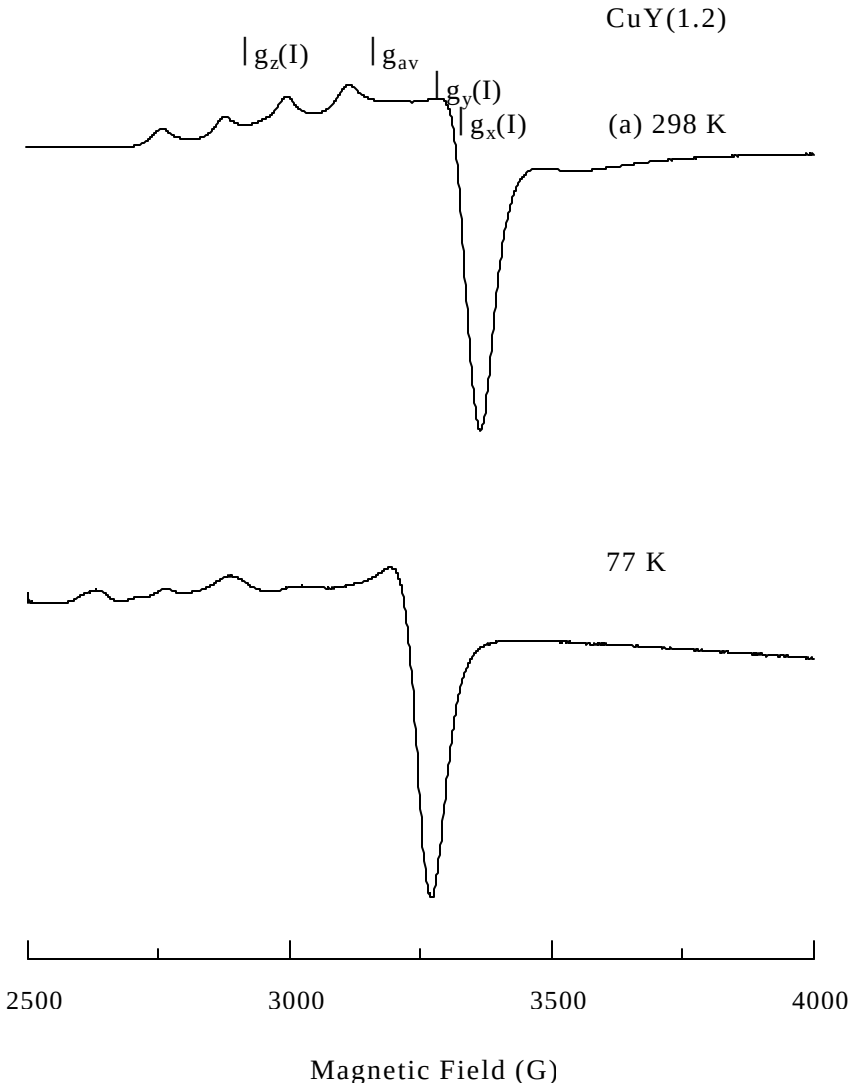

Fig. 3.16 EPR spectra of CuY(1.2) at (a) 298 K and (b) 77 K.

Table 3.11

Electronic spectral data for CuPc, CuPcY(1.2) and CuPcY(m).

Sample	Soret Band, nm	Q-bands, nm
CuPc (neat)	429	545, 588,686, 755
CuPcY(0.6)	429	581, 595, 706, 746
CuPcY(m)	429	574, 592, 699, 755
CuPc in H_2SO_4	443	702, 795
CuPcY(0.6) in H_2SO_4	443	702, 795

(A_x = A_y = 10 G and A_z = 119 G). Species II, on the other hand, exhibited an isotropic signal at g_{iso} = 2.166. As the concentration of copper increased the intensity of the isotropic signal due to species II increased. EPR spectra of CuY at 77 K, corresponded to three distinct Cu(II) species (Fig. 3.16(b)). While the g values of species I were marginally affected, species II which showed an isotropic signal at 298 K transformed into species II' and II'', at 77 K, both characterized by axial g and A(Cu) tensors. The EPR parameters listed in Table 3.12 agree with those reported by others [23-25]. Species I is attributed to Cu(II) ions in the sodalite cages and II' and II" to the ions near the hexagonal prism and in the supercages (α-cages), respectively. The species II' and II" undergo a dynamic Jahn-Teller effect at ambient temperatures which becomes static below 265 K.

3.2.7 EPR spectra of "neat" and encapsulated CuPc complexes

The spectrum for "neat" CuPc reveals near neighbour interactions and shows dipolar broadened EPR signals at $g_{||}$ = 2.133 and $g_{\perp}$ = 2.045. However, when CuPc

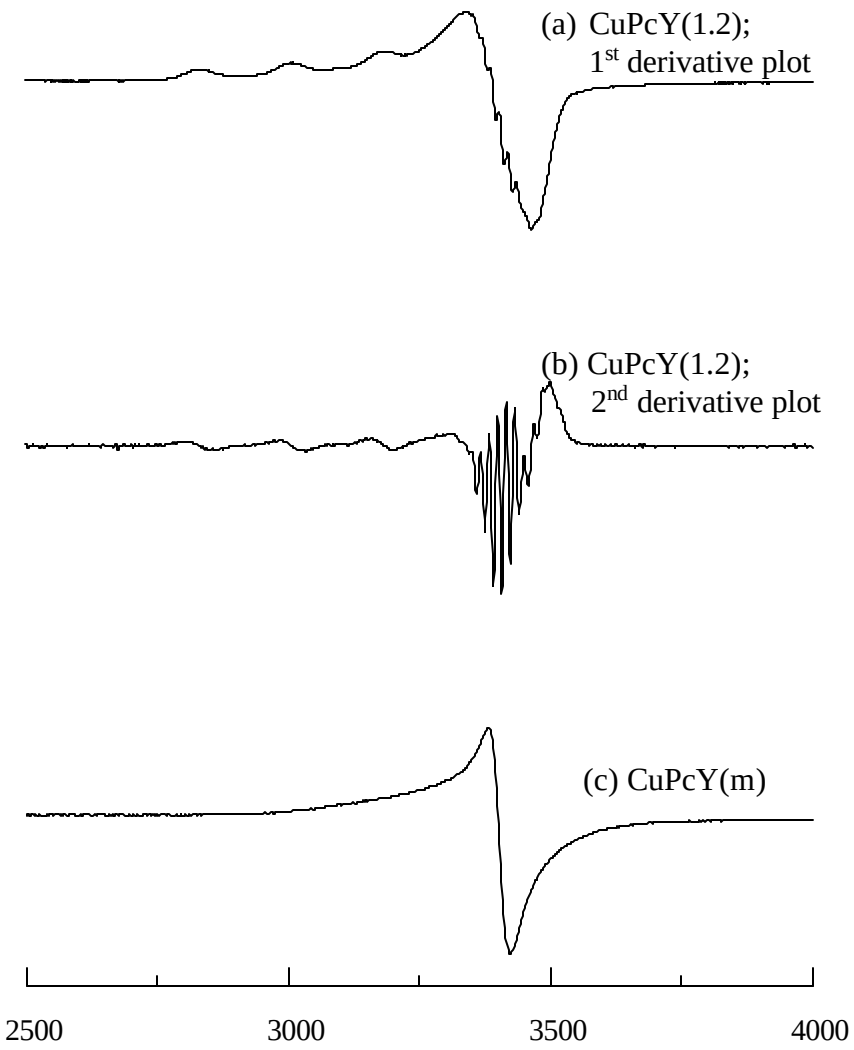

Fig. 3.17 X-band EPR spectra of (a) CuPcY(1.2); 1st derivative spectrum, (b) CuPcY(1.2); 2nd derivative spectrum and (c) CuPcY(m) at 298 K

molecules are isolated (as is the case in doped systems and frozen solutions) one would observe nine superhyperfine features due to four equivalent nitrogens of the isoindole

groups apart from the four hyperfine features due to copper [26, 27]. ^{14}N has a nuclear spin (I) of 1 while ^{63}Cu and ^{65}Cu have nuclear spin of 3/2. Indeed, such superhyperfine

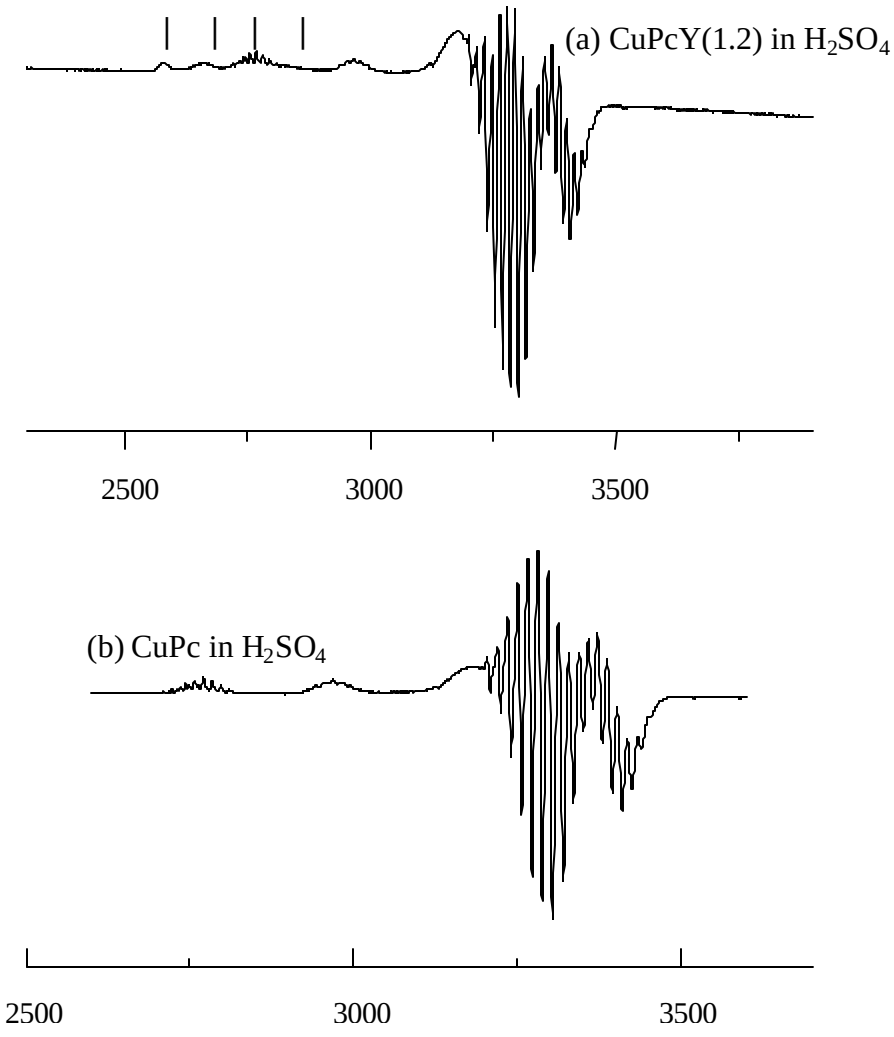

Fig. 3.18 X-band EPR spectra (77 K) of CuPcY(1.2) and CuPc dissolved in conc. H_2SO_4.

features are seen in the perpendicular region of CuPcY(1.2) (Fig. 3.17). A closer look at the spectrum shows additional marked signals corresponding to Cu(II) ions in sodalite cages. The spectrum for the physical mixture, CuPcY(m) is also shown in Fig. 3.17. Although the signals became narrow due to dilution in the physical mixture, the Hamiltonian parameters were different and hyperfine and superhyperfine features are not resolved unlike in CuPcY(1.2). The samples of CuPcY(1.2) dissolved in H_2SO_4 (Fig. 3.18(a)) showed well resolved spectra with a rich number of hyperfine and superhyperfine signals. A comparison of the spectrum with that of "neat" CuPc in H_2SO_4 (Figure 3.18(b)) clearly indicate the formation of CuPc molecules. Interestingly, hyperfine features of ^{63}Cu and ^{65}Cu isotopes were also resolved. Further, the absence of signals due to sites II' and II'' indicated that only the Cu(II) ions in the supercages or those near the hexagonal prism inside the supercages undergo complexation while the ions in the sodalite cages were not accessible for complexation.

The g values (Table 3.12) with $g_{\parallel} > g_{\perp}$ suggest that the unpaired electron of "neat" and encapsulated CuPc occupies a "formal" $3d_{x^2-y^2}$ orbital of the metal ion. Also the deviation of g and A(Cu) values from that of CuPc diluted in ZnPc and H_2Pc [22, 23] and the frozen H_2SO_4 solutions suggest a significant effect of confinement on the molecular geometry of CuPc encapsulated in zeolite Y. The larger $g_{\parallel}$ value for CuPcY(1.2) reveals a pentacoordinated geometry for copper with the Pc moiety puckered in the supercages while it is planar in "neat" complex and frozen solutions.

Spectroscopic studies as well as chemical and thermal analyses clearly indicate the formation and encapsulation of CuPc in the supercages (α-cages) of zeolite Y. The presence of additional IR peaks, a red shift in Q-bands and changes in EPR parameters

(g and A(Cu)) suggest puckering of the phthalocyanine moiety in the encapsulated state. Though exchanged Cu(II) ions are present in both the supercages (α-cages) and sodalite

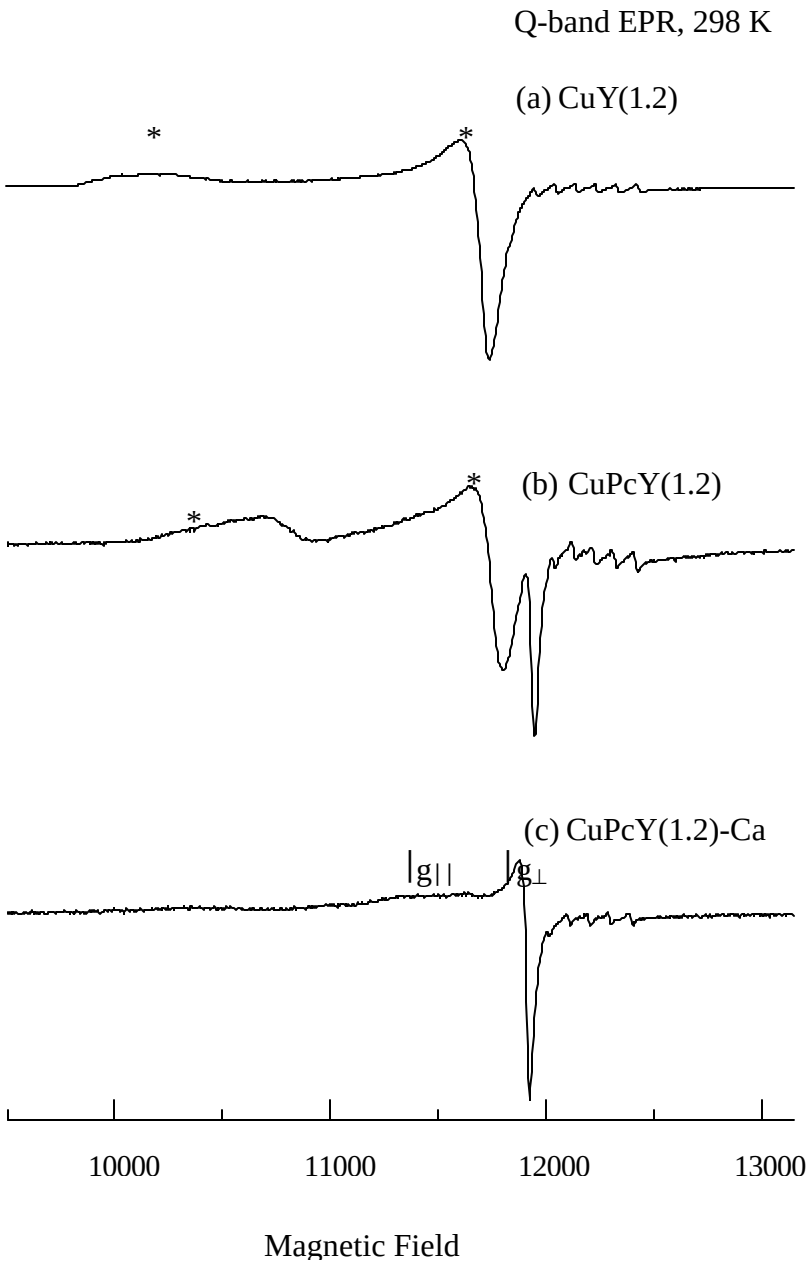

Fig. 3.19 Q-band EPR spectra (at 298 K) of (a) CuY(1.2), (b) CuPcY(1.2) and (c) CuPcY (1.2)-Ca. Asterisk (*) indicates the signals due to uncomplexed Cu(II) ions in the sodalite cages. The $g_{||}$ and $g_{\perp}$ positions of encapsulated CuPc complexes are marked. Back exchange with Ca(II) ions eliminated uncomplexed Cu(II) ions.

cages (β-cages) of CuY, only those ions in the larger α-cages react to form the CuPc complexes. The signals due to uncomplexed Cu(II) ions and encapsulated CuPc are well separated in the spectra taken at Q-band frequency (Fig. 3.19).

Table 3.12 EPR spin Hamiltonian parameters for CuY, CuPcY-1(e) and CuPcY(m)[a].

Sample	Temp. K	Species	G_{ii} (or g_x)	$g_\perp$ (or g_x, g_y)	A_{ii} (Cu) (G)	$A_\perp$ (Cu) (G)	A_{ii} (N) (G)	$A_\perp$ (N)
CuY	298	I	2.376	2.083 2.095	119.0	10.0	-	-
		II	2.166	2.166	NR	NR	-	-
	77	I	2.384	2.086	127.9	NR	-	-
		II'	2.415	2.086	119.4	NR	-	-
		II"	2.280	2.077	137.5	NR	-	-
CuPc	298		2.133	2.045	NR	NR	NR	NR
CuPcY-1 (e)	298		2.246	2.056	189.5	14.2	NR	NR
CuPcY (m)	298		2.205	2.051	NR	NR	NR	NR
CuPc in H_2SO_4	77		2.200	2.062	196.5 (207.0)	11.0 (11.0)	13.2	16.0
CuPcY-1 (e)	77		2.200	2.062	196.5 (207.0)	11.0 (11.0)	13.2	16.0

[a]NR = not resolved

3.3 Characterization of Cobalt Phthalocyanine Encapsulated in Zeolite Y: CoPcY

This section presents the studies on cobalt phthalocyanine (CoPc) complexes encapsulated in zeolite-Y. "Neat" CoPc complexes are blue in colour while the encapsulated complexes are greenish blue.

3.3.1 X-ray diffraction

The XRD patterns of the encapsulated complexes do not reveal any significant differences from that of the pure Y zeolite (Fig. 3.11a) indicating that the molecular sieve has not undergone any structural changes due to the encapsulation of the complex.

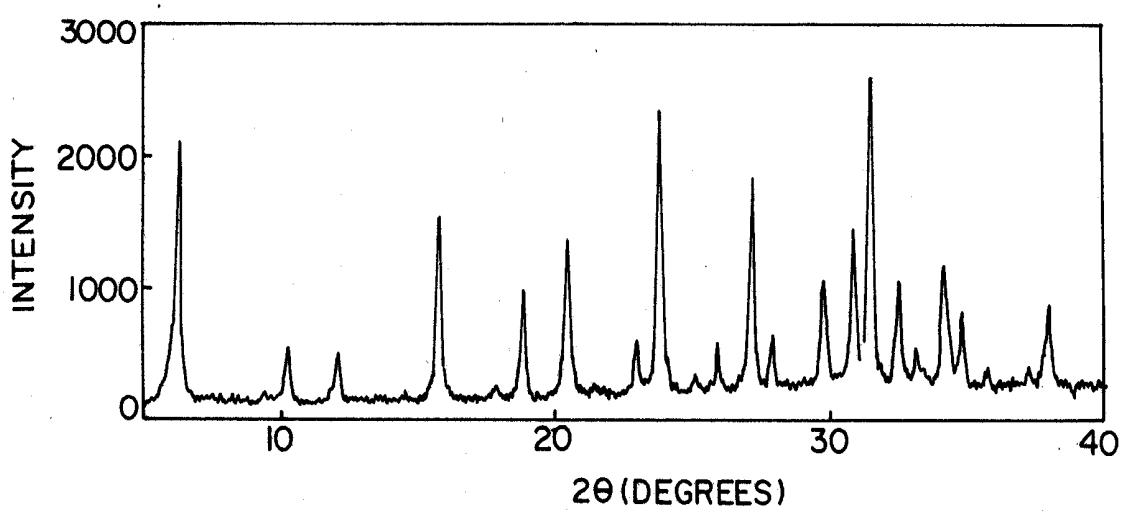

Fig. 3.20 XRD patterns of CoPc encapsulated in zeolite Y (CoPcY (1.2))

The X-ray diffractogram of an enacpsulated CoPc complex (CoPcY (1.2)) is presented in Fig.3.20.

3.3.2 Chemical and thermal analyses of CoPcY

The chemical analysis of the CoPcY samples reveals the presence of organic matter with N/C ratio similar to that of phthalocyanine. The thermal decomposition of the encapsulated CoPc complexes (Fig. 3.21) showed three stages of weight loss. The first

stage below 423 K corresponds to the loss of intra-zeolite water molecules and the other two stages in the temperature range 423 - 873 K correspond to the decomposition of Pc molecules. While the "neat" CoPc complex shows decomposition in a narrow temperature

Table 3.13

TGA/DTG analysis of "neat" CoPc and CoPcY samples: weight loss and decomposition temperatures

Sample	Weight loss (%) in stages		
	Stage I	Stage II	Stage III
CoPc (neat)			86.1 [733 K][a] (550 - 840 K)[b]
CoPcY(0.6)	9.9 [377 K] (303 - 445 K)	8.1 [523 K] (448 - 619 K)	4.8 [735 K] (650 - 863 K)
CoPcY(1.0)	5.8 [374 K] (303 - 423 K)	9.4 [520 K] (423 - 642 K)	7.6 [725 K] (658 - 796 K)
CoPcY(1.2)	6.3 [375 K] (303 - 318 K)	9.4 [530 K] (423 - 673 K)	6.7 [712 K] (673 - 812 K)
Assignments	Condensed and physically adsorbed water in zeolite-Y	Chemisorbed water (in the form of OH groups) in zeolite-Y	Organic matter as Pc moiety in zeolite-Y

[a]Peak temperature.
[b]Weight loss-temperature.

range (550 - 840 K), the encapsulated complexes decompose in a broader temperature range (423 - 873 K). This is in agreement with the observation on CuPcY complexes. The results suggest that thermal stability of CoPc complex is increased on encapsulation. The samples with 1.0 and 1.2 wt.% Co showed the presence of more organic material (as

evidenced from greater weight loss) than that for CoPcY(0.6) sample; Table 3.13 presents the thermal analyses data of the samples.

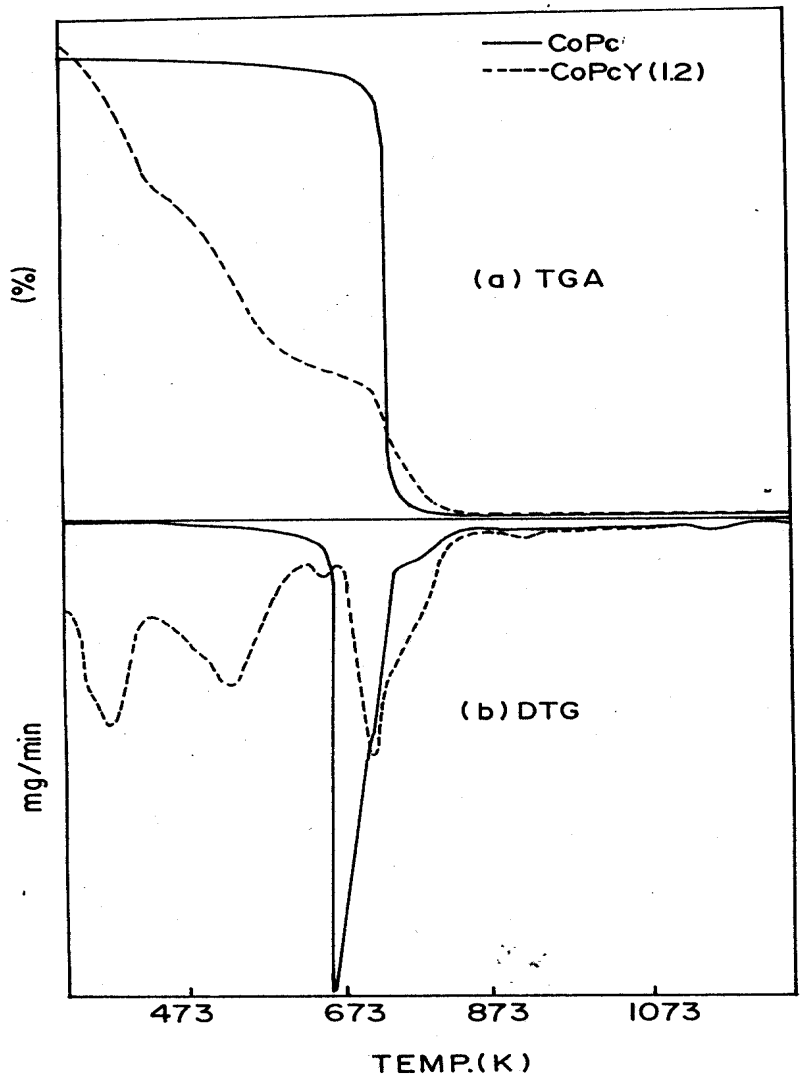

Fig. 3.21 TGA and DTA plots of (a) "neat" CoPc and (b) CoPcY(1.2)

3.3.3 N_2 adsorption studies

The surface areas of CoPcY samples, as measured from N_2 adsorption studies, were smaller than for CoY samples and provide evidence for the formation of CoPc inside the zeolite pores. Further, the S_{BET} of CoPcY samples decreased with an increase in

metal content. Pore volume also decreased from 0.52 (for CoY(1.2)) to 0.26 ml/g (for CoPcY(1.2)).

Table 3.14

N_2 adsorption data for CoPcY

Sample	Co (wt.%)	S_{BET} (m^2/g)*	Pore volume (ml/g)
CoPcY(0.6)	0.6	553.6	0.44
CoPcY(1.0)	1.0	519.9	0.34
CoPcY(1.2)	1.2	312.9	0.26
CoY(1.2)	1.2	667.2	0.52

* degassing of sample done at 423 K and 10^{-5} mm prior to N_2 adsorption

This behaviour is similar to that of CuPcY samples. Table 3.14 presents the micropore volume and BET surface areas of CoY and CoPcY samples. The non-uniformity in decrease of surface area with an increase in metal content is perhaps due to metal complex encapsulation occuring mostly at the periphery of the crystallites.

3.3.4 FT-IR spectra of "neat" and encapsulated CoPc complexes

Fig. 3.22 shows the FT-IR spectra of CoY, CoPcY and "neat" CoPc samples. Though the zeolite bands dominate the spectra of encapsulated complexes, the presence of characteristic bands due to the complex are easily discerned. The bands at 1542, 1487 and 1332 cm^{-1} are attributable to C=C and C=N stretching modes of the macrocycle Pc moiety. The band at 1091 cm^{-1} corresponds to C-N vibrational mode while the bands at 1053 and 1120 cm^{-1} are attributed to the skeletal vibrational modes. The positions of these bands have shifted on encapsulation.

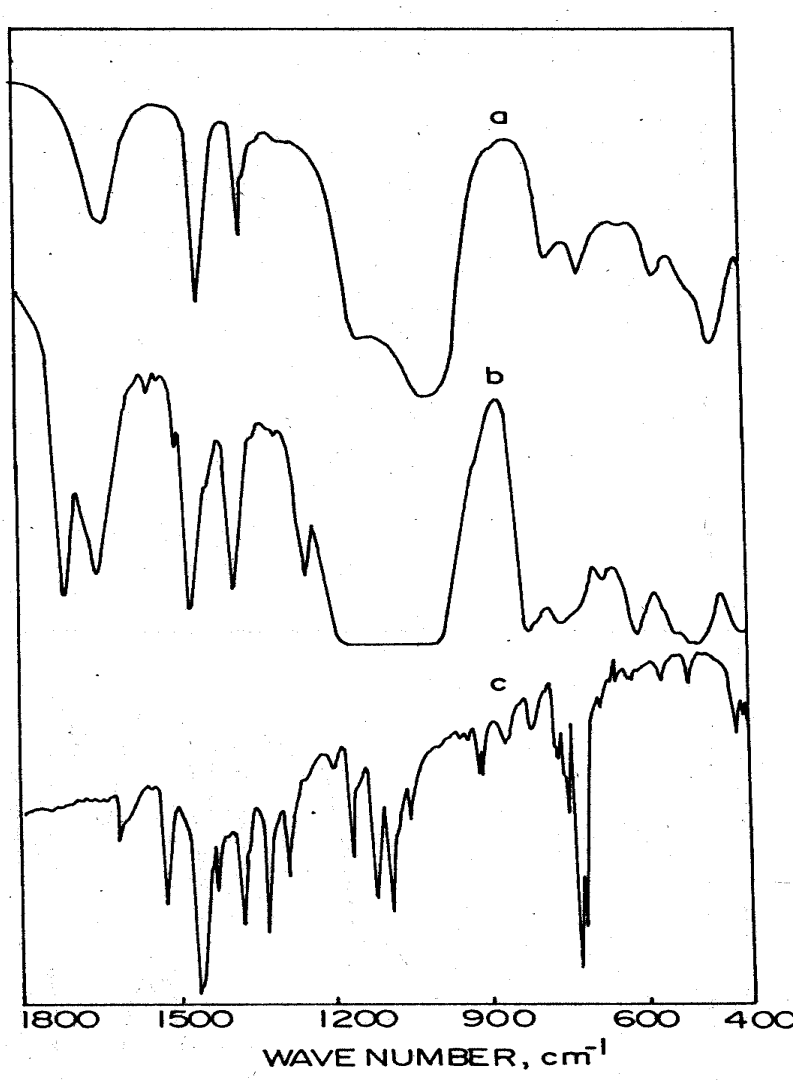

Fig. 3.22 FT-IR spectra of (a) CoY(1.2), (b) CoPcY(1.2) and (c) "neat" CoPc samples as nujol mulls

Table 3.15

FT-IR spectal data for "neat" and zeolite-Y-encapsulated CoPc complexes

Samples	ν (C=C)	ν (C=N)	ν (C-N)	Skeletal
CoPc	1524, 1332	1466	1092	1120, 1053
CoPcY	1543, 1333	1487		

3.3.5 UV-Vis spectra of "neat" CoPc and CoPcY samples

The DRUV-Vis spectra of "neat" CoPc and CoPcY samples are shown in Fig. 3.23. The UV-Vis data are listed in Table 3.16. "Neat" CoPc shows two resolved Q-bands at 618 and 678 nm, respectively. However, CoPc diluted in $BaSO_4$ showed two additional Q-bands as shoulders. These bands for diluted CoPc (5 wt. %) appeared at 572 (sh), 615, 681 and 725 (c) nm. On the other hand the encapsulated complexes showed only three Q-bands. The band in the low energy side was better resolved in encapsulated complexes. These bands for CoPcY appeared at 611, 676 and 736 nm, respectively. In other words, the Q bands appearing in the visible region (572 - 725) due to ligand centered π-π^* transitions have red shifted in zeolite-encapsulated complexes. Similar shifts on encapsulation were observed also for CuPcY samples (*vide supra*). The shift and resolution in Q-bands is due to dilution and deformation of planar Pc moiety as a consequence of encapsulation in the supercages of zeolite-Y. "Neat" complexes showed a partially resolved Soret band at 366 nm. This band could not be identified in encapsulated complexes as it merged with other absorption bands. "Neat" CoPc showed only two bands while "neat" CuPc showed four Q-bands. Also considerable shifts in Q and Soret band positions can be noticed in the "neat" and encapsulated CoPc complexes. The Soret band

Table 3.16

Electronic spectral data for "neat" CoPc and CoPcY

Sample	Soret band, nm	Q-bands, nm
CoPc (neat)	366	618, 678
CoPc(5%)-$BaSO_4$	366	572, 615, 681, 725
CoPcY(0.6)		611, 676, 736

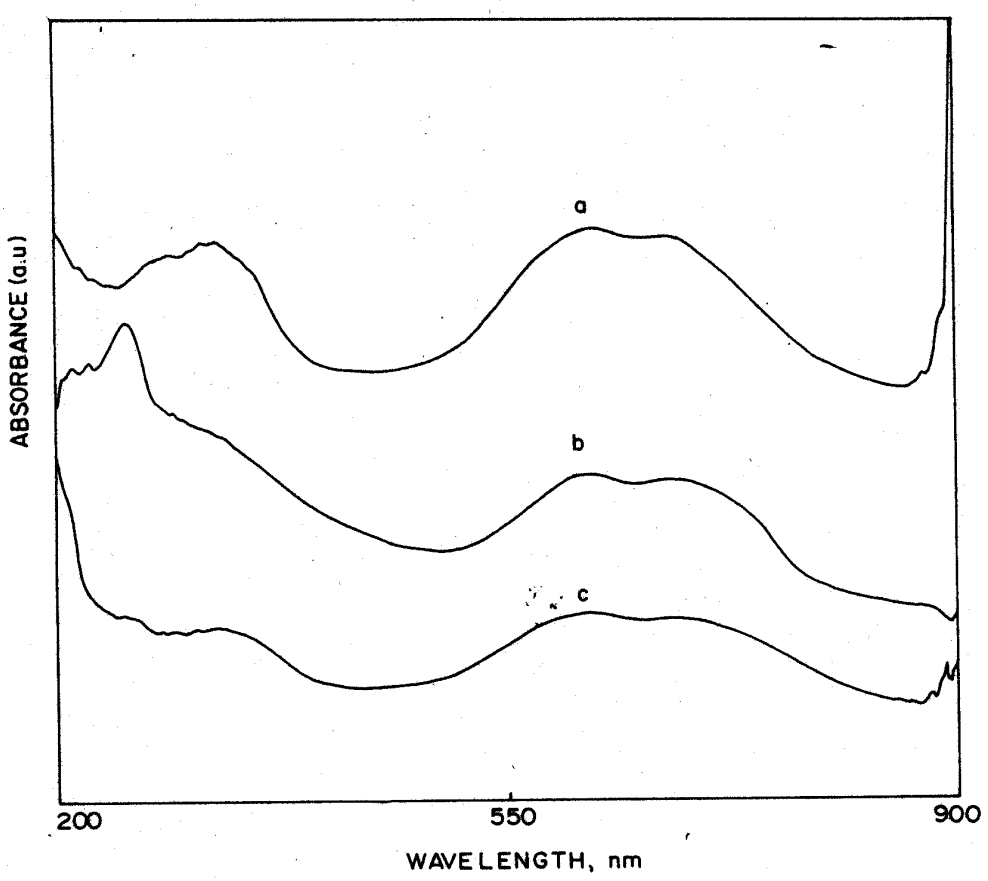

Fig. 23 DRUV-Vis spectra of (a)"neat" CoPc, (b) CoPcY (0.6) and (c) CoPc-$BaSO_4$ (5 wt.%)

is blue shifted (from 429 nm in CuPc to 366 nm in CoPc) while the Q-bands were red shifted. This suggests that the central metal ion modulates the energy levels of π/π^* molecular orbitals.

3.3.6 EPR spectra of "neat" and encapsulated CoPc complexes

Powder samples of "neat" CoPc, at 77 K, showed a broad featureless signal centered at $g \approx 2.6$. In addition to this, weak narrow signals superimposed on the broad signal (Fig. 3.24) appeared at $g \approx 2.05$ and 1.98. The latter signal (at $g \approx 1.98$) is an organic radical impurity.

The cobalt complexes, depending on the ligand field strength, can be in a high spin ($t_{2g}^5e_g^2$; S = 3/2) or low spin ($t_{2g}^6e_g^1$; S = ½) electronic configuration. However, in complexes with nitrogen donor ligands, the electron spin paring energy is, generally, of the order of ligand field stabilizational energy. Hence, these complexes exhibit spin crossover or spin equilibrium phenomenon. A subtle change in physical parameters like temperature or pressure, alters the electronic structure from a high spin to a low spin state or *vice versa*. In spin crossover complexes the system undergoes a complete transition from a high spin (S = 3/2) to a low spin (S = ½) state. While in the spin equilibrium phenomenon both the spin states co-exist even at low temperatures. The EPR signals for a high spin Co(II) system are usually broad at ambient temperatures. Narrow signals can,

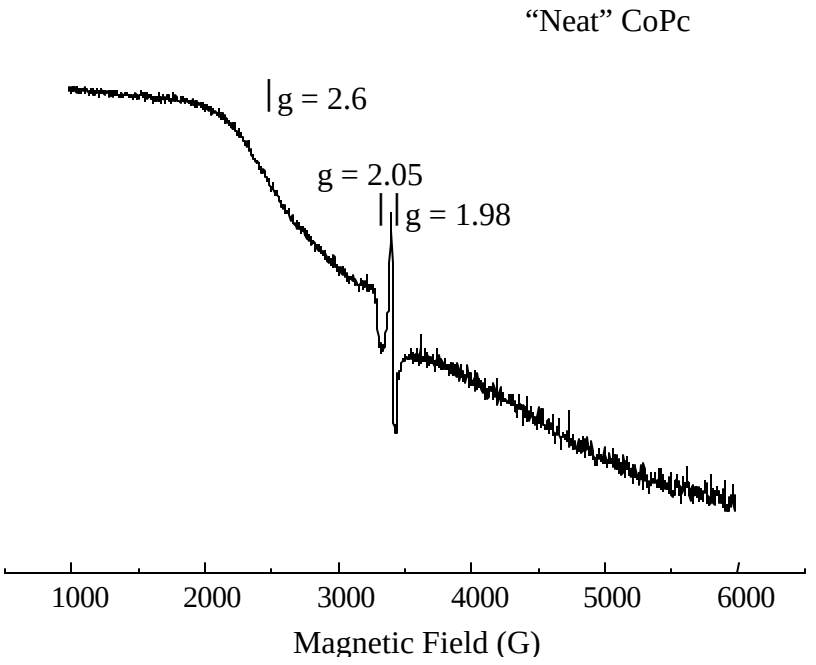

Fig. 3.24 EPR spectrum (77 K) of powder CoPc at 298 K.

however, be observed at liquid He temperatures. The high spin species is characterized by large g-anisotropy (0.6 - 7.0). The low spin Co(II) complex, on the other hand, is characterized by narrow EPR signals with small g-anisotropy (2.4 - 2.0).

The broad signal at g = 2.6 in "neat" CoPc complexes is attributed to high spin electronic configuration. The signal at g = 2.05 corresponds to Co(III)-superoxo ions. The spectra (at 77 K) for CoPcY(0.6), CoPcY(1.0) and CoPcY(1.2) are shown in Fig. 3.25. Distinct changes could be noticed in the EPR spectra with increasing amounts of metal complex in zeolite Y. The spectra of the encapsulated complexes in general contained three types of signals. The broad featureless signal with $g_{\perp}$ = 2.74 corresponds to high spin CoPc complexes. The narrow signals at g_1 = 2.201, g_2 = 2.001 and g_3 = 1.985 correspond to Co(III)-superoxo radical anion species. A closer observation reveals further splitting of g_1 signal due to superhyperfine coupling interaction between the electron spin of $O_2^{-}\cdot$ ions (S = ½) and the nuclear spin of cobalt (I = 7/2). The intensity of the superoxo signals increased with increasing metal content. However, as the concentration of metal ion increased the intensity of high spin CoPc signal (g = 2.74) decreased. The low spin type CoPc complexes were observed in samples with metal loading of 1.2 wt.%. From these observations it can be concluded that CoPc molecules located inside have a high spin electronic configuration while those near the surface (in the case of CoPcY(1.2)) have a low spin electronic configuration. The increase in intensity of superoxo signals with increasing metal content suggests that the CoPc complexes near the surface are

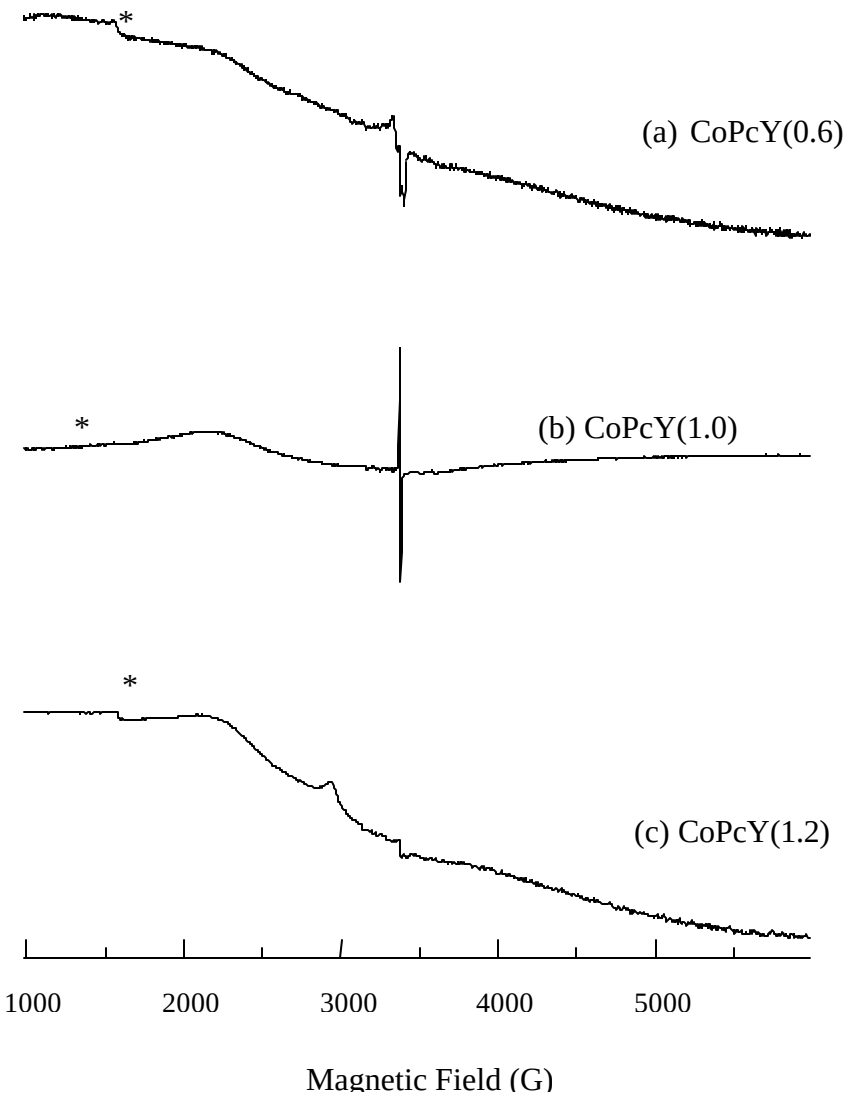

Fig. 3.25 EPR spectra (77 K) of (a) CoPcY(0.6), (b) CoPcY(1.0) and (c) CoPcY(1.2). Asterisk indicates impurity iron(III) signal.

perhaps responsible for the formation of dioxygen adducts. The g parameters of zeolite-encapsulated $Co(O_2^{-}\cdot)$ species fall well within the range of values reported for related cobalt systems.

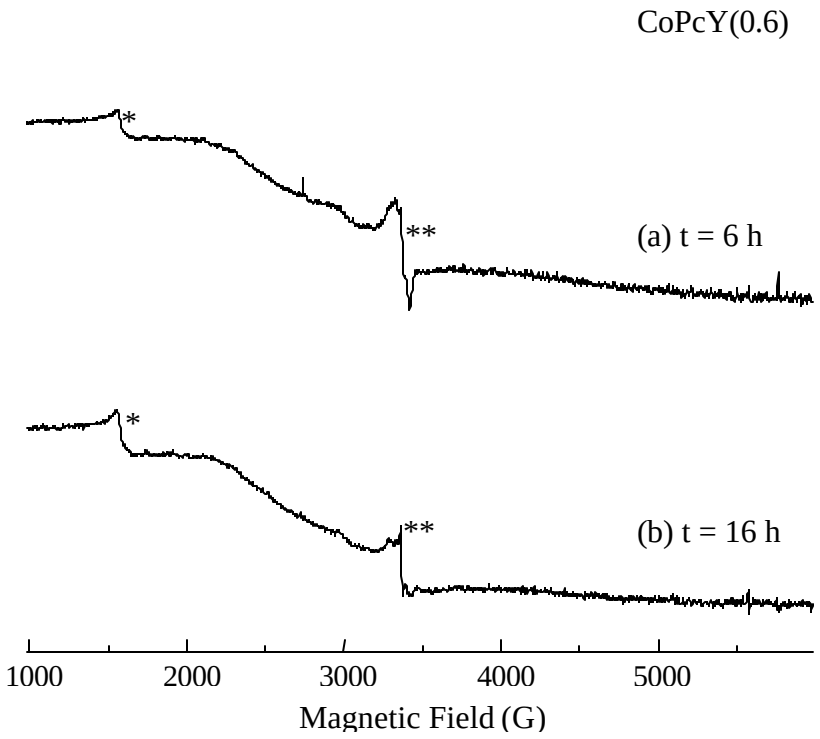

Fig. 3. 26 EPR spectra of CoPcY(0.6) evacuated for (a) 6 h and (b) 16 h. Signal due to iron(III) impurity is denoted by * and signals due to Co($O_2^{-}\cdot$) are donoted by **.

The stability of Co(III)-superoxide species in encapsulated complexes was examined by evaluating (373 K, 10^{-2}mm) the samples for several hours. The spectra of CoPcY(0.6) after 6 and 16 hrs of evacuation are shown in Fig. 3.26. The superoxo species were stable even after 16 hrs of evacuation. In samples evacuated for 16 hrs, a slight decrease in intensity EPR signal of superoxo species (by about 20 %) was noticed. The signals became narrow and the cobalt hyperfine features became more visible in the g_1 region. This suggests that the zeolite mantle stabilizes the Co(III)-superoxo species.

3.4 Characterization of Vanadium Phthalocyanine Encapsulated in Zeolite Y: VpcY

3.4.1 X-ray diffraction

The X-ray diffractogram of VPcY(1.2) is shown in Fig. 3.27. The XRD pattern of the encapsulated complex does not reveal any significant differences from that of the pure Y zeolite (Fig. 3.11) indicating that the molecular sieve has not undergone any structural changes due to the encapsulation of the complex.

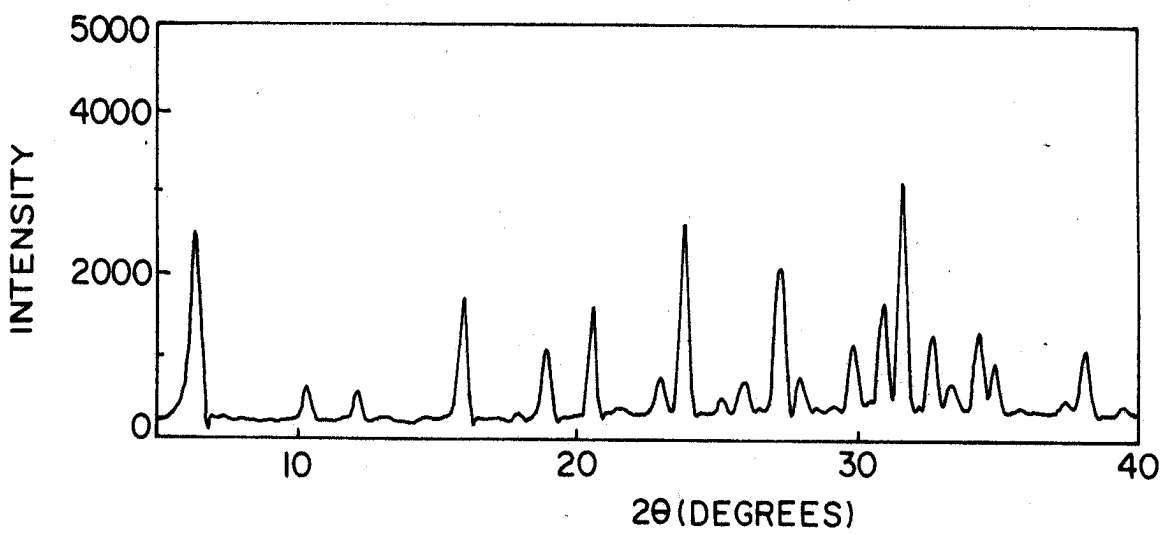

Fig. 3.27 XRD pattern of VPc encapsulated zeolite Y (VPcY(1.2))

3.4.2. Chemical and thermal analyses of VPcY samples

The chemical analysis of VPcY samples revealed the presence of organic matter with N/C ratio similar to that of phthalocyanine (Table 3.17). The total organic contents of the samples suggest the presence of 1 and 3 Pc molecules per unit cell in VPcY samples with metal loading of 1.2 and 1.6 wt%, respectively.

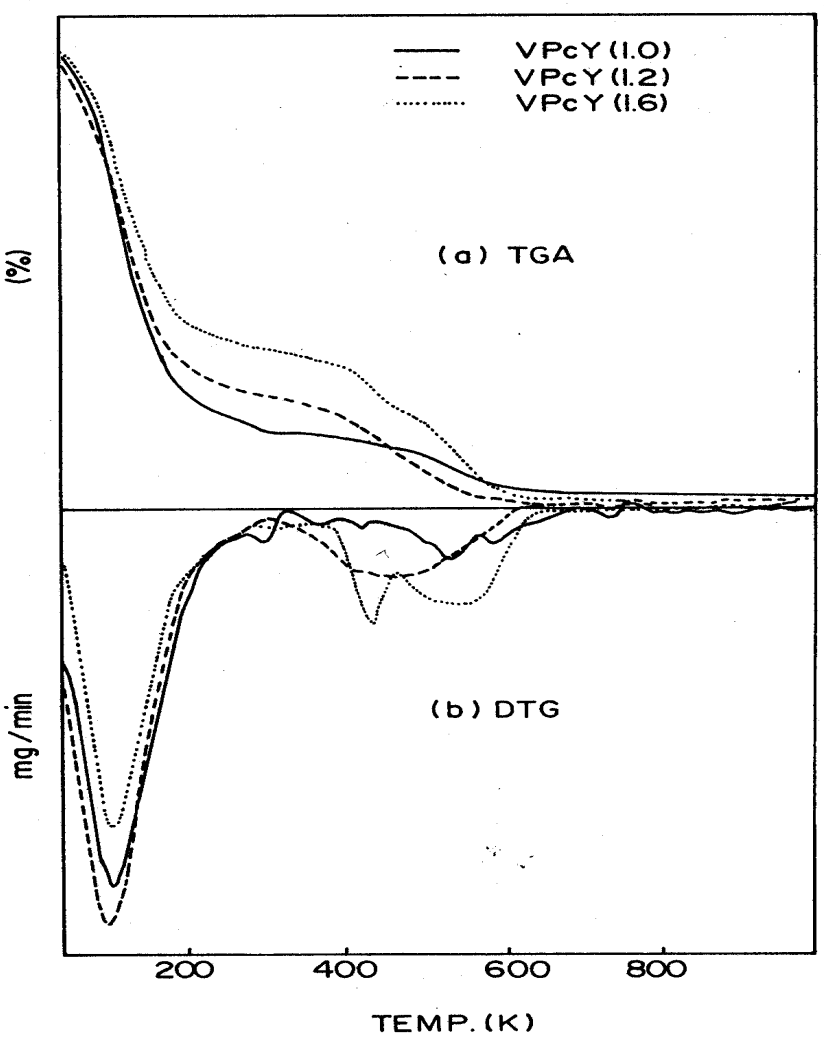

Fig. 3.28 TGA and DTA of (—) VPcY (1.0),(----) VPcY(1.2) and (….) VPcY(1.6)

Encapsulated VPc complexes (Fig. 3.28) showed three stages of weight loss. The first stage (304 - 523 K) corresponds to the loss of intra-zeolite water molecules and the other two stages (523 - 903 K) with peak maxima at 692 and 803 K, respectively, correspond to the decomposition of Pc ligand. The weight loss corresponding to the Pc ligand is low in the samples with metal contents of 1.0 and 1.2 wt.%. Pc decomposition mainly occurs at 692 K. However, the samples with 1.6 wt.% V showed Pc decomposition at peak maxima of 692 and 803 K. This reveals that the complexes with higher metal

loading (1.6 %) contain at least two types of Pc molecules viz., encapsulated VPc in bulk and encapsulated VPc near the surface. The latter type of compounds decompose at lower temperatures (692 K). As observed in CuPcY and CoPcY samples, the encapsulated complexes decompose in a broader temperature range than the "neat" complexes. From the weight losses the VPc molecules in zeolite Y were estimated to be 0.9, 1.0 and 3.0 in samples VPcY(1.0), VPcY(1.2) and VPc(1.6), respectively. A comparative study of Cu, Co and V complexes reveal that the central metal ion and perhaps the metal-ligand bonding affect the Pc decomposition temperature. This temperature for encapsulated MPc complexes varies with the metal ion in the order: Co > Cu > V.

Table 3.17

Chemical and thermal characterization of VPcY

Sample	V (wt.%)	C/N analysis (wt.%)		molecules/ unit cell
		C	N	Pc
VPcY(1.2)	1.2	2.04	0.53	1.0
VPcY(1.6)	1.6	7.02	2.08	3.0

* Degassing of sample was done at 423 K and 10^{-5} mm.

3.4.3 N_2 adsorption studies

The surface areas of VPcY samples as measured from N_2 adsorption studies were found to be lower than VY samples. Table 3.18 presents the micro-pore volume and surface areas of VY and VPcY samples.

Table 3.18

N_2 adsorption data for VY and VPcY samples

Sample	V (wt.%)	S_{BET}* (m^2/g)	Pore volume (ml/g)
VPcY(1.0)	1.0	584.3	0.581
VPcY(1.2)	1.2	448.3	0.558
VPcY(1.6)	1.6	387.8	0.498

* degassing of sample done at 423 K and 10^{-5} mm prior to N_2 adsorption

3.4.4 FT-IR spectra of VPcY samples

The bands due to the Pc moiety were masked by the characteristic zeolite bands in the FT-IR spectra of VPcY samples. However, from the weak bands at 1547, 1489, 1461 and 1335 cm^{-1}, attributable to C=C and C=N stretching modes, the formation of VPc complexes inside zeolite Y can be discerned.

3.4.5 DRUV-Vis spectra of VPcY samples

The UV-Vis spectra of VPcY(1.0 and 1.6) are shown in Fig. 3.29. The encapsulated complexes showed three partially resolved Q-bands at 650, 712 and 810 nm , respectively. These bands were broad in VPcY(1.6) (Fig. 3.29(b)). This is probably due to the presence of more than one type of Pc molecules as revealed from the thermal analysis. It is interesting to note that the position of the Q-bands shifts towards lower energy side with a change in the central metal ion. This shift to lower energy side increases for encapsulated complexes in the order V > Cu > Co. The red shift in Q-band positions was

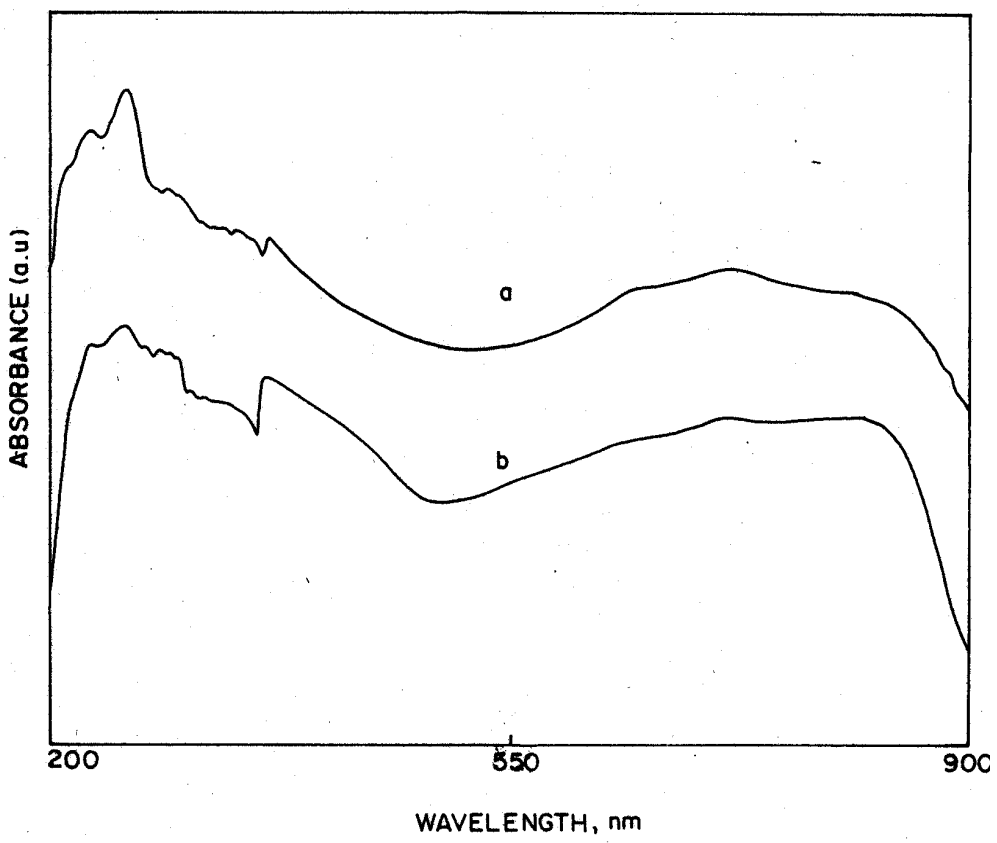

Fig. 3.29 DRUV-Vis spectra of (a) VPcY(1.0) and (b) VPcY(1.2)

attributed to lowering of Pc molecular symmetry and pentacoordination around the metal ions. The order in red shift with different central metal ions perhaps reveals that the Pc moiety is more distorted in encapsulated VPc than in CuPc and CoPc complexes. The vanadium ion probably forms a penta-coordinated structure making an axial coordination with the oxygen atom of zeolite mantle. The shift in Q-band position is in line with the variation in the decomposition temperature of Pc moiety.

3.4.6 EPR studies on VPcY samples

Vanadium(IV) ions are paramagnetic and have one unpaired electron. ^{51}V has a nuclear spin (I) of 7/2. If the symmetry around vanadium is cubic, one would observe eight hyperfine features. On the other hand if vanadium possesses a tetragonal symmetry

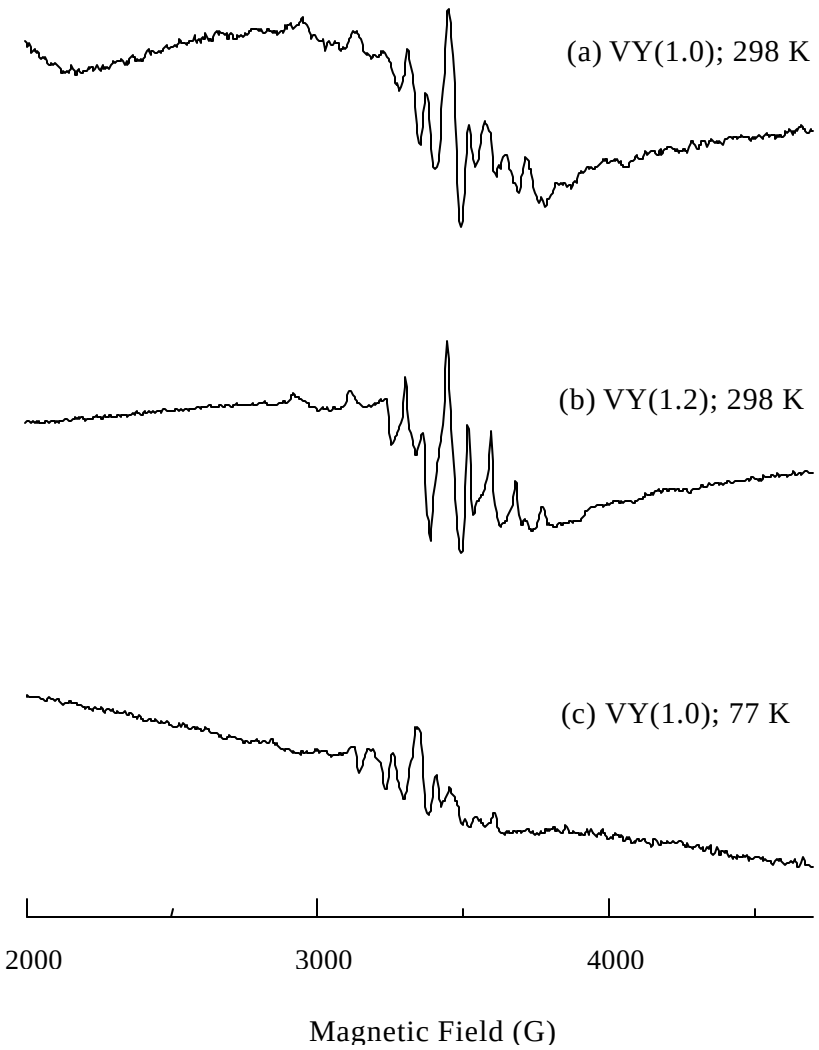

Fig. 3.30 EPR spectra of (a) VY(1.0) at 298 K, (b) VY(1.2) at 298 K and (c) VY(1.0) at 77 K.

two sets of eight hyperfine signals are observed corresponding to parallel and perpendicular orientations. The EPR spectra of vanadium exchanged NaY samples correspond to tetragonal symmetry. Typical spectra for VY (1.0 and 1.2 wt.%) at 298 and 77 K are shown in Fig. 3.30. The spin Hamiltonian parameters are $g_{\|} = 1.937$, $g_{\perp} = 1.995$,

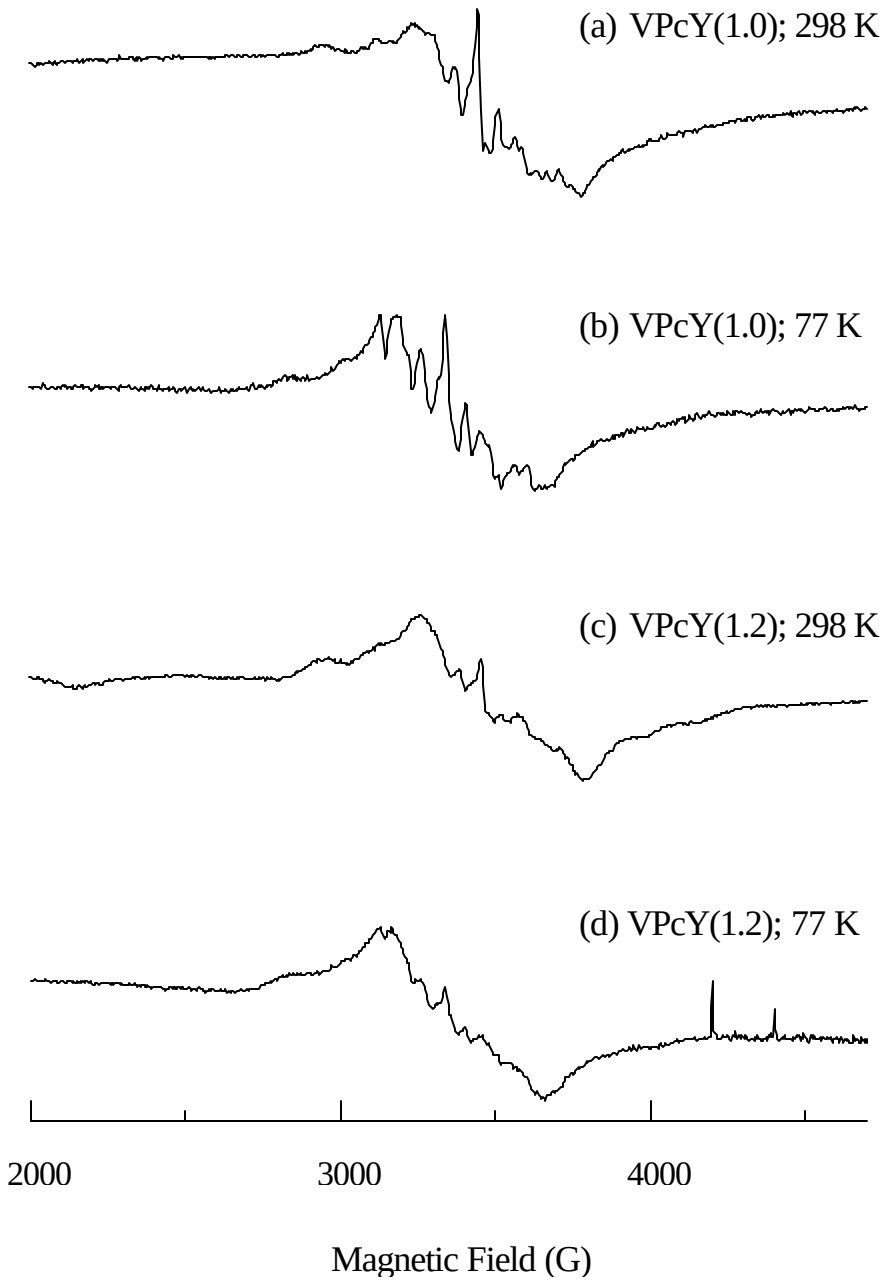

Fig. 3.31 EPR spectra of VPcY samples at 298 K and 77 K.

$A_{||}(V)$ = 195.1 G and $A_{\perp}$ = 77.1 G. The broad signal on which the vanadium hyperfine features are superimposed corresponds to vanadium species with multi-nuclearity. At lower temperatures (77 K), the broad signal disappears due to antiferromagnetic interaction among the vanadium centers.

On metal complex encapsulation, the zeolite samples which were pale green became blue in colour. Also marked changes in the EPR were observed. The spectra for VPcY (1.0 and 1.2) are shown in Fig. 3.31. The spectra of VPcY samples are axially symmetric and the spin Hamiltonian parameters of the encapsulated complexes are $g_{||}$ = 1.968, $g_{\perp}$ = 2.000, $A_{||}(V)$ = 170.0 G and $A_{\perp}(V)$ = 60.7 G. In both VY and VPcY samples, $g_{||} < g_{\perp}$. This suggests that the unpaired electron of vanadium resides in d_{xy} orbital. The vanadium hyperfine coupling constant is reduced for encapsulated complex due to the delocalization of the electron density onto Pc moiety. Similar changes in hyperfine coupling constant due to complexation and encapsulation were also observed in CuPc complexes (*vide supra*). With increasing metal content the signals due to encapsulated VPc became broader as revealed from the spectrum of VPcY(1.2) (Fig. 3.31(c and d)). This broadness is due to dipole-dipole interactions as well as the presence of more than one type of VPc molecules in the zeolite (molecules situated in the bulk and those at the surface).

3.5 Characterization of Iron Phthalocyanine Encapsulated in ETS-10: FePc-ETS-10

3.5.1 X-ray diffraction of FePc-ETS-10

XRD patterns of ETS-10 and FePc-ETS-10 (before and after solvent extractions) are shown in Fig. 3.32 The crystallinity of ETS-10 was retained even after FePc encapsulation.

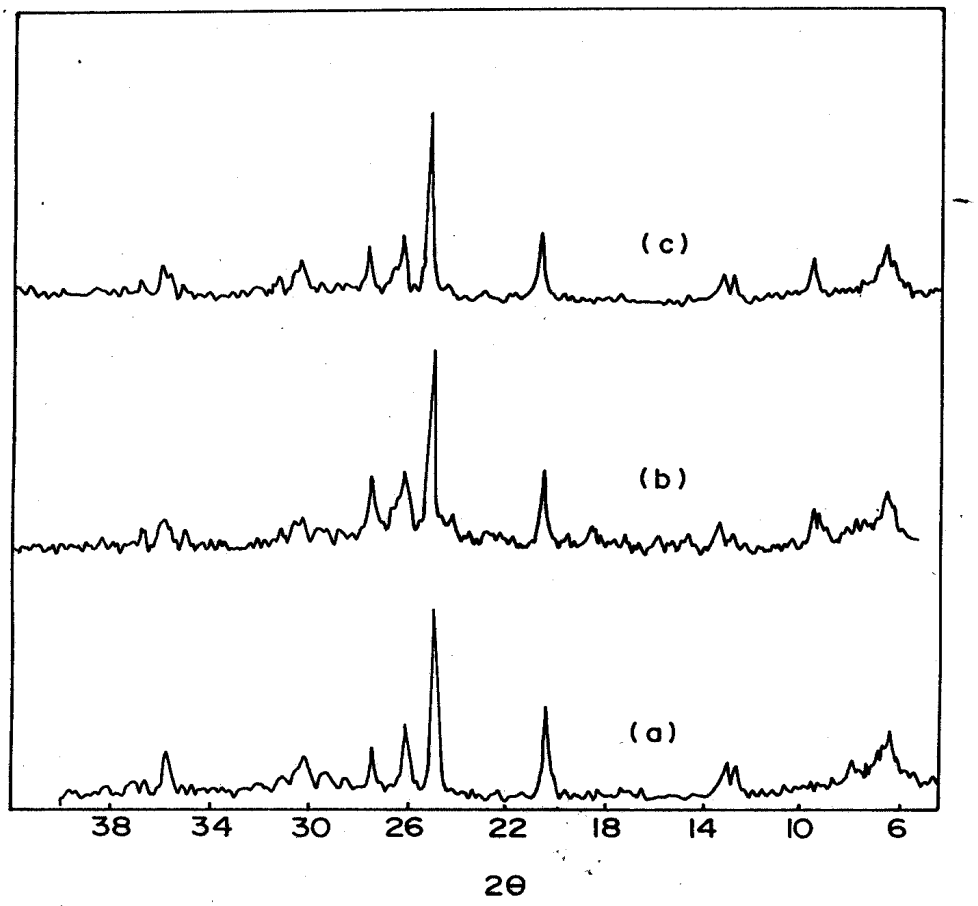

Fig. 3.32 XRD patterns of (a) ETS-10, (b) FePcETS-10 (ne) and (c) FePcETS-10 (e)

3.5.2. Thermal analysis of FePc-ETS-10 samples

The TGA/DTA profiles of ETS-10, "neat" FePc and FePc-ETS-10 are shown in Fig. 3.33. DTA of "neat" FePc shows a broad exotherm in the temperature range 500 - 898 K corresponding to the oxidative decomposition of Pc moiety. The exotherm has T_{max} at 657 K and a shoulder at 873 K. The oxidative decomposition of encapsulated FePc complexes occurs with peak maximum at 748 K. This shift of 91 K in FePc-ETS-10 sample suggests higher thermal stability of FePc complexes when encapsulated in zeolite ETS-10. In contrast to that observed in zeolite-Y, the complexes encapsulated in ETS-10 decompose in a narrow temperature. This suggest a better homogeneity of metal complex structure in ETS-10 than in zeolite-Y samples. The sharp endotherm in the temperature

range 948 - 1023 K in ETS-10 and FePc-ETS-10 is related to distruction zeolite framework structure.

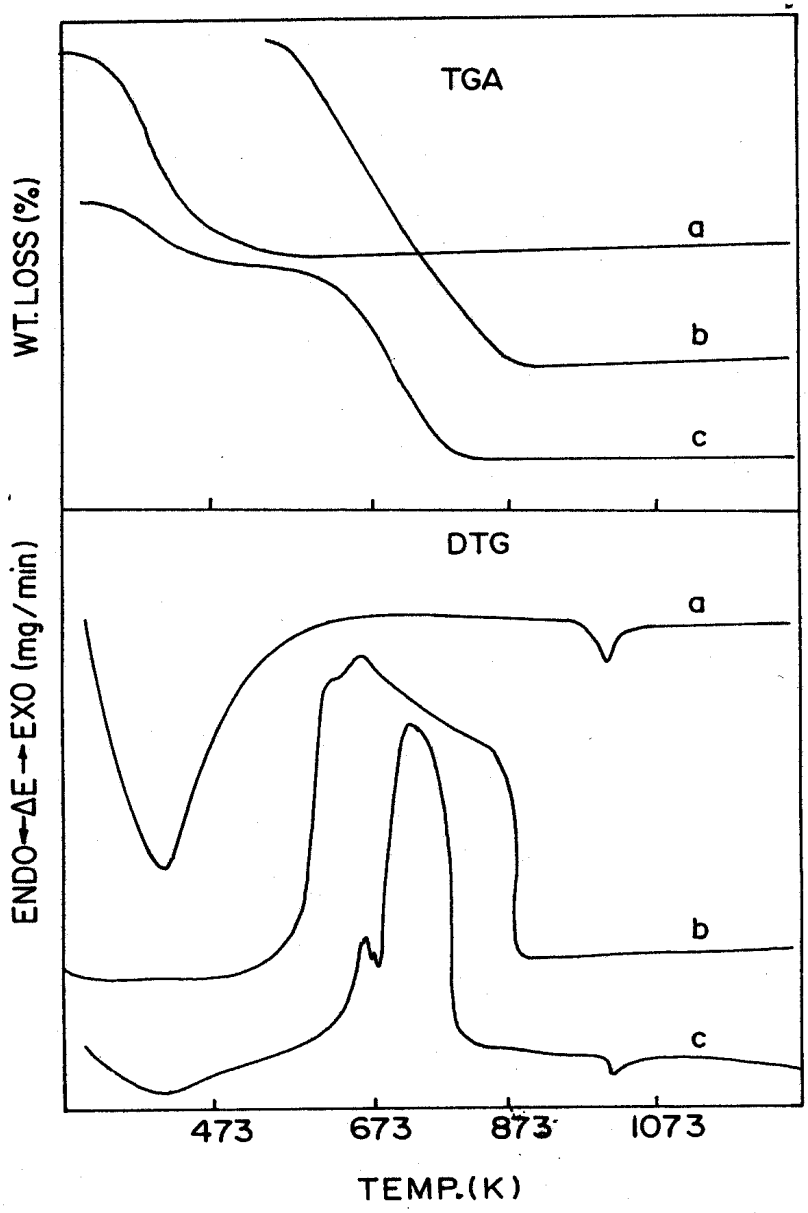

Fig. 3.33 TGA and DTA profiles of (a) ETS-10, (b) FePc and (c) FePcETS-10

3.5.3 FT-IR spectra of FePc-ETS-10 samples

The FT-IR spectra of FePc and FePc-ETS-10 are shown in Fig. 3.34. Encapsulation of FePc complexes in ETS-10 has negligible effect on the positions of the characteristic Pc bands. This is in contrast to that observed for zeolite Y encapsulated complexes where marked shifts in band positions [26] were observed. This observation

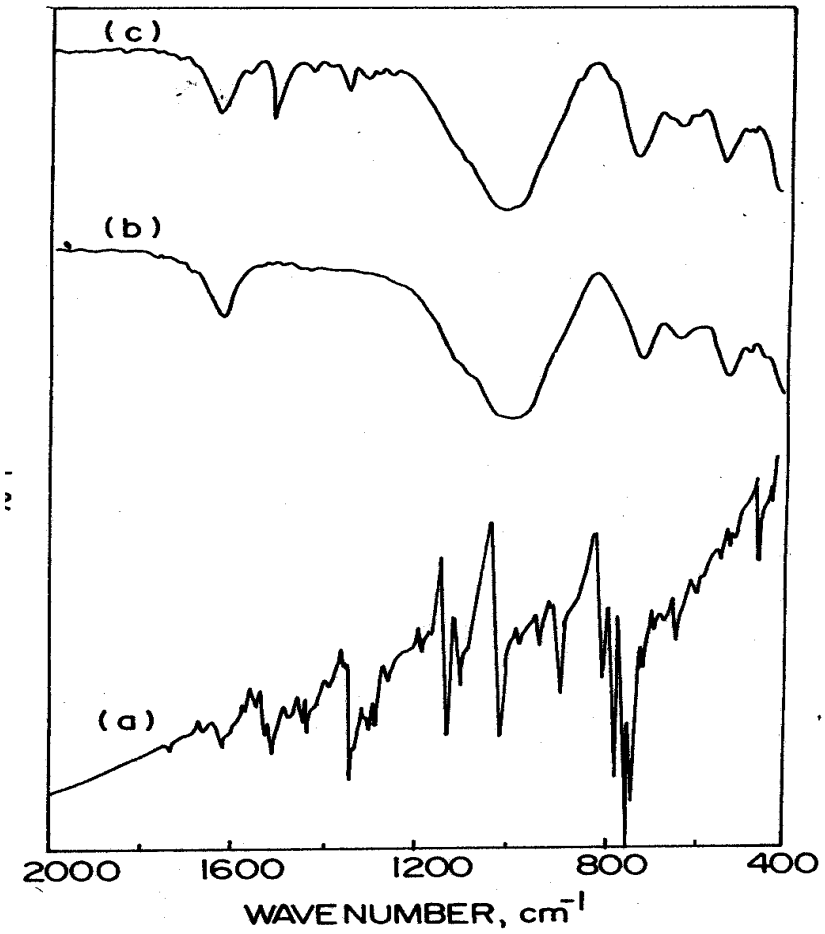

Fig. 3.34 FT-IR spectra of (a) FePc, (b) ETS-10 and (c) FePcETS-10.

reveals that the molecular symmetry of FePc complex is perhaps unchanged even after encapsulation in ETS-10 while the Pc moiety undergoes a considerable change when encapsulated in zeolite-Y.

3.5.4 MAS-NMR studies on FePc-ETS-10 samples

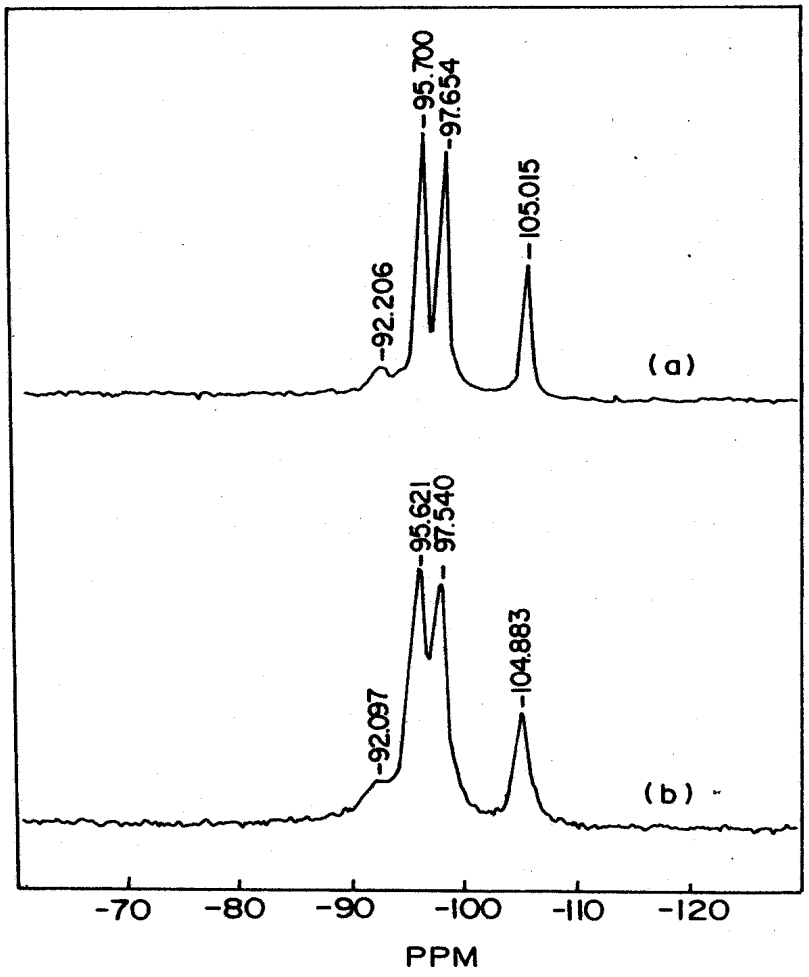

Fig. 3.35 ^{29}Si MAS NMR of (a) ETS-10 and (b) FePcETS-10

The ^{29}Si MAS NMR spectra of ETS-10 (Fig. 3.35(a)) showed three sharp signals at δ = -95.7, -97.7 and –105.0 ppm indicating the presence of at least three magnetically inequivalent silicon ions in ETS-10. The small peak at –92.2 is due a silicon impurity[27].

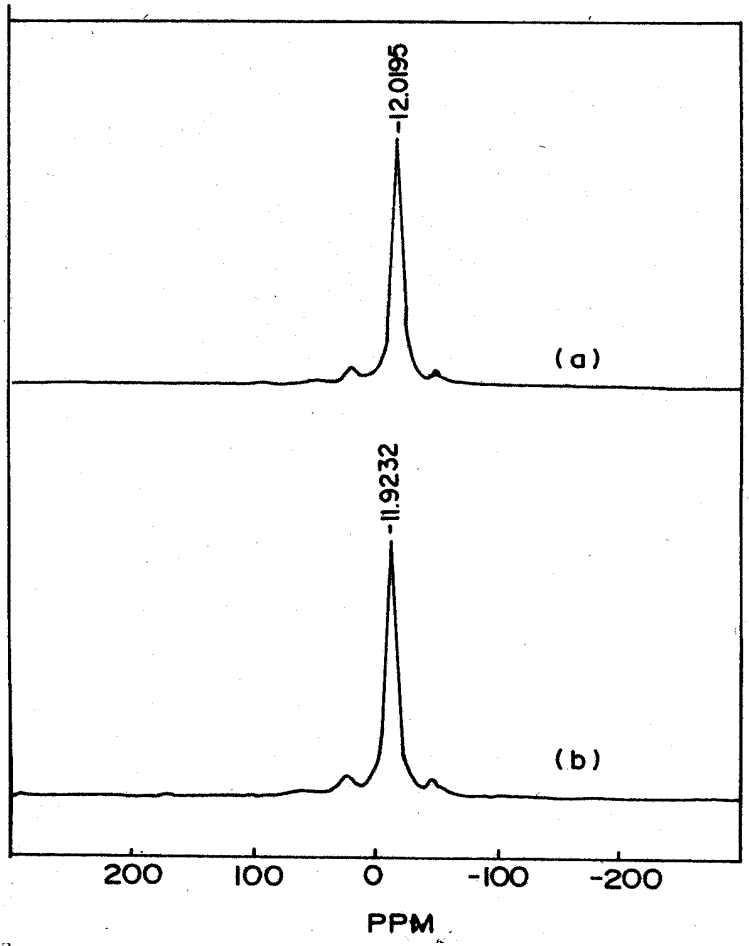

Fig. 3.36 ^{23}Na MAS NMR of (a) ETS-10 and (b) FePcETS-10

impurity [27]. The signals were somewhat broader in encapsulated complexes perhaps due to the presence of Fe ions in ETS-10. No major changes in the chemical shift of silicon signals due to encapsulation were observed (Fig. 3.35(b)).

^{23}Na MAS NMR spectra of ETS-10 samples (Figure 3.36(a)) consist a sharp signal at δ = -11.92 ppm. This signal in FePc-ETS-10 samples occurs at -12.0 ppm (Fig. 3.36(b)).

3.5.5 SEM of FePc-ETS-10

No major difference in the crystallite morphology of ETS-10 was observed due to metal complex encapsulation. Although no direct evidence was observed for the

encapsulation of FePc complexes, the SEM pictures (Figure 3.37) rule out any surface-bound FePc complex.

(a) (b)

Fig. 3.37 Scanning electron micrographs (SEM) of (a) ETS-10 and (b) FePc-ETS-10.

3.5.6. Sorption studies of FePc-ETS-10 samples

The sorption capacity of titanosilicate was measured using H_2O (kinetic diameter = 2.65 Å), n-hexane (4.3 Å) and 1,3,5 trimethylbenzene (8.1 Å). The kinetics of adsorption of these molecules were obtained at 298 K and p/p^0 = 0.5 (Fig. 3.38). The equilibrium sorption capacities observed for FePc-ETS-10, however, are lower than ETS-10. This is due to the incorporation of FePc complex in ETS-10, as also confirmed earlier by FT-IR and TGA-DTA.

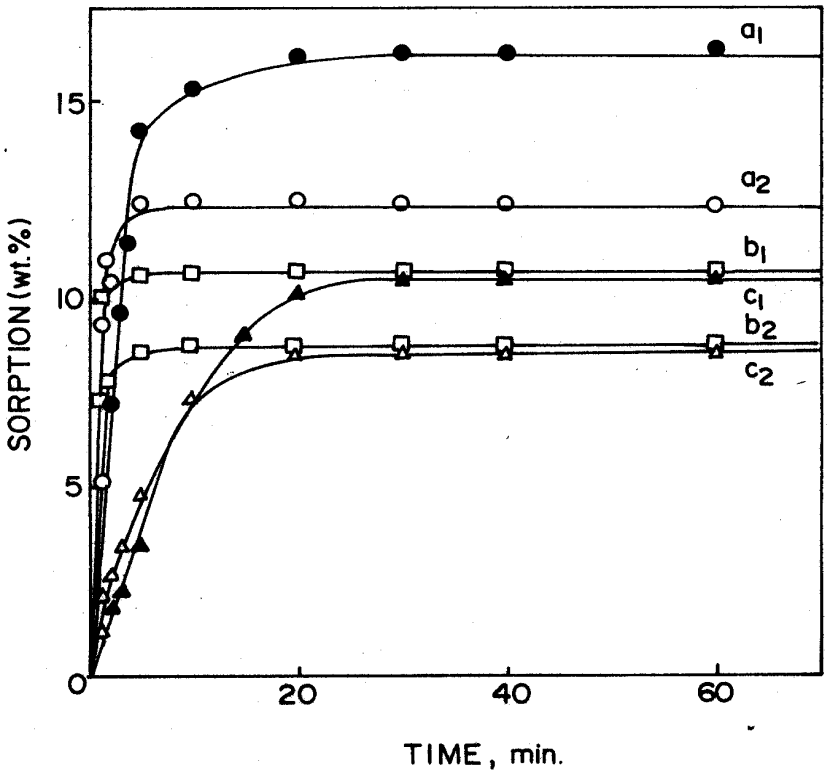

Fig. 3.38 Sorption capacity for (a_1, b_1 and c_1) ETS-10 and (a_2, b_2 and c_2) FePc-ETS-10 using H_2O, n-hexane and 1,3,5 trimethylbenzene, respectively.

3.5.7 EPR of FePc-ETS-10 samples

Iron in FePc-ETS-10 can have +2 or +3 oxidation states. While the former ions do not show EPR signals, the latter are paramagnetic and hence, EPR active. As in Co(II), the iron complexes are also prone to spin crossover phenomenon. Depending on the ligand field stabilizational energy Fe(III) ions can be in a high spin electronic configuration ($t_{2g}^3 e_g^2$; S = 5/2) showing EPR signals at g = 4.2 or in a low spin configuration (t_{2g}^5; S = ½) showing EPR spectra with low g-anisotropy. FePc-ETS-10 (Fig. 3.39) samples showed weak EPR signals at $g_\perp$ = 2.329 and $g_\parallel$ = 1.928 indicating that FePc-encapsulated in ETS-

10 is in +3 oxidation state with low spin electronic configuration (t_{2g}^5; S = ½). However the presence of Fe^{2+}cannot be ruled out as they are EPR silent. The signals at free spin g value are those arising from Pc radical species.

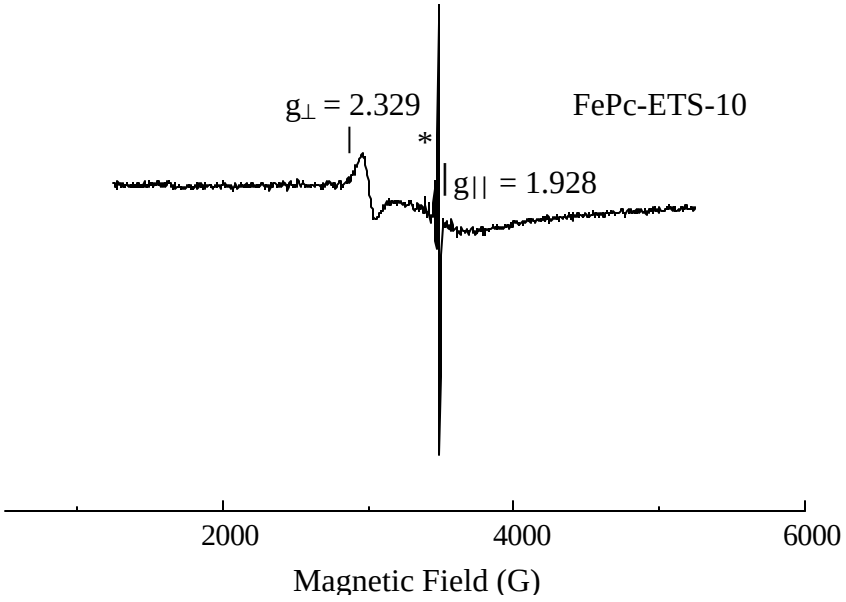

Fig. 3.39 EPR spectrum of FePc-ETS-10 at 298 K. Asterisk denotes signals due to Pc radical species.

3.6 Characterization of Copper(II)hexadecachlorophthalocyanine ($CuCl_{16}Pc$)

Encapsulated in Zeolite X

As the molecular dimension of $CuCl_{16}Pc$ is larger than the size of the zeolite supercages, encapsulation of these complexes were not successful by the "template synthesis" method. Hence, attempts were made to encapsulate this complex in X zeolite by the "zeolite synthesis" method as described in chapter 2. The encapsulated complexes, thus prepared, were green in colour. The formation and integrity of the complex was investigated by XRD, TG-DTA, sorption studies, FT-IR, DRUV-Vis and EPR techniques.

3.6.1. X-ray diffraction of $CuCl_{16}PcX$

The encapsulated samples showed X-ray diffraction patterns typical of X-zeolite. In other words, the presence of $CuCl_{16}Pc$ did not alter the zeolite framework structure. Typical XRD patterns of NaX (Linde) and $CuCl_{16}PcX$ are shown in Fig. 3.40. The samples did not show diffraction patterns corresponding to $CuCl_{16}Pc$ suggesting the absence of bulk $CuCl_{16}Pc$ complex.

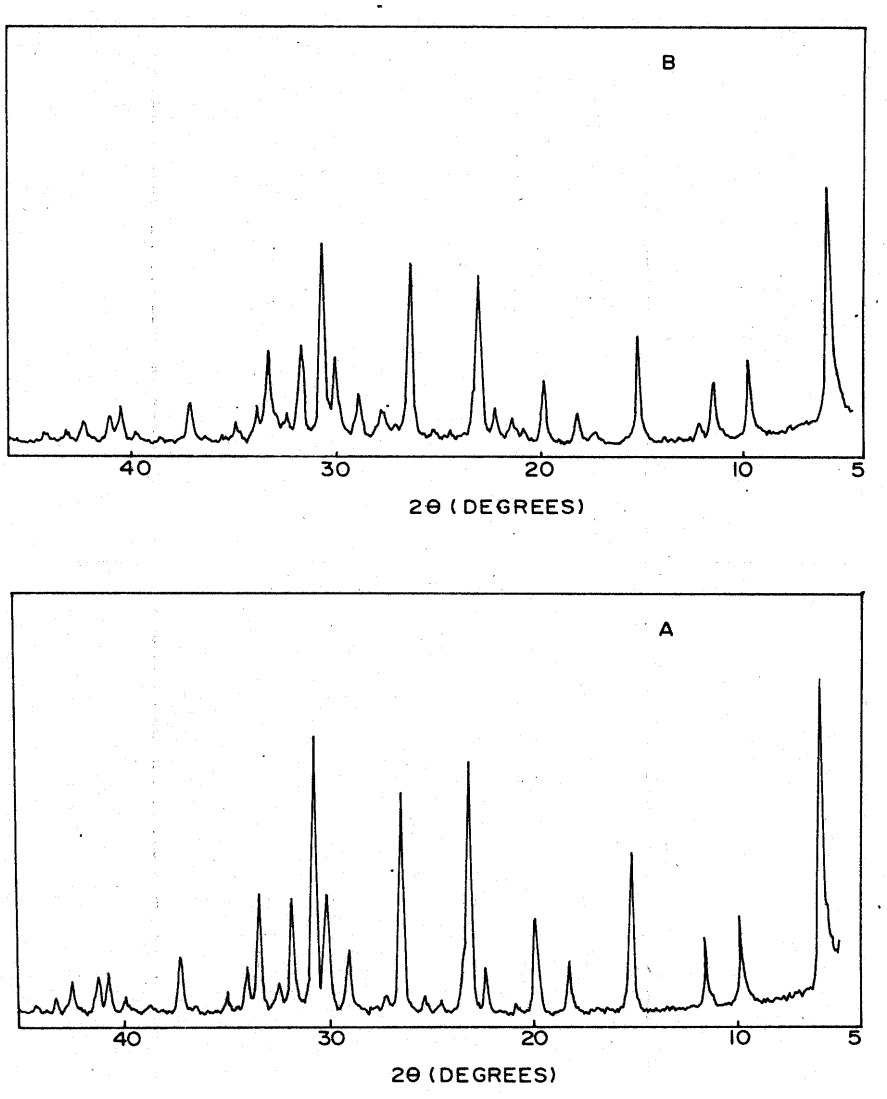

Fig. 3.40 XRD patterns of (A) NaX (linde) and (B) $CuCl_{16}PcX$

3.6.2. N_2 and n-hexane adsorption studies of $CuCl_{16}Pc$

The surface area of encapsulated complexes were estimated from nitrogen adsorption studies. The surface area (S_{BET}) of Linde X and $CuCl_{16}PcX$ and were 600 m^2/g and 420 m^2/g, respectively. The amount of n-hexane adsorbed on the samples was also estimated. It was found that 16.97 wt.% of n-hexane was adsorbed on NaX at $p/p_0 = 0.5$ and temperature = 298 K while it was only 14.25 wt.% in $CuCl_{16}PcX$ samples. The reduction in BET surface area and n-hexane adsorption capacity of $CuCl_{16}PcX$ is either due to encapsulation of the complexes in the super cages or blockage of the surface pores. Therefore, further studies by spectroscopic techniques were carried out to differentiate the encapsulated from surface-bound species.

3.6.3. FT-IR spectra of $CuCl_{16}PcX$

Unlike the samples prepared by the "template synthesis" method, the $CuCl_{16}PcX$ samples prepared by the "zeolite synthesis" method did not show any shift in the band positions of the characteristic ligand bands which were very weak. The spectra was dominated by the intense broad bands due to the zeolite framework.

3.6.4. DRUV-Vis spectra of $CuCl_{16}PcX$

Representative DRUV-Vis spectra of "neat" $CuCl_{16}Pc$, $CuCl_{16}PcX$ and impregnated $CuCl_{16}Pc$ on zeolite X are shown in Fig. 3.41. The Q-bands in $CuCl_{16}PcX$ have red shifted compared to "neat" $CuCl_{16}Pc$. These bands for "neat" $CuCl_{16}Pc$ occur at 600, 732 and 790 nm while the bands for $CuCl_{16}PcX$ appear at 659, 732 and 790 nm. The spectrum of impregnated samples resemble those of $CuCl_{16}PcX$. This observation indicates that the red shift in Q-bands for $CuCl_{16}PcX$ is perhaps due to dispersion of the Pc molecules and not necessarily be due to encapsultion of molecules in the supercages.

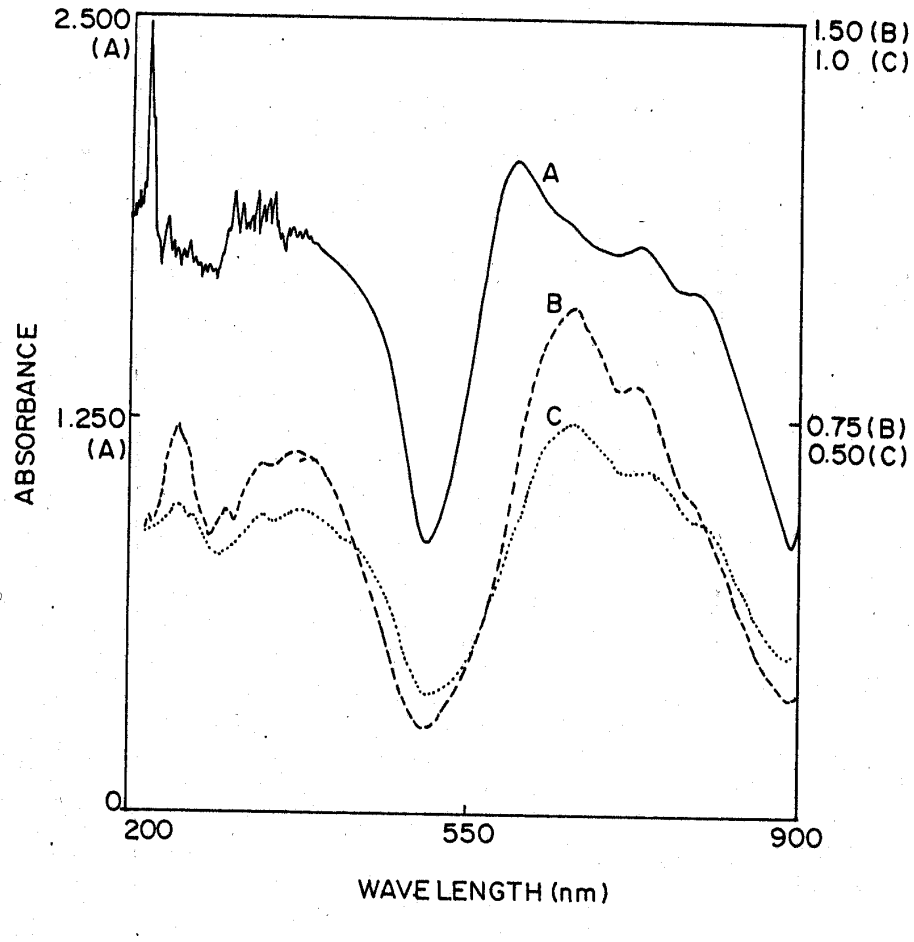

Fig. 3.41 DRUV-Vis spectra of $CuCl_{16}Pc$: A, "neat" complex ; B, $CuCl_{16}PcX$; C, $CuCl_{16}Pc$ impregnated on zeolite X

3.6.5. EPR spectra of $CuCl_{16}PcX$

The EPR spectrum of $CuCl_{16}PcX$ at 298 K is shown in Fig. 3.42 The spectrum is characterized by an axial g-tensor with $g_{||}$ = 2.145 and $g_{\perp}$ = 2.045. Unlike the encapsulated CuPc complexes synthesized by "template synthesis" method, the $CuCl_{16}PcX$ sample did not show copper hyperfine features. The spectrum and spin Hamiltonian parameters the are same as those of the "neat" $CuCl_{16}Pc$ complex ($g_{||}$ = 2.142 and $g_{\perp}$ = 2.045). These observations reveal that $CuCl_{16}Pc$ is not "truely" encapsulated in the supercages of zeolite X but could be present in the intercrystalline

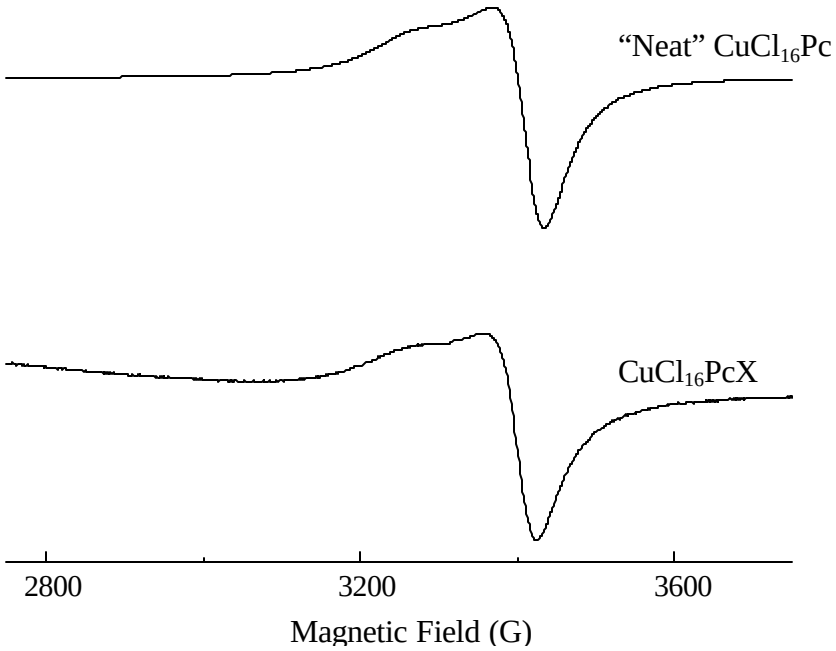

Fig. 3.43 A comparative EPR spectra for the solid samples of "neat" $CuCl_{16}Pc$ and CuCl16PcX (prepared by the "zeolite synthesis method) at 298 K

void spaces or on the surface of zeolite X. The absence of shift in the positions of the IR bands as well as similar UV-Vis spectral behaviour of $CuCl_{16}PcX$ and impregnated zeolite X samples further confirm the conclusions derived from EPR spectra.

3.7 Molecular Modeling Studies

Molecular modelling studies of zeolite encapsulated MPc complexes were performed using the MSI software Insight II and O2 Silicon Graphics Workstation. The molecular graphics pictures with 3-dimensional views of MPc encapsulated inside the zeolite-Y and ETS-10 are shown in Fig. 3.44. The studies confirmed the possibilities of

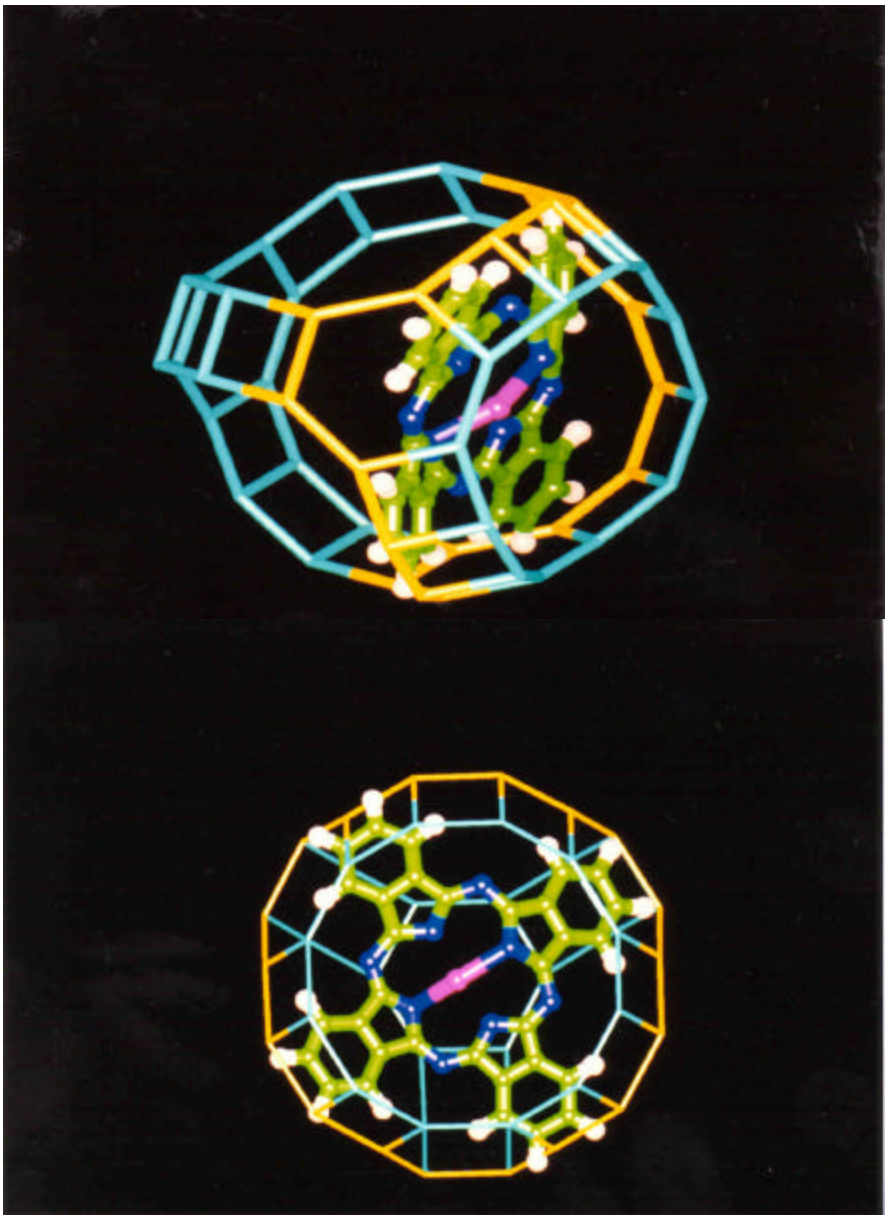

Fig. 3.44 Structure of MPc encapsulated in the supercage of zeolite NaY using molecular modelling methods ; represents Carbon, represents Nitrogen , represents Hydrogen and represents MPc.

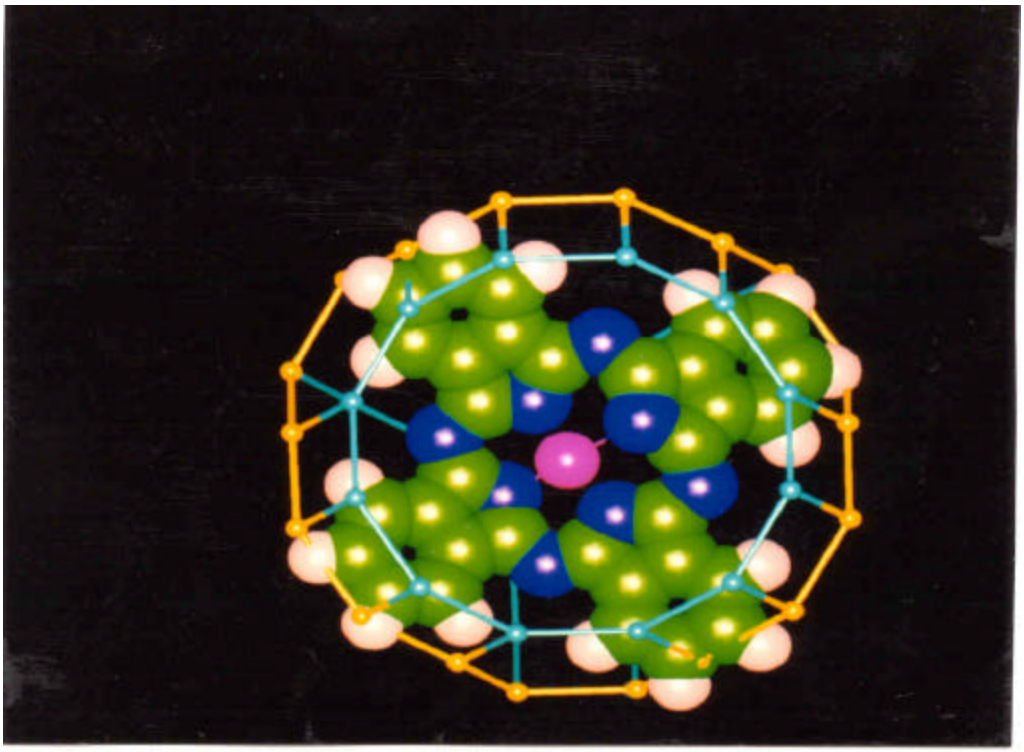

Fig. 3.44 Structure of MPc encapsulated in the supercage of zeolite NaY using molecular modelling methods ; represents Carbon, represents Nitrogen , represents Hydrogen and represents MPc.

encapsulation of MPc complexes inside the supercages of zeolite Y and in the channel intersections of ETS-10 (Fig. 4.45). Energy minimization of molecular structure was done using MM3 module. The studies reveal that the complexes are puckered on encapsulation. This puckering is more in the supercages of zeolite-Y than in ETS-10. The modeling studies on the molecular conformation support the experimental observations.

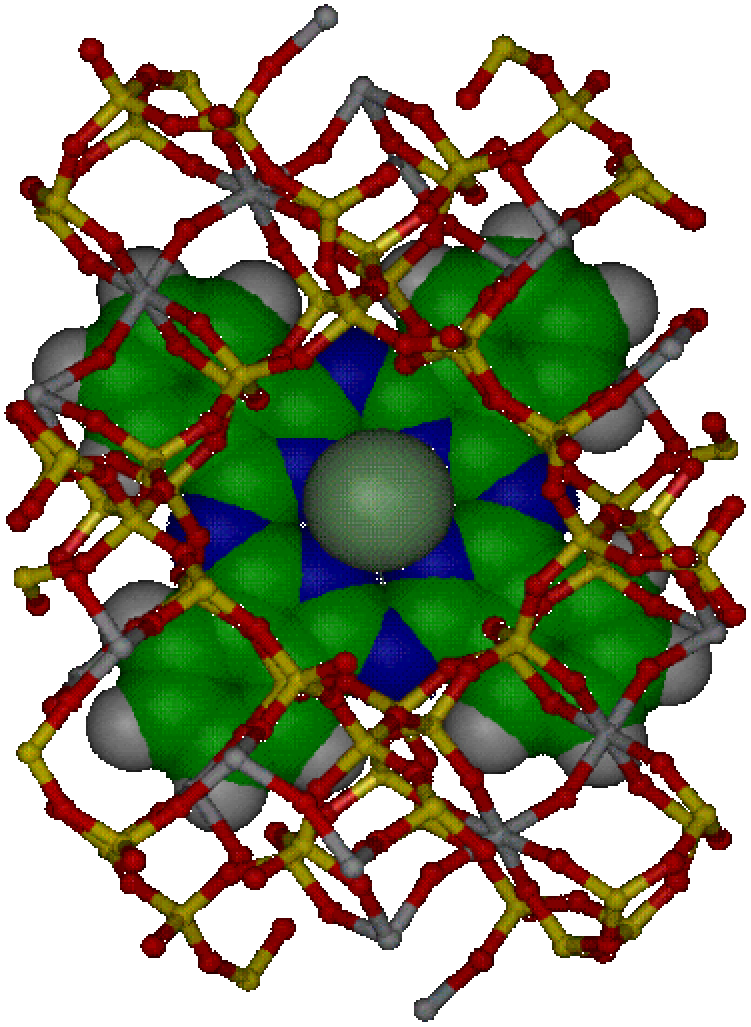

Fig. 3.45 Encapsulation of FePc in ETS-10

3.8 Conclusions

CuPc, CoPc and VPc complexes were encapsulated in the supercages of zeolite Y and FePc was encapsulated in the titanosilicate ETS-10. A comparative physicochemical study of metal exchanged zeolites, "neat" MPc and encapsulated complexes revealed that the complexes are encapsulated inside the supercages of zeolite Y and in the channel intersections of ETS-10. The metal ions located in sodalite cages are inaccessible for

complexation with Pc moiety. The surface areas of MPcY samples are lower than MY consistent with the encapsulation of metal complex inside the cages or channel intersections of zeolite Y and ETS-10, respectively. The changes in the FT-IR and UV-Vis band positions along with the EPR spin Hamiltonian parameters revealed a distorted molecular symmetry for Pc moiety due to encapsulation or molecular confinement in zeolite Y. However, FePc encapsulated in ETS-10 is little affected. The results of this chapter reveal that the spectroscopic techniques are ideal to differentiate the encapsulated MPc from the surface-bound complexes.

3.9 References

1. P.A. Reynolds, B.N. Figgis *Inorg. Chem.* 30 (1991) 2294.
2. N. Kobayashi in "*Phathalocyanines-Properties and Applications*", C. C. Leznoff, A.B.

   P. Lever (Eds.) VCH Publishers, Inc., New York, Vol. 2 (1993) 97.
3. J. P. Linsky, T. R. Paul, R. S. Nohr and M. E. Kenney., *Inorg. Chem*., 19 (1980) 3131.
4. A. Abragam and B. Bleaney., *Electron Paramagnetic Resonance of Transition Ions*., Oxford University Press, London, 1970.
5. A. B. P. Lever., *Advances in Inorganic Chemistry and Radiochemistry*.,

   H. J. Emeleus, A. G. Sharpe., eds. Academic Press, New York, 7 (1965) 28.
6. E. M. Roberts and W. S. Koski., *J. Am. Chem. Soc*., 83 (1961) 1865.
7. D. Kivelson and R. Neiman., *J. Chem. Phys*., 35 (1961) 149.
8. C. M. Guzy, J. B. Raynor and M. C. R. Symons., *J. Chem. Soc.A.*, (1969) 2299.
9. S. E. Harrison and J. M. Assour., *J. Chem. Phys*., 40 (1964) 365.
10. R. M. Deal, D. J. E. Ingram and R. Srinivasan., Proc. XII Colloq. Ampere., 1963.

11. A.H. Maki and B.R. McGarvey, *J. Chem. Phys*. 29 (1958) 31 and 35.

12. D. Kivelson and R. Neiman, *J. Chem. Phys*. 35 (1961) 149.

13. P.T. Manoharan and M.T. Rogers in*: Electron Spin Resonance of Metal Complexes*, T. F. Yen (Ed.), Plenum Press, New York, 1969, p. 143.

14. J. S. Griffith., *Disc. Faraday Soc*., 26 (1958) 81.

15. M. Gouterman and M. Zerner., *Theoret. Chim. Acta.*, 4 (1996) 44.

16. R. Raja and P. Ratnasamy, *J. Catal.*, 170 (1997) 244.

17. M. Fukui, N. Katayama, Y. Ozaki, T. Araki, and K. Iriyama, *Chem. Phys. Lett*., 177 (1991) 247.

18. R. Aroca, Z.Q. Zeng and J. Mink, *J. Phys. Chem. Solids*., 51 (1990) 135

19. R. Parton, *Ph.D Thesis*, K. U. Leuven (Belgium), May 1993

20. J. Dowdy, J.J. Hoagland, and K.W. Hipps , *J. Phys. Chem*., 95 (1991) 3751.

21. K. J. Balkus, Jr., A.G. Gabrielov, S.L. Bell, F. Bedioui, L. Roue and L. Davynck., *Inorg. Chem*. 33 (1994) 67-72.

22. K.J. Balkus Jr., M. Eissa and R. Lavado, *Stud. Surf. Sci.Catal*., 94 (1995) 713.

23. R.G. Herman and D.R. Flentge, *J. Phys. Chem*., 82 (1978) 720.

24. C. Naccache and Y. Ben Taarit, *Chem. Phys. Lett*., 11 (1971) 11.

25. E. Páez-Mozo, N. Gabriunas, R. Maggi, D. Acosta, P. Ruiz and B. Delmon., *J. Mol. Catal.*, 91 (1994) 251.

26. E. M. Flanigen and H. Katani., Molecular Sieve *Zeolites. I* Adv. Chem. Ser., 101 (1971) 201.

27. T. K. Das, A. J. Chandwadkar, A. P. Budhkar and S. Sivasanker., *Microporous Materials*., Part I., 4 (1995) 195 ; Part II., 5 (1995) 401.

CHAPTER 4
CATALYTIC PROPERTIES

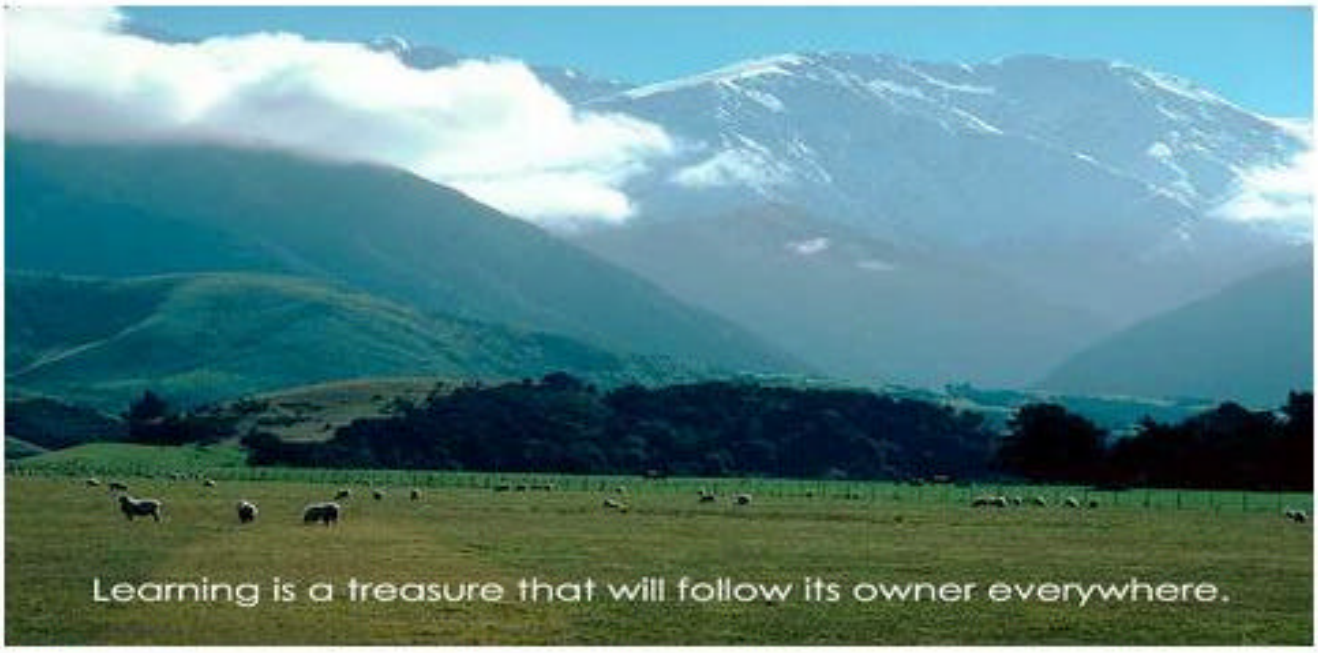

4.1 Oxidation of Styrene over CuPc and CuPcY Catalysts

Catalytic oxidations of olefins to epoxides, carbonyl compounds and diols are industrially important reactions. Epoxidation has traditionally been carried out using peracids, which are hazardous to use and expensive. These procedures also generate much waste. The use of H_2O_2 or TBHP in metal catalyzed oxidation reactions has mostly been restricted to homogeneous catalysts. The use of heterogeneous catalysts in liquid phase oxidation reactions is not commercially practiced to any significant extent even though they offer advantages of easy separability and reuse. The major problem with solid catalysts is their dissolution in the reaction medium in the presence of peroxides. One notable exception is TS-1, a microporous crystalline titanosilicate which has been found to catalyze many selective oxidation reactions such as epoxidation of alkenes, hydroxylation of phenols, oxidation of alcohols and oxidation of aldehydes and ketones [1-4]. Ti does not leach out from TS-1 materials as it is part of their framework structure. Similarly, TiO_2–SiO_2 (Shell catalyst) has been commercially used in the epoxidation of propylene with TBHP [5].

Metal phthalocyanines (MPc) are well known oxidation catalysts but tend to autoxidize resulting in a rapid loss of activity [6]. They oxidize a remarkably wide range of electron rich to electron deficient olefins using single oxygen donors like PhIO, NaOCl, H_2O_2 and TBHP [7,8].

The encapsulation of metal phthalocyanine complexes in zeolites can, besides favouring dispersion and preventing auto-oxidation, benefit from the favourable influences exerted by the zeolite matrix. These benefits could arise from the stereochemistry of the encapsulated complexes dictated by the zeolite framework, the

stabilization of the charged transition states by electrostatic fields inside the zeolite cages and alteration of the redox behaviour of the metal. Titanium tartarate catalysed enantioselective epoxidation of allyl alcohols discovered by Sharpless [9]] was a major milestone in catalytic epoxidation. The Sharpless catalyst however, requires directing groups on the substrate to effect high enantiomeric efficiency. The steric restrictions imposed by the zeolite cages can also (in principle) affect the stereochemistry of the product through restrictions imposed on the transition state. Interest in the study of encapsulated complexes as selective oxidation catalysts has been growing in recent years. A number of review articles have already been published on the subject [10 - 13]. Herron et al. first reported the oxidation of alkanes by iodosylbenzene catalyzed by FePc encapsulated in zeolites NaX and NaY [12]. Subsequently Parton et al. reported that using t-butylhydroperoxide and FePc in NaY zeolites for oxidation of alkanes resulted in high turn over numbers [14,15]. MnPc encapsulated in NaY has been reported to catalyze the oxidation of alkenes using iodosylbenzene [7]. NaX encapsulated CoPc was found to facilitate the oxidation of propene to formaldehyde and acetaldehyde, while the free complex was unreactive and CoY produced acetone [8].

Styrene oxide is manufactured industrially by the reaction of benzene with ethylene oxide or by the epoxidation of styrene by NaOCl. It is an intermediate in the manufacture of the perfumery chemical, phenylethyl alchohol. The epoxidation of styrene has been studied, so far, mostly in homogeneous systems [16] or over titanosilicate zeolites [17-19] or heteropolytungstates [20]. There are also a few reports on styrene epoxidation using Ru porphyrin encapsulated in MCM-41 [21] and using Cu and Mn Salen encapsulated in Y zeolite [22]. This section describes the epoxidation of styrene

using TBHP as the oxidant over CuPcY catalysts whose synthesis and characterization have been described in chapters 2 and 3, respectively. Also, some substituted CuPc complexes have been tested for their catalytic activity in styrene epoxidation to study the influence of peripheral substitution on activity.

Experimental details of styrene epoxidation reaction by MPc complexes are given in Chapter 2.

4.1.1 Epoxidation using "neat" CuPc complexes

The catalytic activities of different CuPc complexes in the epoxidation of styrene in acetonitrile are presented in Table 4.1. The substituted CuPc complexes yielded

Table 4.1

Product distribution in epoxidation of styrene over substituted CuPc complexes

Catalyst	Conv. (wt.%)	Product distribution[a](wt.%)				TON[b] (h^{-1})
		-CHO	EPO	$-CH_2CHO$	Others	
CuPc	8.8	84.5	9.6	1.6	4.3	10.2
$CuCl_8Pc$	18.9	51.3	40.6	6.1	2.1	14.9
$Cu(SO_3Na)_4Pc$	26.0	37.5	51.1	10.2	1.7	17.6
$CuCl_{16}Pc$	31.5	43.7	50.6	4.3	1.4	18.7

Conditions: styrene, 4.8 mmol; acetonitrile, 5 g; TBHP, 4.8 mmol; catalyst, 0.001 g; temperature, 333 K; duration, 24 h.

[a] -CHO = benzaldehyde, EPO = styrene epoxide, $-CH_2CHO$ = phenylacetaldehyde.

[b] TON = moles of styrene converted per mole of catalyst per hour.

styrene epoxide (EPO) and benzaldehyde (-CHO) as major products. On the contrary, CuPc was highly selective for benzaldehyde. Phenylacetaldehyde ($-CH_2CHO$) was

observed as a minor product. The turnover number (TON; number of moles of substrate converted per mole of catalyst per hour) is more for complexes with electronegative substituents and decreases in the order $CuCl_{16}Pc > Cu(SO_3Na)_4Pc > CuCl_8Pc > CuPc$.

An attempt has been made to correlate bonding parameters with the catalytic activity of the complexes in the homogeneous medium. The MO coefficients estimated from UV-Vis and EPR data (see chapter 3) reveal that the metal-ligand bond is in general covalent. The characterization results reveal greater depletion of electron density at the metal site in the case of sulphonic acid substituted complexes than CuPc and chloro substituted CuPc complexes. Though no one to one correspondence of catalytic activity with electron depletion at the metal centres of the complexes is noticed, the general observation is that complexes with electron deficient Cu possess larger catalytic activity. The depletion of electron density perhaps promotes the nucleophillic attack of the oxidant molecule (*tert*-butylhydroperoxide) at the metal centre forming the catalytically active intermediate metal-hydroperoxide. Further, heterolytic cleavage of the metal-hydroperoxy complex is also facilitated. The ease of heterolytic cleavage of metal-hydroperoxy complexes is said to be related to the epoxidation activity of transition metal complexes [23]. The ease of formation and heterolytic cleavage of hydroperoxy intermediates is more in complexes with electron withdrawing substituents and hence an increased catalytic activity is observed in these complexes (Table 4.1).

4.1.2 Epoxidation using encapsulated CuPc complex

4.1.2.1 Comparison of catalysts

Detailed studies on the epoxidation of styrene with two encapsulated CuPcY catalysts are presented in this section. The results of the catalytic activity studies carried

out on the epoxidation of styrene over the encapsulated and neat CuPc complexes and a parent CuY sample are presented in Table 4.2. It is noticed that the encapsulated complexes are more active than the neat complex and the parent CuY. For example CuPcY(1.2) gives a conversion of 94.2% whereas, the neat complex (4 mg, more than double the 1.8 mg of CuPc present in 0.05 g of CuPcY(1.2) used in the reaction) gives a conversion of only 29.3%. Again, CuY(1.2) gives a conversion of 20.9%. Analyzing the above data, in terms of TON (moles converted per mole of CuPc or Cu ions per hour) yields a value of 8.4 for CuPc and 4.5 for CuY. After correcting for the anticipated conversion due to the exchanged (uncomplexed) Cu present in CuPcY(1.2), one gets a TON of 50.3 for the encapsulated Pc molecules. The TON for CuPc in CuPcY(0.6) and

Table 4.2

Product distribution in styrene epoxidation over CuPc and CuPcY catalysts.

Catalyst (wt %)	Cu[1] (exch) (%)	Cu as CuPc (%)	Conv. (wt%)	TON[2] (h^{-1})	Product distribution[3] -CHO	EPO	$-CH_2CHO$	Others
CuPc(1.2)	0.79	0.41	94.2	50.3*	43.5	39.1	13.7	3.8
CuPc(0.6)	0.14	0.46	95.2	51.2*	53.0	23.8	12.6	10.5
CuPc(1.2)Ca	0.09	0.41	63.4	38.7*	52.4	34.3	9.0	4.2
CuPc	-	(4 mg)	29.3	8.4*	50.1	40.6	7.8	1.7
CuY (1.2)	1.2	-	20.9	4.5^{+}	64.2	29.5	6.2	0.2

Conditions: Styrene, 4.8mmole; acetonitrile, 5g; TBHP, 4.8 mmole; catalyst, 0.05 g except where noted; temperature, 333K

1: Cu in exchange sites (uncomplexed with Pc)

2: Moles of styrene converted per mole of active component per hour (*, based on CuPc; +, based on Cu ions)

3: -CHO = benzaldehyde, EPO = styrene epoxide, $-CH_2CHO$ = phenylacetadehyde

CuPcY(1.2)-Ca are 51.2 and 38.7, respectively. Though the values for CuPcY(1.2) and CuPcY(0.6) are similar (50.3 and 51.2), the TON for CuPcY(1.2) after Ca-exchanging is slightly lower (38.7). The reasons for the observed effect of Ca on activity are not clear. The above results indicate that activation of the CuPc molecules takes place when they are encapsulated inside the cages of Y. A similar enhancement in the activity of CuPc on encapsulation in zeolite Y has been reported by Ernst et *al.* [24] in the case of ethylbenzene oxidation. The higher activities of the complexes noticed on encapsulation may be a result of the distortion of the molecules (revealed by spectroscopic studies) and the consequent ease of redox transformation of Cu ions.

4.1.2.2 Influence of reaction time on styrene epoxidation

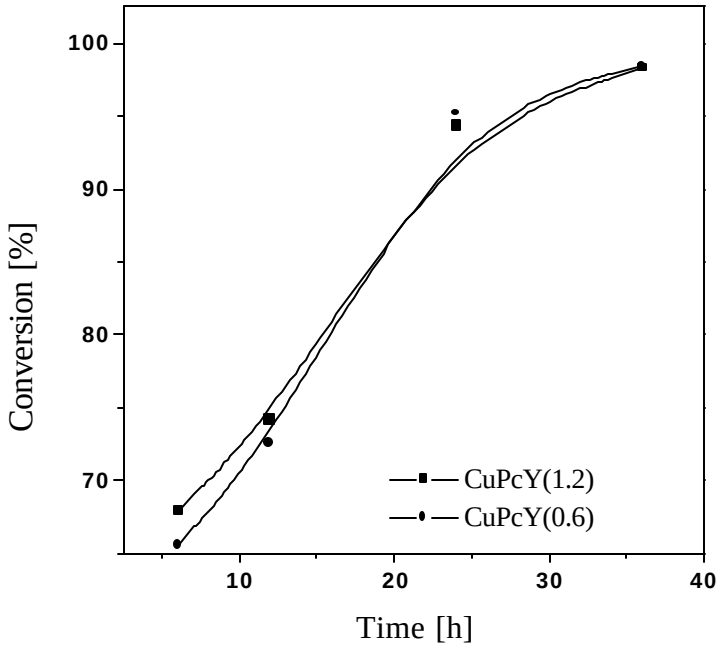

Fig. 4.1a Epoxidation of styrene over different encapsulated catalysts

Conditions : Styrene, 4.8mmole ; acetonitrile,5g ; tertiary butylhydroperoxide, 4.8mmole ; catalyst, 0.05g; temp., 333K

The kinetics of styrene epoxidation and variation in product distribution with reaction time are presented in Figs. 4.1a and 4.1b for CuPcY(1.2) and CuPcY(0.6). Styrene conversion is found to increase with increasing reaction time up to 36 h beyond which there was little increase in conversion (data after 36 h not shown in the figures). Styrene conversion was found to be similar at all reaction times for both the samples. This is not surprising because the amount of the active component, CuPc, is similar in

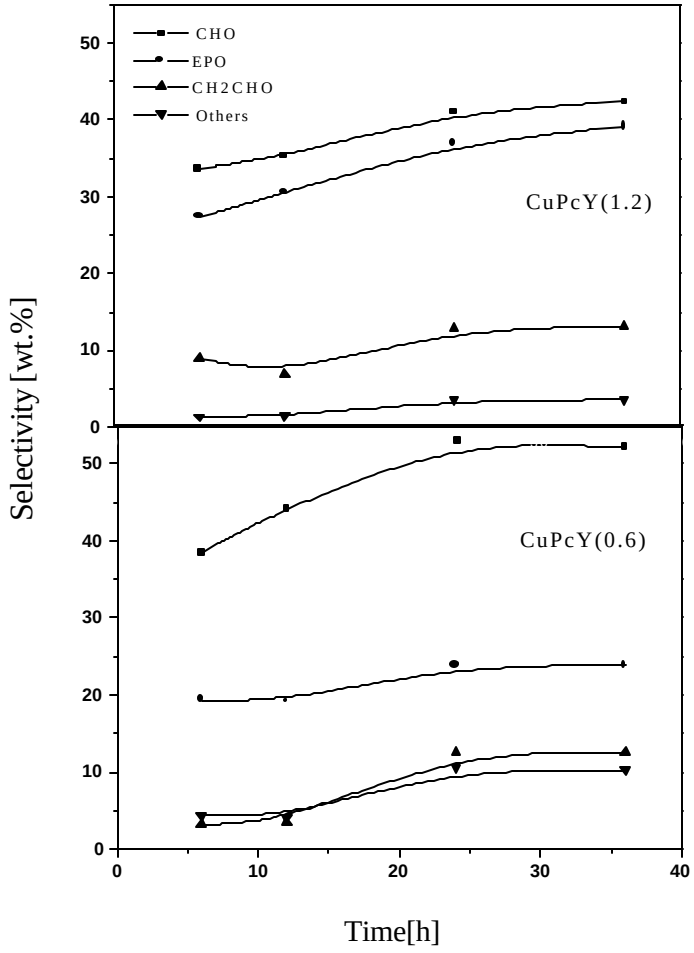

Fig. 4.1b Epoxidation of styrene over different CuPc encapsulated catalysts : product distribution

Conditions : Styrene, 4.8mmole ; acetonitrile,5g ; tertiary butylhydroperoxide, 4.8mmole ; catalyst, 0.05g; temp., 333K

-CHO = benzaldehyde ; EPO = styrene epoxide ;

-CH_2CHO = phenylacetaldehyde

both the samples (0.41 - 0.46%). Though both at 0.6 wt.% and 1.2 wt.% of Cu loading the activity is almost same (Fig. 4.1), the product distribution is slightly different over the two catalysts (Fig. 4.1b). CuPcY(0.6) produces more benzaldehyde and other impurities (benzoic acid and unidentified compounds) than CuPcY(1.2). Benzaldehyde is a cleavage product of styrene epoxide while phenyl acetaldehyde is the isomerized product.

The reactions in the epoxidation of styrene are :

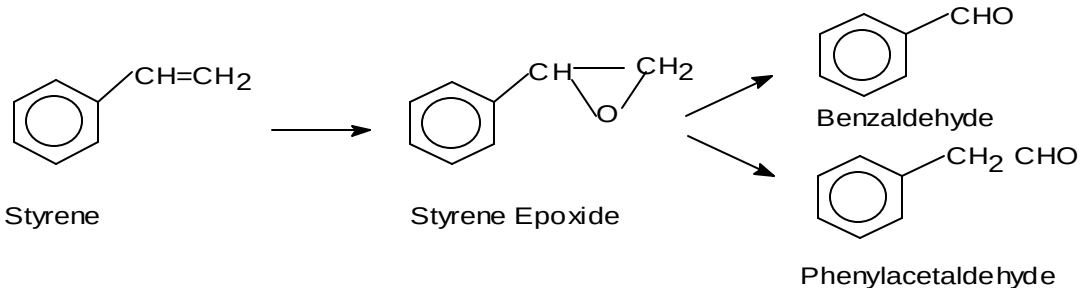

4.1.2.3 Influence of temperature on styrene epoxidation over encapsulated CuPc

Styrene epoxidation was studied using CuPc(0.6) at different reaction temperatures to follow the effect of temperature on conversion and selectivity (Fig. 4.2). The activation energy for the styrene conversion reaction is found to be 33.2 kJ/mol at a time on stream (TOS) of 24 h. At higher reaction temperatures, 333 K and 338 K (higher conversions) the reaction is found to be more selective towards benzaldehyde formation while at lower reaction temperatures, 328 K (lower conversions) comparable selectivity for benzaldehyde and styrene epoxide is observed (Fig. 4.2). It is probably because benzaldehyde is formed mainly via the further reaction of the epoxide, and a higher reaction temperature favours the oxidation of epoxide to benzaldehyde [24]. Also, phenylacetaldehyde selectivity does not appear to be much influenced by reaction temperature (Fig. 4.2).

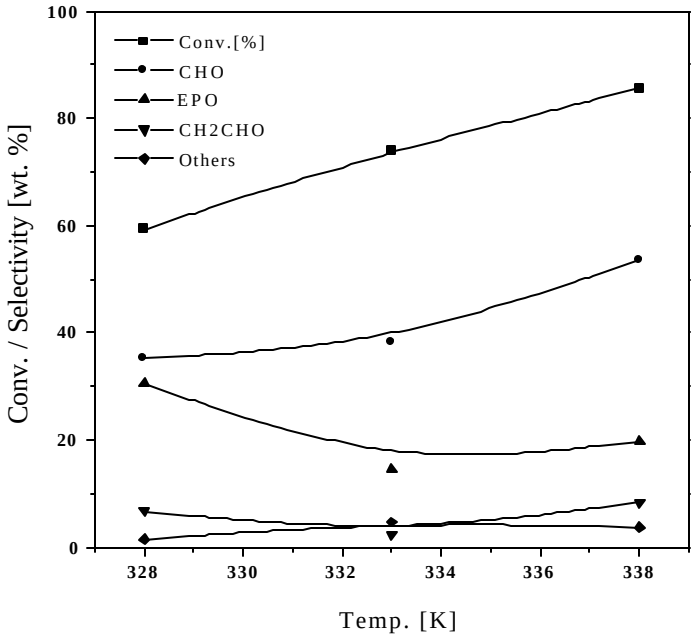

Fig. 4.2 Influence of temperature on conversion and selectivity.
Conditions : Styrene, 4.8mmole ; acetonitrile,5g ; tertiary butylhydroperoxide, 4.8mmole ; catalyst, CuPc (0.6) 0.05g; TOS = 24hrs
-CHO = benzaldehyde ; EPO = styrene epoxide ;
-CH_2CHO = phenylacetaldehyde

4.1.2.4 Influence of solvent on styrene epoxidation

Conversion of styrene is more when acetonitrile is used as solvent (95.2 wt.%) than when acetone is used (56.1 wt.%) (Table 4.3). However, use of different solvents does not appear to influence product selectivity (Table 4.3). It is also worth noting that the two catalysts with similar CuPc contents (but different amounts of Cu in exchange positions (see Table 4.2)) possess similar conversions in acetonitrile and acetone (Table 4.3). The enhanced activity in acetonitrile may be due to its higher polarity. The reasons for the two catalysts differing in amount of exchanged Cu-ions possessing similar activities is a result of the low activity of the free Cu^{2+} ions in epoxidation.

Table 4.3

Influence of solvent in styrene epoxidation

Catalyst (wt. %)	Solvent	Conv. (%)	Product distribution (wt.%)				TON[1] [h^{-1}]
			CHO	EPO	-CH_2CHO	Others	
CuPcY(1.2)	ACN	94.2	43.5	39.1	13.7	3.7	50.3
CuPcY(0.6)	ACN	95.2	53.2	23.8	12.6	10.5	51.2
CuPcY(1.2)	Acetone	54.6	22.4	19.0	11.6	1.7	29.6
CuPcY(0.6)	Acetone	56.1	32.2	15.7	5.5	2.8	30.2

Conditions: Styrene, 4.8mmoles; solvent (5g); tertiary butylhydroperoxide, 4.8 mmoles; catalyst, 0.05 g; temperature, 333 K; ACN = acetonitrile; -CHO = benzaldehyde; EPO = styrene epoxide; -CH_2CHO = phenylacetadehyde.
1: Moles of styrene converted per mole of active component per hour based on CuPc.

4.1.2.5 Influence of styrene: TBHP mole ratio

Decreasing the concentration of tertiary-butylhydroperoxide (TBHP) resulted in considerable suppression of the reaction. When the concentration of TBHP was decreased to half, the catalytic activity decreased considerably (more than half) (Table 4.4). The conversion is less for CuPcY(0.6) than CuPcY(1.2) at lower TBHP concentration. This is probably due to the greater contribution of uncomplexed copper to the reaction in the latter catalyst at lower TBHP : phenol (mole) ratios. The overall product distributions appear similar at both TBHP concentrations, the yield of benzaldehyde being more than -EPO or -CH_2CHO.

Table 4.4

Influence of TBHP concentration in styrene epoxidation

Catalyst (wt.%)	Phenol : TBHP (mole ratio)	Conv. (%)	Product distribution			
			-CHO	-EPO	-CH_2CHO	Others (wt.%)
CuPcY(1.2)	1	94.3	41.0	36.9	12.9	3.5
CuPcY(0.6)	1	95.2	50.5	22.6	12.0	10.0
CuPcY(1.2)	2	33.3	14.6	14.6	3.0	1.0
CuPcY(0.6)	2	24.9	15.6	6.4	1.8	1.1

Conditions: Styrene, 4.8mmoles; acetonitrile, (5g); catalyst, 0.05 g; temperature, 333 K; TOS = 24hrs.
-CHO = benzaldehyde; EPO = styrene epoxide; -CH_2CHO = phenylacetadehyde

4.2 Hydroxylation of Phenol over MPcY Catalysts (M = Cu, Co, V)

Use of solid catalysts for selective oxidation of phenols preferably at near – ambient conditions and using clean oxidants like O_2 or H_2O_2 is a research area of growing importance. Hydroxylation of phenol with H_2O_2 using microporous titanosilicate, TS-1 and its commercial utilization by Enichem workers [25] is a major advance in this area. Hydroquinone and catechol are obtained with high selectivity over TS-1. Strong mineral acids or Fenton's reagent are other efficient catalysts for the hydroxylation of phenol using H_2O_2 as the oxidant, producing peroxonium ion and hydroxyl radical, respectively. Various metal phthalocyanines have been studied for the hydroxylation of phenol by H_2O_2 [26]. It was found that the metal ion of the catalyst influences both activity and selectivity of the reaction as well as the distribution of catechol and hydroquinone. Since H_2O_2 alone is not a hydroxylating agent, catalysts have to be added to make it a hydroxylating agent. An active oxidant for the hydroxylation of phenol is an ionic species formed by the activation or reaction of H_2O_2 with metal phthalocyanines. Bimetallic Sn–Mo and Sn–Sb phthalocyanines have also been used to hydroxylate phenols using H_2O_2 as the oxidant [26]. The main products are catechol and hydroquinone, but the rate of hydroxylation with mineral acids is much faster than with metal phthalocyanines. Since very little (2%) of the dihydroxy benzene (resorcinol) was formed, the authors [26] suggest that the hydroxylation proceeds via an electrophilic substitution mechanism, which is typical for hydroxylation of phenol catalysed by strong acids or organic peracids. However, metal phthalocyanines facilitate hydrolysis of peroxide bonds [27] and hydroxyl radicals are always produced during the reaction. Amberlite supported Fe and Mn sulfonated phthalocyanines are efficient catalysts for the

H_2O_2 oxidation of chlorinated phenols [28]. Orita et al [29], have recently reported that copper(II) chloride coupled with amine, hydroxylamine or oxime catalyse the oxidation of 2,3,6-trimethyl phenol to the corresponding p-benzoquinone with dioxygen. Cobalt tetraphenylporphyrins have also been used for the oxidation of phenols to quinones using molecular oxygen as the oxidant [30]. 2, 6-Di-tert-butyl phenol was oxidised in water by cobalt phthalocyanine–tetrasulfonate bound to polymer colloids using dioxygen as the oxidant [2].

The catalytic activity of copper, cobalt and vanadium phthalocyanines encapsulated in zeolite Y in the hydroxylation of phenol to hydroquinone and catechol using H_2O_2 as the oxidant is reported in this section.

Experimental details of phenol hydroxylation reaction by MPc complexes are given in Chapter 2.

4.2.1 Hydroxylation of phenol over CuPcY catalysts

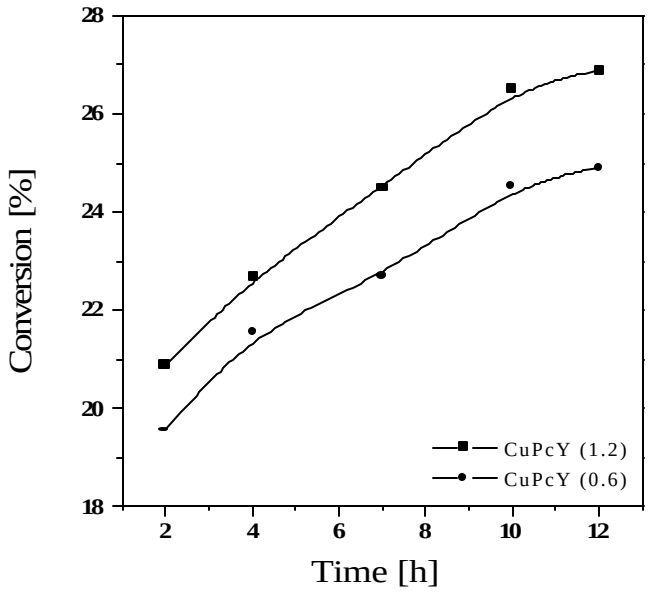

Fig. 4.3a Effect of Cu content of CuPcY catalysts on conversion

Conditions : Catalyst wt. = 0.1 g; Phenol:H_2O_2 = 3 mole; Temp. = 348 K; Solvent, water = 20 g;

When phenol is oxidized with H_2O_2, catechol and hydroquinone are formed as the major products and parabenzoquinone as a minor product. The results of the hydroxylation of phenol over the two CuPcY catalysts, CuPcY(0.6) and CuPcY(1.2) are presented in Fig. 4.3 (a and b).

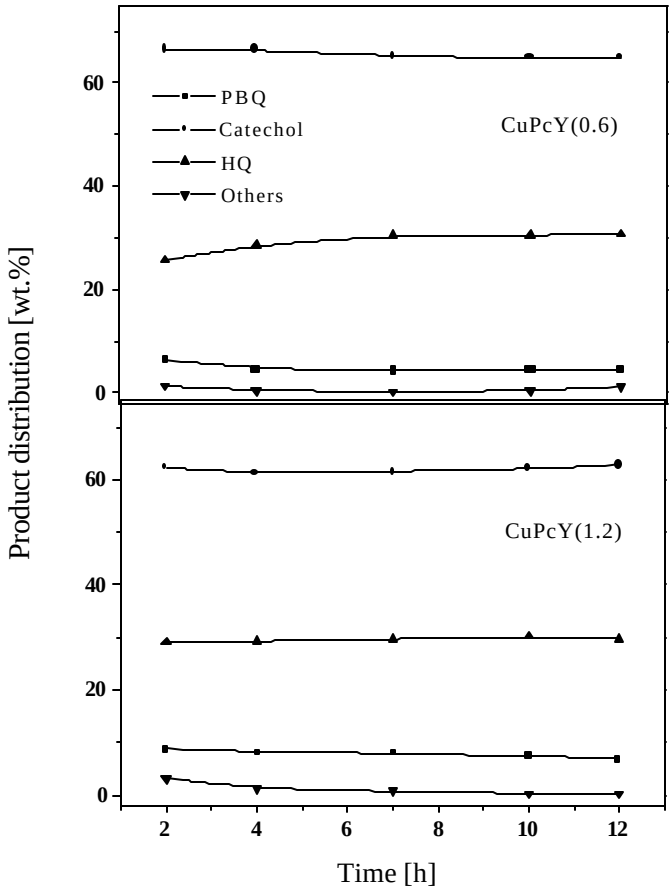

Fig. 4.3 b Influence of Cu content of CuPcY catalysts on yield of catechol, hydroquinone (HQ) and parabenzoquinone (PBQ).

Conditions : Catalyst wt. = 0.1 g; Phenol:H_2O_2 = 3 mole; Temp. = 348 K; Solvent, water = 20 g;

There is a small difference in the activity of the two catalysts containing 0.6 and 1.2 wt% Cu (Fig. 4.3a), the catalyst containing more Cu is slightly more active than the

one with less Cu. As both catalysts contain the same amount of CuPc, but different amounts of exchanged Cu^{2+} ions, the activity of Cu^{2+} ions is much smaller than that of CuPc. Both the catalysts also show similar product selectivities (Fig. 4.3b) again due to same amount of the active component (CuPc) in both the catalysts.

The results of the studies on the influence of temperature on phenol conversion and product selectivity over the two catalysts are presented in Fig. 4.4a and 4.4b. As expected, conversion increases with temperature, the activation energy, E_a value being 27.7 and 38.8 kJ/mol for CuPcY(0.6) and CuPcY(1.2) respectively at 12 h . Product selectivities are similar for the two catalysts at the two temperatures (Fig. 4.4b). At the higher reaction temperature, the selectivity for parabenzoquinone is more than that at the lower temperature (Fig. 4.4b) over both the catalysts.

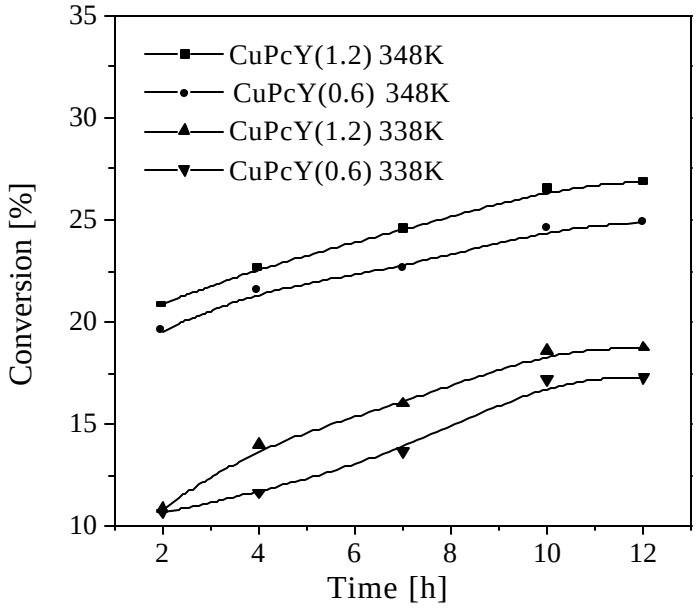

Fig. 4.4a Influence of temperature on phenol conversion over CuPcY catalysts.

Conditions : Catalyst wt. = 0.1 g; Phenol:H_2O_2 = 3 mole; Solvent, water = 20 g;

The results of studies on the influence of the weight of the catalyst charged on the conversion of phenol are presented in Table 4.5. The data confirm the catalytic nature of the reaction (Table 4.5). Phenol conversion effficiency increases with catalyst

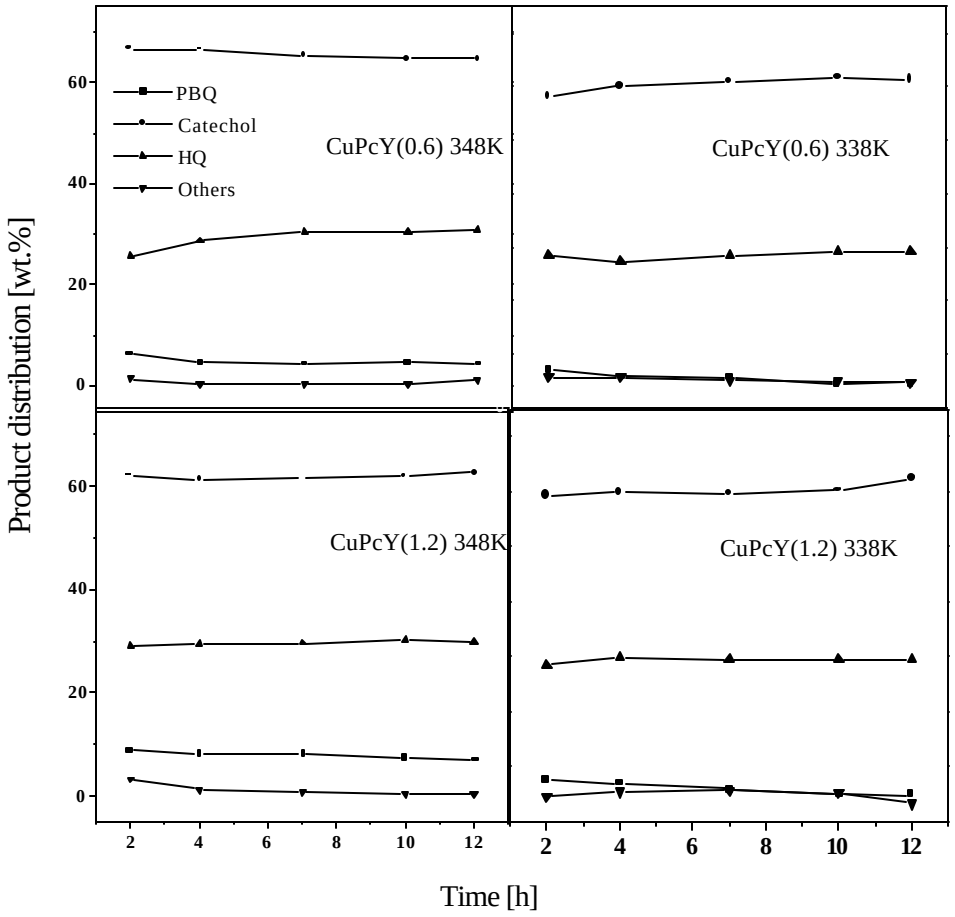

Fig. 4.4b Influence of temperature on product distribution.

Conditions : Catalyst wt. = 0.1 g; Phenol/H_2O_2 = 3 mole;
Solvent, water = 20 g PBQ = parabenzoquinone;
HQ = hydroquinone

concentration (Table 4.5). There is little variation in product distribution with variation in catalyst concentration. Catechol and hydroquinone are the major reaction products at all concentrations.

Phenol conversion is found to decrease with decrease in H_2O_2 concentration in the reaction (Fig. 4.5a, Table 4.6). But the product distribution for catechol, hydroquinone and parabenzoquinone formation was not affected by variation in H_2O_2 concentration (Fig. 4.5b, Table 4.6). An examination of the influence of H_2O_2 concentration on product distribution (Fig. 4.5b) shows that the phenol : H_2O_2 (mole) ratio should be kept high for maximum utilization of H_2O_2 in the conversion of phenol to (HQ + CAT) and minimum formation of quinones. However, lower H_2O_2 concentrations lead to lower phenol conversions. At higher H_2O_2 concentrations not only more hydroquinone is produced but also part of the H_2O_2 is decomposed non catalytically to $H_2O + O_2$. This results in lower phenol conversion efficiencies at higher H_2O_2 concentration.

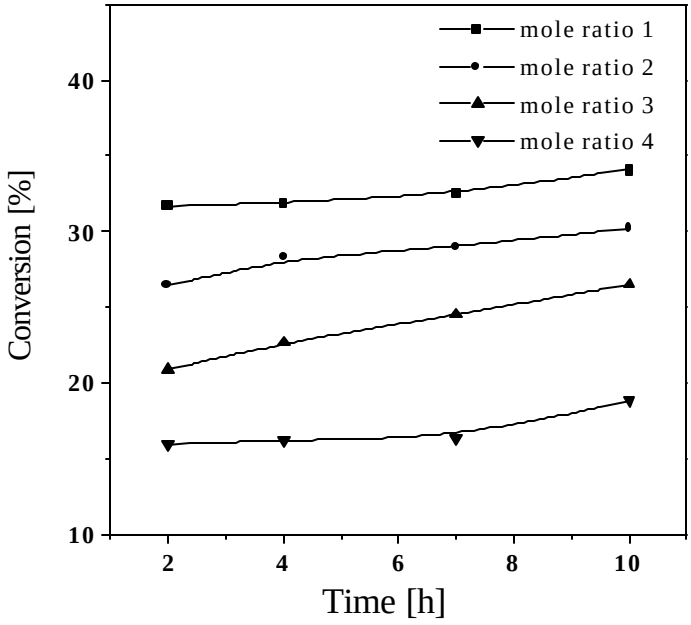

Fig. 4.5a Influence of phenol : H_2O_2 mole ratio on phenol conversion over CuPcY(0.6).

Conditions : Catalyst wt. = 0.1 g; Temp. = 348 K; Solvent, water = 20 g

Table 4.5
Effect of catalyst concentration in phenol hydroxylation (CuPc)

Catalyst conc. (g)	Time [h]	Conv. (%)	Conv. Efficiency[a](%)	Selectivity			
				PBQ	Catechol	HQ	Others
0.05	12	20.3	61.0	4.5	63.6	31.1	0.8
0.10	12	26.5	79.5	6.4	62.0	31.2	0.3
0.20	12	35.1	90.3	7.80	62.1	29.3	0.7

Phenol/H_2O_2 = 3 mole; Temperature = 348 K; solvent, water = 20 g; PBQ = para benzoquinone; HQ = hydroquinone

[a]% theoretical maximum for phenol conversion based on phenol : H_2O_2(mole) ratio.

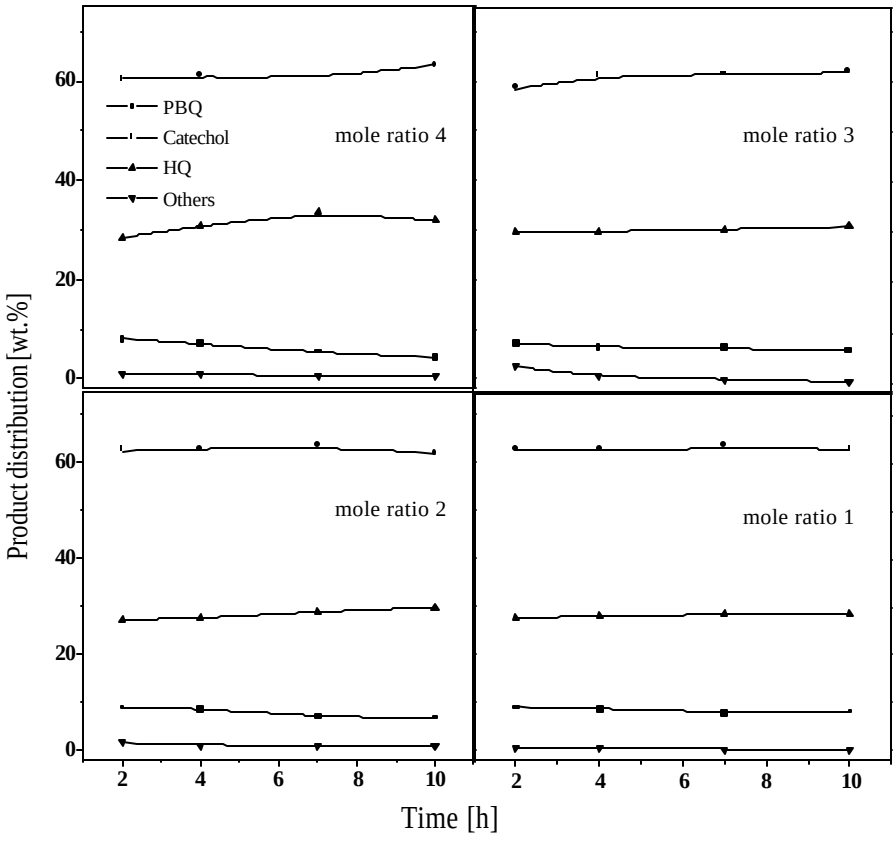

Fig. 4.5b Influence of phenol : H_2O_2 mole ratio on product distribution [CuPcY (0.6)]

Conditions : Catalyst wt. = 0.1 g; Phenol:H_2O_2 = 3 mole;
Temp. = 348 K; Solvent, water = 20 g;
PBQ = parabenzoquinone; HQ = hydroquinone.

Table 4.6

Effect of phenol: H_2O_2 mole ratio in phenol oxidation (CuPc)

Mole ratio	Time [h]	Conv (%)	Conv. Efficiency(%)[a]	Product distribution (wt. %)			
				PBQ	Catechol	HQ	Others
1	12	35.0	35.0	8.2	62.9	28.5	0.2
2	12	30.2	60.4	6.6	63.0	29.7	0.6
3	12	26.5	79.6	6.4	62.0	31.2	0.3
4	12	18.9	75.6	4.3	63.3	31.9	0.4

Catalysts wt = 0.1 g; Temperature = 348 K; solvent, water = 20 g; PBQ = para benzoquinone; HQ = hydroquinone

[a]% of theoretical maximum for phenol conversion based on phenol : H_2O_2 (mole) ratios.

4.2.2 Hydroxylation of phenol over CoPcY catalysts

Three different catalysts with 0.6, 1.0 and 1.2 wt % Co loading prepared and characterized according to procedures described in chapters 2 and 3 (respectively) were tested for their catalytic activity in phenol oxidation. The catalyst with 0.6 wt% Co loading was used to study the influence of catalyst weight, H_2O_2 concentration on activity and product selectivity. After 12 h reaction time the catalyst with 0.6 and 1.0 wt% Co loading showed similar activities which were larger than that shown by 1.2 wt% Co loading catalyst (Table 4.7). This difference can be attributed to pore blockage (as evidenced from large decrease in surface area; see chapter 2) in the case of the catalyst containing more Co (1.2 wt%) due probably to the formation of more CoPc complex. The changes in conversion with duration of run in the case of CoPcY(1.0) and CoPcY(1.2) are presented in Fig. 4.6a. Analysis of the product distribution (Fig. 4.6b) shows that catechol and hydroquinone are the major reaction

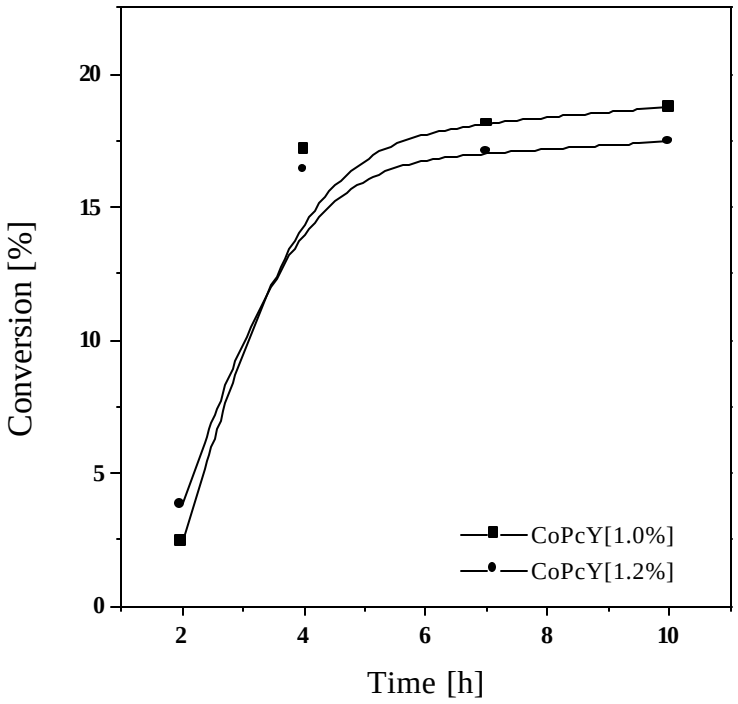

Figure 4.6a Effect of Co content of CoPcY catalysts on phenol conversion.

Conditions : Catalyst wt. = 0.1 g; Phenol:H_2O_2 = 3 mole; Temp. = 348 K; Solvent, water = 20 g;

Table 4.7

Effect of Co content of CoPcY catalysts in phenol oxidation

Catalyst	Conversion (%)	Product distribution (wt%)			
		PBQ	Catechol	HQ	Others
CoPcY(0.6)	20.6	4.4	63.6	31.1	0.9
CoPcY(1.0)	20.4	4.9	63.2	29.9	2.0
CoPcY(1.2)	17.4	8.1	62.7	28.2	1.1

Catalyst wt = 0.1 g; Temperature = 348 K; Solvent-water = 20 g; Reaction time = 12 h
PBQ = para benzoquinone; HQ = hydroquinone

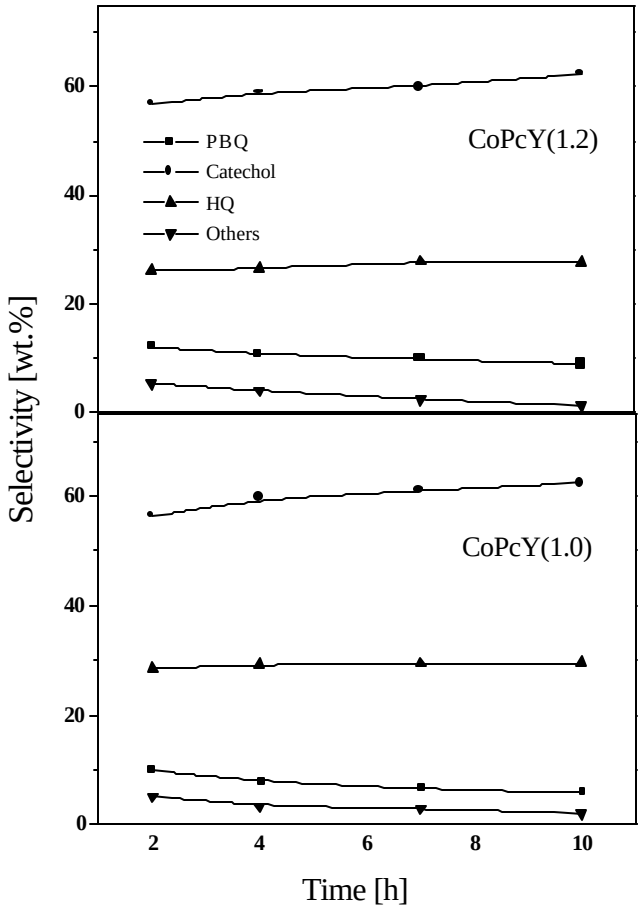

Figure 4.6b Influence of Co content of CoPcY catalysts on product selectivity.

Conditions : Catalyst wt. = 0.1 g; Phenol:H_2O_2 = 3 mole;
Temp. = 348 K; Solvent, water = 20 g;
PBQ = parabenzoquinone; HQ = hydroquinone.

products with parabenzoquinone forming in small amounts. It is found that with increasing Co content in the catalysts, parabenzoquinone selectivity increases along with a slight decrease in hydroquinone selectivity. This may be due to both higher CoPc content and more uncomplexed Co in the catalyst. These Co ions probably cause the oxidation of hydroquinone further into parabenzoquinone.

The influence of changing catalyst loading on phenol conversion and selectivity is presented in Table 4.8. The increase in conversion with increasing catalyst CoPcY(1.2) weight confirms the catalytic nature of the reaction. Though the conversion increases significantly (from 12.3 to 22.7%) with increase in catalyst loading from 0.05 to 0.1 g, further increase in catalyst loading from 0.1 to 0.2 g causes only a marginal increase in activity (22.7 to 24.8%). There is a slight increase in parabenzoquinone selectivity while hydroquinone selectivity decreases with increasing catalyst concentration (Table 4.8). More importantly, phenol conversion efficiency increases only marginally after 0.1 g catalyst charge.

Table 4.8

Effect of catalyst concentration in phenol hydroxylation over CoPc(0.6)

Catalyst amount (g)	Time [h]	Conv. (%)	Conv. Efficiency[a] (%)	Selectivity			
				PBQ	Catechol	HQ	Others (wt.%)
0.05	12	12.3	36.8	5.0	62.3	28.6	4.2
0.10	12	22.7	68.1	5.3	63.0	30.6	1.1
0.20	12	24.8	74.5	9.2	60.5	23.2	7.2

Phenol/H_2O_2 = 3 mole; Temperature = 348 K; solvent, water = 20 g;

[a]% of theoretical amount of phenol converted based on H_2O_2 : Phenol(mole) ratio

PBQ = para benzoquinone; HQ = hydroquinone.

The influence of phenol : H_2O_2 mole ratio on conversion and product distribution are presented in Figs. 4.7a and b and Table 4.9. With the decrease in H_2O_2 concentration, the phenol conversion is found to decrease (Fig. 4.7a, Table 4.9) and also formation of parabenzoquinone is suppressed. So lower H_2O_2 concentration favours the formation of

catechol and hydroquinone (Fig. 4.7b, Table 4.9). Higher H_2O_2 concentration not only favours parabenzoquinone formation but also some H_2O_2

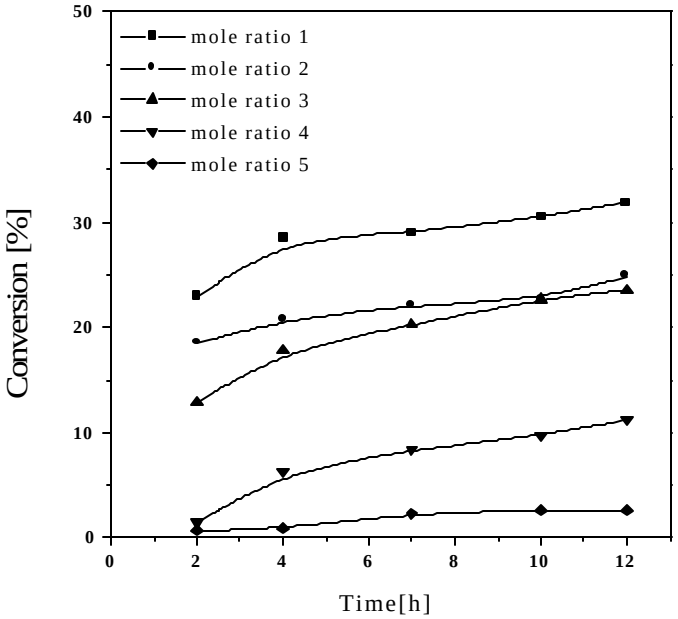

Fig. 4.7a Influence of phenol : H_2O_2 mole ratio on phenol conversion over CoPcY(1.0) catalysts.
Conditions : Catalyst wt. = 0.1 g; Temp. = 348 K; Solvent, water = 20 g

Table 4.9

Effect of phenol: H_2O_2 mole ratio on phenol oxidation over CoPcY(0.6)

Mole ratio	Time [h]	Conv. (%)	Conv. Efficiency[a](%)	Product distribution (wt. %)			
				PBQ	Catachol	HQ	Others
1	12	30.51	30.5	8.90	61.74	28.74	0.62
2	12	22.67	45.4	6.75	64.22	27.99	1.03
3	12	22.69	68.1	5.26	63.01	30.64	1.09
4	12	18.74	75.0	4.20	63.59	29.82	2.39

Catalyst wt. = 0.1 g; Temperature = 348 K; Solvent-water = 20 g;
[a]% of theoretical amount of phenol converted based on H_2O_2 : Phenol (mole ratio)
PBQ = parabenzoquinone; HQ = hydroquinone.

decomposes non-catalytically into $H_2O + O_2$. This is clear from the lower % phenol conversion efficiency at higher H_2O_2 contents (Table 4.9).

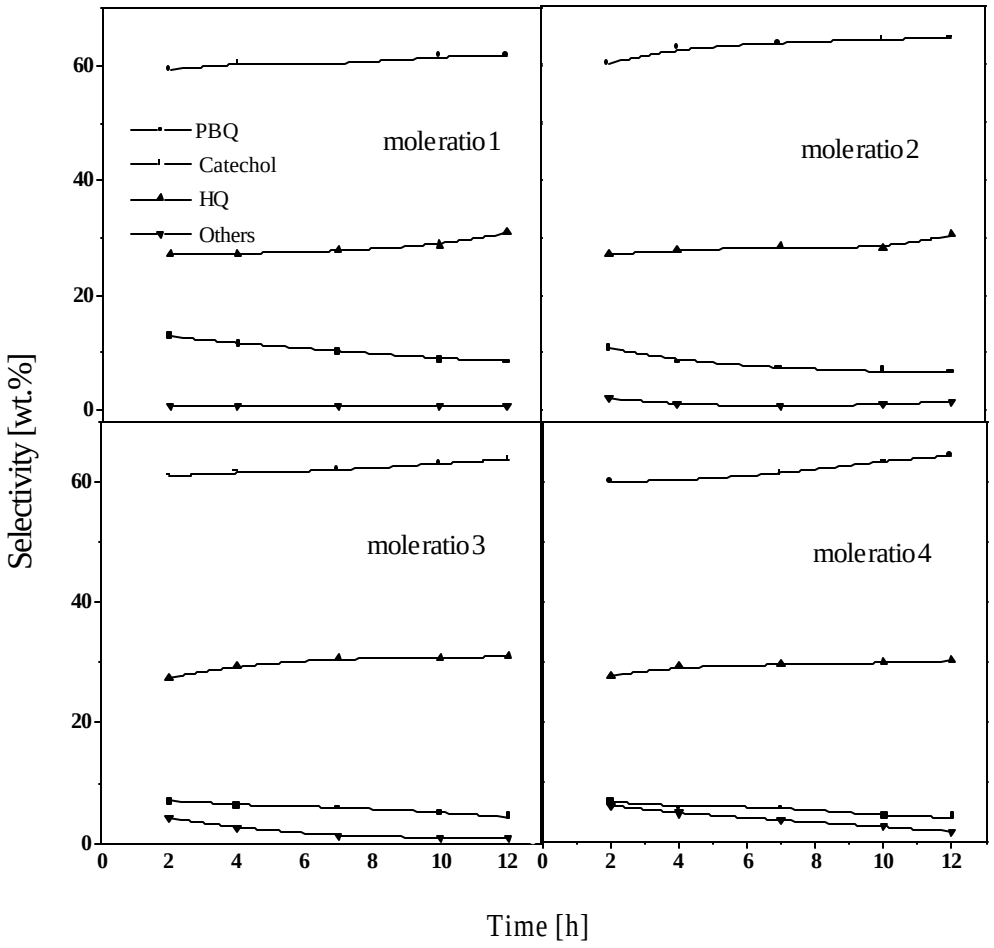

Fig. 4.7b Influence of phenol : H_2O_2 mole ratio on product distribution.

Conditions : Catalyst wt. = 0.1 g; Temp. = 348 K; Solvent,
water = 20 g;
PBQ = parabenzoquinone; HQ = hydroquinone.

4.2.3 Hydroxylation of phenol over VPcY catalysts

Three different catalysts with 1.0, 1.2 and 1.6 wt% vanadium loading were tested for their catalytic activity in phenol hydroxylation. Catalyst with 1.0 wt% Co loading was used to study the influence of catalyst weight, H_2O_2 concentration and reaction temperature on activity and product selectivity.

Comparison of the catalytic activities of VPcY catalysts (with different V contents) shows that with increasing V content from 1.0 to 1.6 wt% the catalytic activity decreases (Fig. 4.8a) This decrease can be attributed to pore blockage at higher V contents. Product distribution analysis shows that the reaction is highly selective towards catechol formation (Fig. 4.8b). Formation of parabenzoquinone is found to increase with increasing V content of the catalyst while the hydroquinone selectivity decreases.

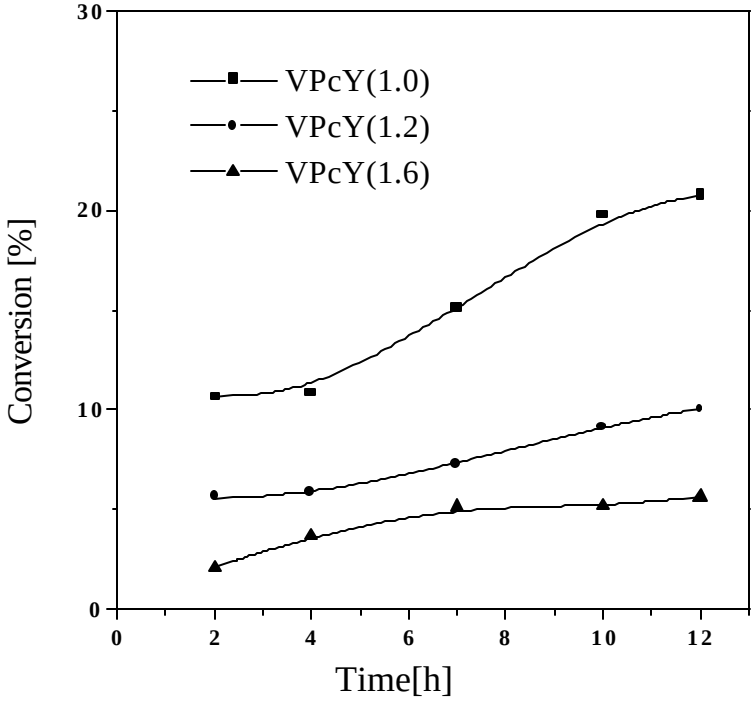

Fig. 4.8a Hydroxylation of phenol over V catalysts with different V contents.

Conditions : Catalyst wt. = 0.1 g; Phenol:H_2O_2 = 3 mole; Temp. = 348 K; Solvent, water = 20 g

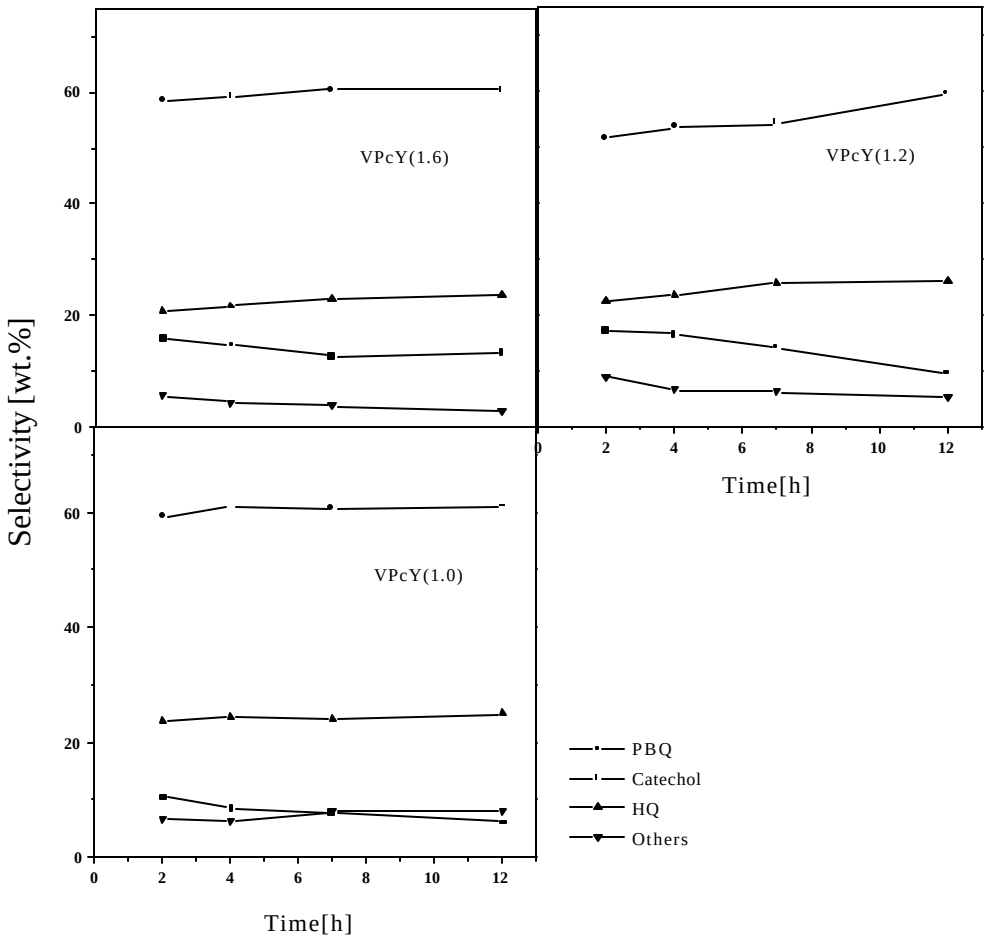

Fig. 4.8b Product distribution in oxidation of phenol over different VPcY catalysts

Conditions : Catalyst wt. = 0.1 g; Phenol:H_2O_2 = 3 mole;
Temp. = 348 K; Solvent, water = 20 g;
PBQ = parabenzoquinone; HQ = hydroquinone.

Influence of catalyst weight on phenol conversion is illustrated in Fig. 4.9a. Product distribution at different loadings are presented in Fig. 4.9b and Table 4.10. Increase in phenol conversion with increasing catalyst concentration shows that the reaction is catalytic in nature. The conversion levels off (and then decreases) beyond 0.1 g of catalyst which is probably due to more rapid H_2O_2 decomposition at larger catalyst

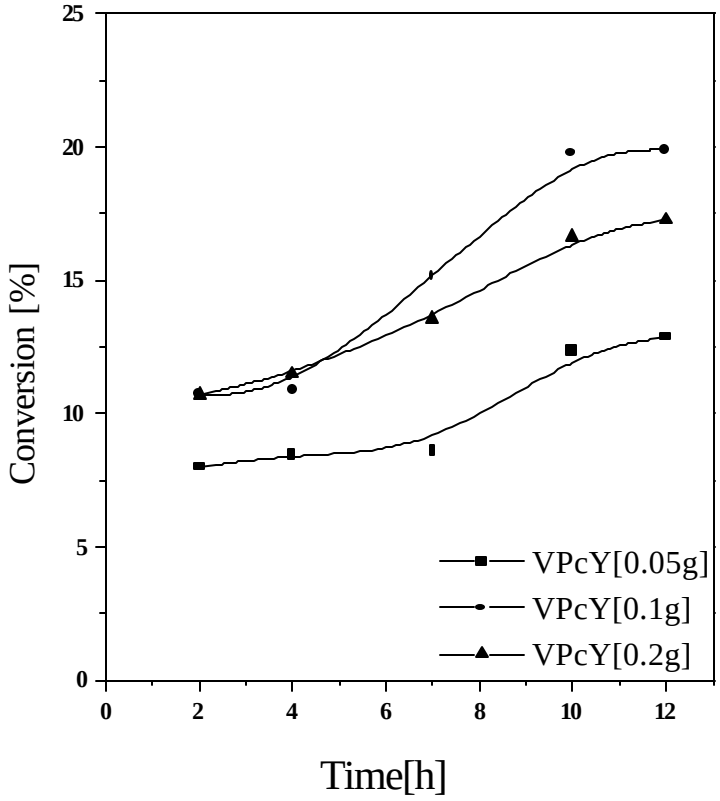

Fig. 4.9a Hydroxylation of phenol over different VPcY catalysts

Conditions : Catalyst wt. = 0.1 g; Phenol:H_2O_2 = 3 mole;
Temp. = 348 K; Solvent, water = 20 g;

loading. Analysis of the product distribution (Fig. 4.9b; Table 4.10) shows that with increasing catalyst content, the selectivity for parabenzoquinone is enhanced while hydroquinone selectivity is slightly suppressed. It is seen from the Fig. 4.9a that though the conversion at 0.1 g and 0.2 g loadings are similar at 2 to 4 h duration of run, the conversion increases less rapidly when 0.2 g catalyst is present due presumably to the rapid decomposition of H_2O_2 by the large amount of catalyst. Phenol conversion efficiency is actually smaller when more catalyst (0.2 g) is used (Table 4.10).

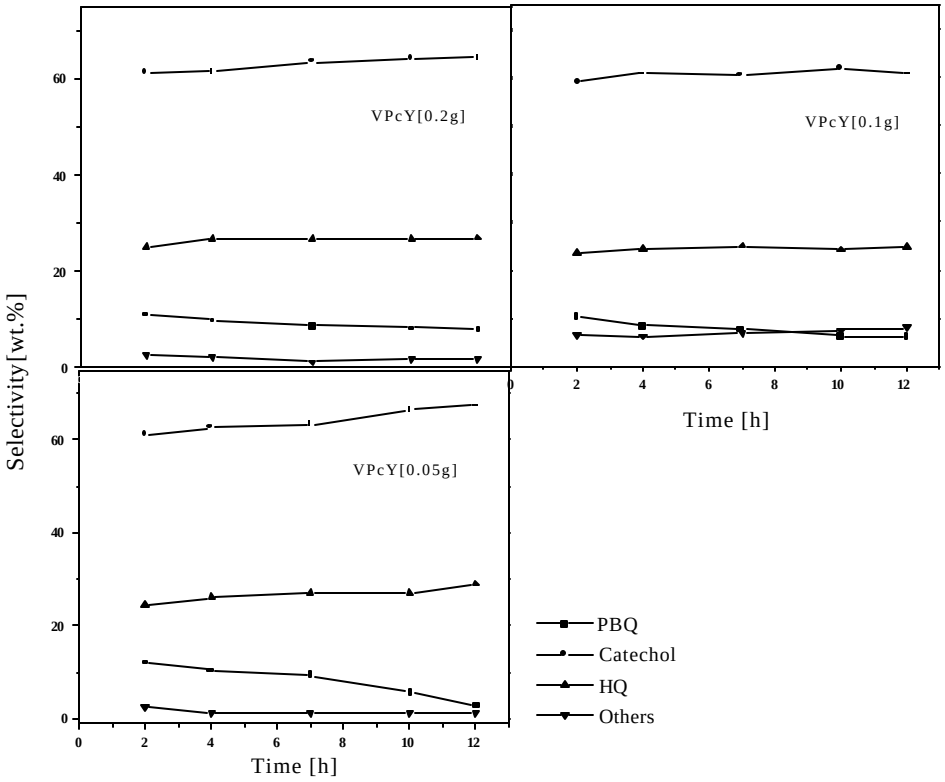

Fig. 4.9b Effect of catalyst concentration on product selectivity in phenol hydroxylation.

Conditions : Catalyst wt. = 0.1 g; Phenol:H_2O_2 = 3 mole; Temp. = 348 K; Solvent, water = 20 g;
PBQ = parabenzoquinone; HQ = hydroquinone.

Table 4.10

Effect of catalyst concentration in phenol hydroxylation over VPcY(1.0)

Catalyst amount (g)	Time [h]	Conv. (%)	Conv. Efficiency[a] (%)	Selectivity			
				PBQ	Catechol	HQ	Others
0.05	12	12.3	37.0	2.6	61.4	30.0	6.1
0.10	12	19.8	59.3	6.3	62.0	24.2	7.5
0.20	12	16.6	49.9	8.3	63.0	23.9	4.8

Phenol/H_2O_2 = 3 (mole ratio); Temperature = 348 K; Solvent-water = 20 g, PBQ = parabenzoquinone; HQ = hydroquinone.
[a]% of theoretical amount of phenol converted based on H_2O_2 : Phenol (mole ratio)

The influence of changing the phenol : H_2O_2 (mole) ratios on conversion and product yields are presented in Table 4.12. Decreasing H_2O_2 concentration in the reaction medium resulted in decreased phenol conversion (Table 4.12). Variation in H_2O_2 concentration was not found to affect product selectivities. Catechol, hydroquinone and parabenzoquinone selectivities were nearly similar. This observation is quite different from that found in the case of titanosilicates. For example, in the case of phenol hydroxylation with H_2O_2 over TS-1 molecular sieves [23], the relative concentration of catechol was higher at larger concentrations of H_2O_2. The differences in shape selectivity and relative hydrophobicity/hydrophilicity of TS-1 and NaY are probably factors that play a role in this difference (TS-1 being highly silicic, is more hydrophobic than NaY). Due to the smaller nature of the pores in TS-1, diffusion limitations become more severe at higher H_2O_2 contents leading to more surface reaction and catechol formation.

Table 4.12

Effect of phenol: H_2O_2 mole ratio in phenol hydroxylation over VPcY(1.0)

Mole ratios	Time [h]	Conv (%)	Conversion Efficiency[a](%)	Product distribution (wt. %)			
				PBQ	Catachol	HQ	Others
1	12	25.2	25.2	14.9	65.4	16.1	3.7
2	12	20.0	40.0	11.6	65.7	18.6	3.3
3	12	19.8	59.5	6.3	62.0	24.2	7.5
4	12	10.2	40.8	4.5	59.9	24.1	6.9

Catalyst wt. = 0.1 g; Temperature = 348 K; Solvent-water = 20 g;

[a]% of theoretical amount of phenol converted based on H_2O_2 : phenol (mole ratio);

PBQ = parabenzoquinone; HQ = hydroquinone.

4.2.4 Comparative study of CuPcY, CoPcY and VPcY catalysts in phenol hydroxylation

A comparison of activity and selectivity of the most active MPcY catalysts namely CuPcY(0.6), CoPcY(0.6) and VPcY(1.0) shows (Fig. 4.10a, Table 4.13) that catalytic activity for the three catalysts varies in order, CuPcY (0.6) > CoPcY (0.6) > VPcY (1.0). The selectivities for catechol and parabenzoquinone are found to be similar for the three catalyst systems but hydroquinone selectivity was found to vary in the order CuPcY(0.6) > CoPcY(0.6) > VPcY(1.0).

Table 4.13

Comparative study of CuPcY, CoPcY and VPcY catalysts in phenol hydroxylation

Catalyst	Conversion (%)	Product distribution (wt %)			
		PBQ	Catechol	HQ	Others
CuPcY(1.2)	26.9	7.1	63.8	28.8	0.3
CoPcY(1.2)	17.4	8.1	62.7	28.2	1.1
VPcY(1.2)	9.1	16.4	52.6	25.9	5.2

Catalyst wt = 0.1 g; phenol:H_2O_2 = 3 (mole ratio); Temperature = 348 K; Solvent-water = 20 g; Reaction time = 12 h; PBQ = parabenzoquinone; HQ = hydroquinone

A comparison of the activity and selectivity of CuPcY(1.2), CoPcY(1.2) and VPcY(1.2) shows that the order of conversion over the three catalysts is, CuPcY(1.2) > CoPcY(1.2) > VPcY(1.2). The product selectivities over the three catalysts show a similar trend. The differences in the activity of the catalysts arises in part from the differences in the relative amounts of phenol hydroxylated and H_2O_2 decomposed.

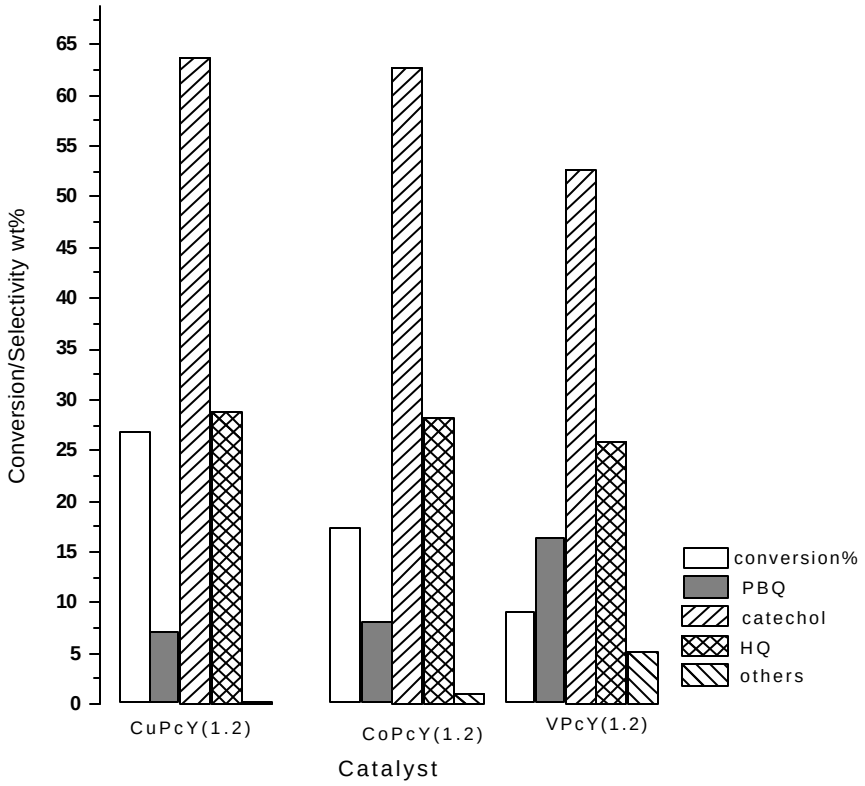

Figure 4.10 Comparison of various MPcY (M= Cu, Co, V) catalysts in phenol Oxidation reaction

Metals with higher redox potentials tend to decompose H_2O_2 more as they easily switch between two valencies as shown below:

Decomposition of H_2O_2 :

$M [n^+] + H_2O_2 \longrightarrow M [(n-1)^+] + HOO. + H^+$ (**rate = k_d**)

$M[(n-1)^+] + H_2O_2 \longrightarrow M [n^+] OH + .OH$

$HO. + H_2O_2 \longrightarrow HOO. + H_2O$

$2\ HOO. \longrightarrow O_2 + HO.$

The redox potential of Co (III) ⟶ Co (II) is 1.82 V and that for Cu (II) ⟶ Cu (I) is 0.15 V. Hence one would expect Co to decompose H_2O_2 faster than Cu.

Hydroxylation of Phenol

$$M\,[n^+] + H_2O_2 + \text{phenol} \rightarrow M\,[n^+] + \text{HQ or Catechol} + H_2O \quad (\textbf{rate } \mathbf{k_h})$$

The phenol conversions observed over the different catalysts will depend on the ratio of the rates of the two reactions : phenol conversion $\propto k_h / k_d$. In our observations, the order of activity is Cu > Co > V. The very low activity of V is also related to the large amount of extraframework V present in higher oxidation states (IV or V) which undergo redox transformation easily. These ions decompose H_2O_2 rapidly. This is also evident from the studies on catalyst concentration; in the case of Cu, increasing catalyst loading from 0.1 to 0.2 g increased phenol hydroxylation significantly (Table 6); the effect was less marked in the case of Co (Table 9) and the activity decreased (Table 11) in the case of V.

As HO**.** free radicals are also formed easily, there is more free radical hydroxylation of phenol over metals which undergo redox transformation more easily (like Co, Fe, etc.). Though both free radical (**.**OH) and hydroxonium ion (OH^+) hydroxylation may be occuring over all the catalysts investigated, the proportion of free radical hydroxylation is expected to be more over V and Co catalysts than over Cu catalysts.

4.3 Conclusions

Comparison of the catalytic activity of substituted copper phthalocyanine complexes shows that TON is more for complexes with electronegative substituents and decreases in the order $CuCl_{16}Pc > Cu(SO_3Na)_4Pc > CuCl_8Pc > CuPc$ which is attributed

to electron depletion at the metal site resulting in easier cleavage of metal-hydroperoxy complexes and hence higher epoxidation activity.

CuPcY catalysts are found to be active in styrene epoxidation using TBHP as the oxidant. Encapsulated CuPcY catalysts show higher catalytic activity than neat CuPc sample which is attributed to the distortion of the molecules and the consequent ease of redox transformation of Cu ions. Both the low Cu content catalyst (CuPcY(0.6)) and high Cu content catalyst (CuPcY(1.2)) show similar activities but CuPcY(0.6) produces more benzaldehyde.

CuPcY, CoPcY and VPcY were compared for their catalytic activity in phenol using H_2O_2 as the oxidant. CuPcY showed the highest activity while VPcY catalyst was the least active of the three catalysts. The three catalysts showed similar selectivities for catechol and parabenzoquinone but CuPcY had a higher selectivity for hydroquinone than CoPcY and VPcY. The difference in the activities of the catalysts is explained on the basis of the redox characteristics of the metal ions.

4.4 References

1. A. V. Ramaswamy and S. Sivasanker., *Catal. Lett*., 22 (1993) 239.
2. A. Thangaraj, R. Kumar and P. Ratnasamy, *J. Catal*. 131 (1991) 294
3. A. Bhaumik, R. Kumar and P. Ratnasamy., *Stud. Surf. Sci. Catal*., 84C (1993).
4. W. Hoelderich, M. Hesse and F. Newman., *Angew. Chemie*. Int. Ed. Engl., 27 (1988) 226.
5. R. A. Sheldon, *J. Mol. Catal*., 7 (1980) 107.
6. R. Belal and B. Meunier, *J. Mol. catal*., 44 (1988) 187.
7. T. Katsuki and K.B. Sharpless, *J. Am. Chem. Soc*., 102 (1980) 5974.

8. K. J. Balkus, Jr. and A. G. Gabrielov., *J. Inclu.Phenom. and Mole. Recog. in Chem.*., 21 (1995) 159.

9. D. E. De Vos, F. Thibault-Starzyk, P. P. Knops-Gerrits, R. F. Parton and P. A. Jacobs., *Macromol. Symp*., 80 (1994) 157.

10. A. A. Ozin and C. Gil., *Chem. Rev*., 89 (1989) 1749.

11. N. Jaeger, P. Plath and G. Shultz-Ekloff., *Acta. Phys. Chem*., 31 (1985) 189.

12. N. Herron, C.A. Tolman and G.D. Stucky, *J. Chem. Soc. Chem. Commun*., 1521 (1986).

13. R.F. Parton, D.R.C. Huybrechts, Ph. Buskens and P.A. Jacobs, *Stud. Surf. Sci. Catal.*, 70 (1991) 47.

14. R.F. Parton, L. Utyhervoen and P.A. Jacobs, *Stud. Surf. Sci. Catal*., 59 (1991) 395.

15. R. Parton, Dissertation, Katholieke Universiteit Leuven (1993).

16. K. Srinivasan, P. Michaud and J.K. Kochi, J. *Am. Chem. Soc*., 108 (1986) 2309.

17. S.P. Varkey, C.R. Jacob and P. Ratnasamy, *J. Mol. Catal*.

18. P.P.K. Gerrits, D.de Vos, F.T. Starzyke and P.A. Jacobs, *Nature*, 369 (1994) 543.

19. R. Irie, Y. Ito and T. Katsuki, *Syn. Lett*., (1991) 265.

20. P. Pietikainen, *Tetrahedron Lett*., 36 (1995) 319.

21. C-J. Liu, S.-G. Li, W.-Q. Pang and C.-M. Che, *Chem. Commun*., 65 (1997).

22. C.R. Jacob, S.P. Varkey and P. Ratnasamy, *Microporous and Mesoporous Materials*., 22 (1998) 465.

23. R.A. Sheldon and J.K. Kochi, in "*Metal catalyzed oxidation of organic compounds"* Academic Press, N.Y., 1981.

24. S. Eenst, Y. Traa and U. Deeg., *Stud. Surf. Sci. Catal*., 84 (1994) 925.

25. Q. Yang, C. Li, S. Yuan, J. Li, P. Ying, Q. Xin and W. Shi, *J. Catal*. 183 (1999) 128.

26. Y. Masri and M. Hronee., Stud. *Surf. Sci. Catal*., 66 (1991) 455.

27. M. Hronee, G. Kiss and J. Sitek., *J. Chem. Soc*. *Faraday Trans. 1*.,79 (1983) 1091.

28. S. Alexander and B. Meunier., *J. Chem. Soc. Chem. Commun*., 15 (1994) 1799.

29. K. Takehira., M. Shimizu, T. Hayakawa and H. Orita., *Stud. Surf. Sci. Catal*., 66 (1991) 279.

30. Y. Omura, M. Nakamura, M. Oka, and Y. Fujiwara., Japanese Patent, J.P., 74, 127, 937.

CHAPTER 5
SUMMARY AND CONCLUSIONS

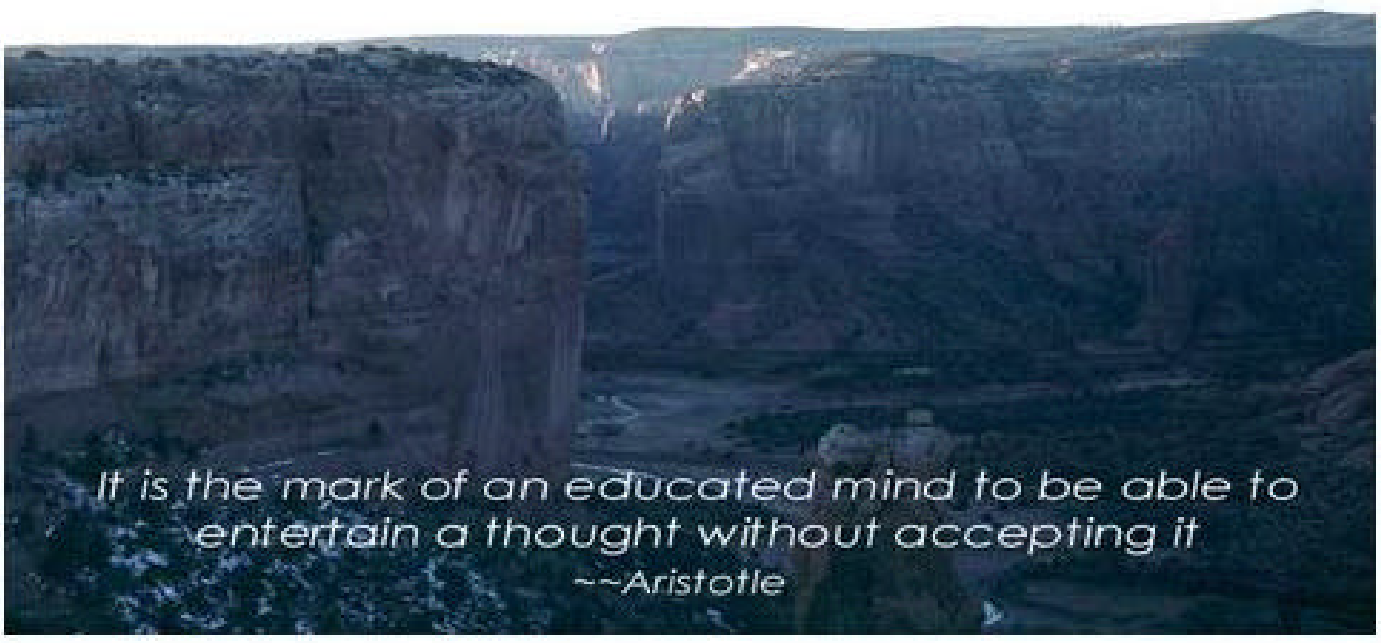

The synthesis, characterization and catalytic properties of copper, cobalt and vanadium phthalocyanine complexes encapsulated in zeolite Y and iron phthalocyanine encapsulated in ETS-10 have been investigated. The encapsulated complexes were prepared by the "template synthesis" method [1] (also known as "*in situ* ligand synthesis" method by some workers [2]) by using metal exchanged zeolite NaY and ferrocene occluded ETS-10 samples (with metal content in the range 0.6 to 1.6 wt.%) and 1,2-dicyanobenzene (DCB). Attempts were also made to encapsulate copper phthalocyanine complexes, especially $CuCl_{16}Pc$, by "zeolite synthesis" method.

The formation and structural integrity of the complexes were investigated by using a variety of physicochemical studies such as elemental analysis (C, H and N), AAS, XRD, TG-DTA, sorption studies and FT-IR, DRUV-Vis and EPR spectroscopic techniques. The comparative spectroscopic studies on "neat" metal phthalocyanine complexes, metal exchanged zeolites and encapsulated complexes have revealed that MPc complexes can be encapsulated in the supercages of zeolite Y and in the channel intersections of ETS-10 by the "template synthesis" method. The spectral properties of the complexes prepared by the "zeolite synthesis" method have resembled those of the "neat" complexes and hence they are not isolated or "truely" encapsulated. The catalytic activity of the "neat" and zeolite-encapsulated MPc complexes were studied in two industrially important reactions viz., styrene epoxidation and hydoxylation of phenol. The encapsulated complexes showed enhanced catalytic activities than the "neat" complexes.

Peripheral substitution has a marked effect on the structure and catalytic activity of "neat" CuPc complexes. The electronic and vibrational band positions shifted as a consequence

of substitution. The EPR spectroscopic studies revealed lower symmetry for chloro-substituted complexes. The substituted complexes showed higher activity in phenol hydroxylation. The catalytic activity of the complexes varied in the order: $CuCl_{16}Pc$ > $Cu(SO_3Na)_4Pc$ > $CuCl_8Pc$ > CuPc. The studies have revealed that the lower symmetry of the complexes and electron withdrawing effects of the substituents are perhaps responsible for the higher catalytic activity of the substituted CuPc complexes. The depletion of electron density perhaps promotes the nucleophillic attack of the oxidant molecule (TBHP) at the metal center forming the catalytically active intermediate metal-hydroperoxide. Further, the heterolytic cleavage of the metal-hydroperoxy complex is also facilitated by the electron withdrawing substituents. The ease of formation and eterolytic cleavage of metal-hydroperoxy intermediate in complexes with electron withdrawing substituents has been correlated to the increased catalytic activity of these complexes in selective oxidation reactions.

A comparative physicochemical study of metal exchanged zeolites, "neat" MPc and zeolite-encapsulated MPc complexes has unequivocally proved the encapsulation of MPc complexes in zeolite Y and ETS-10. Quantitative estimation of the encapsulated metal complex was possible by microanalysis, thermal studies and AAS techniques. The integrity of the complex and its structure was determined from FT-IR, UV-Vis and EPR spectroscopic techniques. EPR spectroscopy, especially of CuPcY complexes has provided clear evidence for the encapsulation of phthalocyanine molecules inside the supercages of zeolite Y. The spectra of the encapsulated complexes were different from that of "neat" and surface adsorbed samples. Sorption studies have also provided an indirect evidence for the encapsulation of the complexes. The encapsulated complexes have lower surface area than the metal exchanged zeolites

samples. By and large the spectroscopic studies revealed that the metal phthalocyanine moiety is puckered as a consequence of encapsulation.

EPR studies of CoPc in zeolite Y and FePc in ETS-10, revealed that the metal ion in these complexes exhibits spin equilibrium phenomenon. Presence of both high and low spin phthalocyanine complexes were noticed in the samples with metal loadings in the range 0.6 to 1.6 wt%. The encapsulated complexes at the outer layers were found to be in a low spin electronic configuration while those in the bulk have a high spin electronic configuration. From the studies on CoPcY complexes it was inferred that the encapsulated CoPc complexes in the outer layers readily interact with molecular oxygen to form stable cobalt superoxide $Co(O_2^{-\cdot})$ radical species.

The zeolite Y-encapsulated CuPc catalysts have been found to be active in styrene epoxidation with TBHP as the oxidant. The encapsulated complexes showed higher catalytic activity than the "neat" CuPc complexes. The enhanced catalytic activity of the encapsulated complexes is attributed to the distortion of Pc moiety and the consequent ease of redox transformation of Cu ions.

A comparative study has revealed that the central metal ion indeed plays a significant role in the catalytic hydroxylation of phenol. The catalytic activity varies with the metal ion in the order: CuPcY > CoPcY > VPcY. The encapsulated CuPc catalysts have shown higher selectivity for hydroquinone than the other Pc catalysts. The product distribution for catechol and parabenzoquinone is similar for all the catalysts.

The studies presented in the thesis on encapsulated MPc complexes have provided definite convincing evidence for their biomimitic nature. Just as the protein environment in

metalloenzymes dictates the geometry and redox properties of the active site in addition to providing sterio- and regio-selectivities, the zeolite mantle as revealed from the present investigations also modifies the molecular and electronic structural properties of MPc complexes and enhances the rate of the chemical trasformations. Thus the modified solid catalysts can be called as inorganic mimics of enzymes. These catalyst systems are found to be advantageous and hold promise for application in chemical industry due to the following reasons: (1) the catalysts have high thermal stability, (2) deactivation via. dimerization and aggregation is avoided, (3) the activity of the encapsulated complexes is higher than the corresponding "neat" complexes, (4) the solid encapsulated catalysts have significant processing advantages in industrial operations when compared to homogeneous catalysts and (5) the catalyst system utilizes cheap singlet oxygen source like H_2O_2 which leave no harmful dissociation products.

5.1 References

1. K. J. Balkus, Jr. and A. G. Gabrielov., *Journal of Inclusion Phenomena and Molecular Recognition in Chemistry*., 21 (1995) 159.
2. D. E. De Vos, F. Thibault-Starzyk, P. P. Knops-Gerrits, R. F. Parton and P. A. Jacobs., *Macromol. Symp*., 80 (1994) 157.

List of Publications

1. Spectroscopic investigation and catalytic activity of copper(II) phthalocyanine encapsulated in zeolite-Y
   Sindhu Seelan, A. K. Sinha, D. Srinivas and S. Sivasanker
   J. Mol. Catal. 157 (2000) 163.

2. Effect of peripheral substitution on the EPR spectra and catalytic properties of copper phthalocyanine complexes
   Sindhu Seelan, D. Srinivas and S. Sivasanker
   (Communicated).

3. Thermodynamic and transport properties of ionized solutes in molten state continuously miscible in org. solvents : A class of systms with interesting features.
   Sindhu Seelan & Anil Kumar
   Indian Journal of Chemistry, Vol. 36A (1997) 121

List of Papers Presented in Symposia/Workshops

1. Preparation and characterization of iron phthalocyanine encaged ETS-10 molecular sieves
   Sindhu Seelan, Tapan Kr. Das, A. J. Chandwadkar and S. Sivasanker
   Presented in the National Worshop on Catalysis at Regional Research Laboratory, Trivendrum (1997).

2. Spectroscopic studies of Cu(II) phthalocyanine complexes encapsulated in zeolite Y
   Sindhu Seelan, D. Srinivas and S. Sivasanker
   Presented in the International *Symposium on Catalysts* at National Chemical Laboratory, Pune. January 1999.

3. Characterization of copper(II) phthalocyanine encapsulated in zeolite-Y by spectroscopic techniques
   Sindhu Seelan, A. K. Sinha, D. Srinivas and S. Sivasanker
   Presented in the National Workshop on Catalysis held at Indian Institute of Chemical Technology, Hyderabad during January 7-8, 2000.